U.S.NRC

United States Nuclear Regulatory Commission

Protecting People and the Environment

Methodology for Estimating Fabrication Flaw Density and Distribution – Reactor Pressure Vessel Welds

Office of Nuclear Regulatory Research

U.S.NRC

United States Nuclear Regulatory Commission

Protecting People and the Environment

Methodology for Estimating Fabrication Flaw Density and Distribution – Reactor Pressure Vessel Welds

Prepared by
G.J. Schuster, M. Morra, S.R. Doctor

Pacific Northwest National Laboratory
P.O. Box 999
Richland, WA 99352

W.E. Norris, NRC Project Manager

Office of Nuclear Regulatory Research

Abstract

The Pacific Northwest National Laboratory has developed a generalized fabrication flaw distribution for the population of U.S. nuclear reactor pressure vessels in operating nuclear power plants. The U.S. Nuclear Regulatory Commission (NRC) will use the generalized flaw distribution to predict component-specific flaw rates. The estimates of fabrication flaws are intended for use in fracture mechanics structural integrity assessments. Structural integrity assessments, such as estimating the frequency of loss-of-coolant accidents, are performed by computer codes that require, as input, accurate estimates of flaw rates. Machine-made welds using the submerged arc method were destructively examined to measure and characterize fabrication flaws to provide empirical estimates of the density.

This report describes the fabrication flaw distribution and characterization in the submerged arc weld of four vessels. The work indicates that flaw density changed over the years of vessel construction. Furthermore, the results show that flaw distributions differ by manufacturer. Parametric analysis using an exponential fit is performed on the data.

This report describes the validation methods employed on the detected fabrication flaws. Nondestructive examination (NDE) measurements were applied to the clad surface of the vessel, large and small weld segments, and cubes of material. Ultrasonic, radiographic, and metallographic testing methods and results are described in the report. The implementation and application of high-resolution ultrasonic methods for imaging the fabrication flaws is also reported.

Foreword

NUREG/CR-6945, *Fabrication Flaw Density and Distribution in Repairs to Reactor Pressure Vessel and Piping Welds*, was published in April 2008. The report provides details regarding the fabrication flaws that were found in the repair weld metal of reactor pressure vessels (RPV) and piping. To determine the distribution and density of fabrication flaws, empirical studies were performed on RPV welds obtained from Shoreham, Hope Creek Unit 2, River Bend Unit 2, and the Pressure Vessel Research User Facility (PVRUF). Sections of pipe obtained from Pilgrim Unit 2 and from the Beaver Valley Nuclear Power Plant were analyzed to assess repairs that were performed and determine the fabrication flaw distribution. The primary focus of this study was RPVs; however, a limited number of piping segments were available for evaluation. Thus, it would be difficult to make any generic conclusions with regard to piping. The NRC is further investigating the effects of repairs to piping welds.

The research was initiated because analyses have shown that vessel behavior is sensitive to flaw location, type, size, orientation, and other flaw characteristics. Accurate estimates of flaw density and distribution are required as input to the computer codes that are used in performing structural integrity assessments. The objective of the research was to determine the relevant properties of flaws created during the fabrication of nuclear components and develop data on the density and distribution of fabrication flaws in the base materials, cladding, and welds. This research was conducted over a 15-year time period. In addition to NUREG/CR-6945 mentioned above, the following three reports were previously published: NUREG/CR-6471, Volume 1, *Characterization of Flaws in U.S. Reactor Pressure Vessels ─ Density and Distribution of Flaw Indications in PVRUF*, (NRC Agencywide Documents Access and Management System [ADAMS] Number ML070300576 [report] and ADAMS Number ML070300579 [Appendix A]; NUREG/CR-6471, Volume 2, *Characterization of Flaws in U.S. Reactor Pressure Vessels ─ Validation of Flaw Density and Distribution in the Weld Metal of the PVRUF Vessel*, (ADAMS Number ML003754908); and NUREG/CR-6471, Volume 3, *Characterization of Flaws in U.S. Reactor Pressure Vessels ─ Density and Distribution of Flaw Indications in the Shoreham Vessel*, (ADAMS Number ML003727107). Finally, NUREG/CR-6817, *A Generalized Procedure for Generating Flaw-Related Inputs for the FAVOR Code*, is expected to be published in the first quarter of 2009.

The U.S. Nuclear Regulatory Commission used the data from all of these reports in its re-evaluation of the technical basis for Title 10 of the *Code of Federal Regulations* (CFR) 50.61, "Fracture toughness requirements for protection against pressurized thermal shock events." Based on the experimental data from this study in conjunction with calculations and expert judgment, it has been concluded that the risk of through-wall cracking due to pressurized thermal shock events is much lower than previously calculated. The NRC has initiated rulemaking activities to revise 10 CFR 50.61.

As summarized above, NUREG/CR-6945 describes the research conducted to analyze repair weld metal. This subsequent report (*Methodology for Estimating Fabrication Flaw Density and Distribution ─ Reactor Pressure Vessel Welds*) documents the empirical methodology that evolved for reliably detecting the fabrication flaws in nuclear components and accurately characterizing them through advances/ improvements in the NDE methods, as well as the destructive characterization processes being employed. The methodology evolved to become more effective, thus requiring fewer resources to develop validated fabrication flaw density and distribution values. This report also documents the fabrication flaws in the River Bend Unit 2 and the Hope Creek Unit 2 RPV material exclusive of the repairs. This new data and findings assist in the development of a generalized flaw density and distribution that can be used to

estimate flaws created during the fabrication of nuclear component weldments. As previously stated, estimates of flaw density and distribution are required as input to the computer codes that are used in performing structural integrity assessments. The development of a generalized approach has been further validated, supporting an accurate estimation of flaw density and distribution in weldments in operating nuclear power plants.

Contents

Figures

Tables

Executive Summary

This report presents results of empirical studies on nuclear materials from cancelled U.S. nuclear power plants. The studies were conducted to develop data on the density and distribution of fabrication flaws in selected nuclear reactor components and product forms. These inspection-based empirical results are intended to help characterize the initial fabrication flaw distributions in weldments for use in probabilistic fracture mechanics codes. The results were used, for example, by the NRC in the recent reassessment of the requirements in Title 10, Part 50, Section 50.61, of the *Code of Federal Regulations* (10 CFR 50.61), "Fracture Toughness Requirements for Protection Against Pressurized Thermal Shock Events." Reactor pressure vessel segments with machine-made welds were examined from Shoreham, Hope Creek Unit 2, River Bend Unit 2, and the Pressure Vessel Research User Facility (PVRUF).

Pacific Northwest National Laboratory (PNNL) found many fabrication flaws in the machine-made weld passes, and the data were analyzed for density and distribution. Descriptions of the source of the welds are provided in the report. An estimate of flaw density and distribution was made, and the results for through-wall size distribution are given in Figure ES.1.

The report describes the methodology used by PNNL to produce flaw rates. High-resolution synthetic aperture focusing technique ultrasonic testing (SAFT-UT) was refined and performed using immersion testing. Work on the SAFT algorithm is reported that produced an improvement of three orders of magnitude in processing times. High-resolution reconstructions that previously required greater than 24 hours can now be completed in under a minute. The refined SAFT-UT was shown to resolve closely spaced small flaws and more accurately size them as well.

Among the principal findings of this study is that flaw density changed over the years of vessel construction. The results show that flaw distributions differ by manufacturer. Parametric analysis using an exponential fit was performed on the data. The Combustion Engineering (CE) vessels, Shoreham and PVRUF, have a similar through-wall size dependence and a factor of three difference in overall density. The vessels by Chicago Bridge and Iron (CB&I) do not share the same through-wall size dependence as the vessels by CE. The slope for the cumulative flaw density vs. size curve is much greater for CB&I vessels compared to CE vessels as shown in Figure ES.1. For flaws greater than 4 mm, the cumulative flaw density is a factor of 10 less for River Bend Unit 2 than for Hope Creek Unit 2 showing the change in flaw rate over the years for vessel construction.
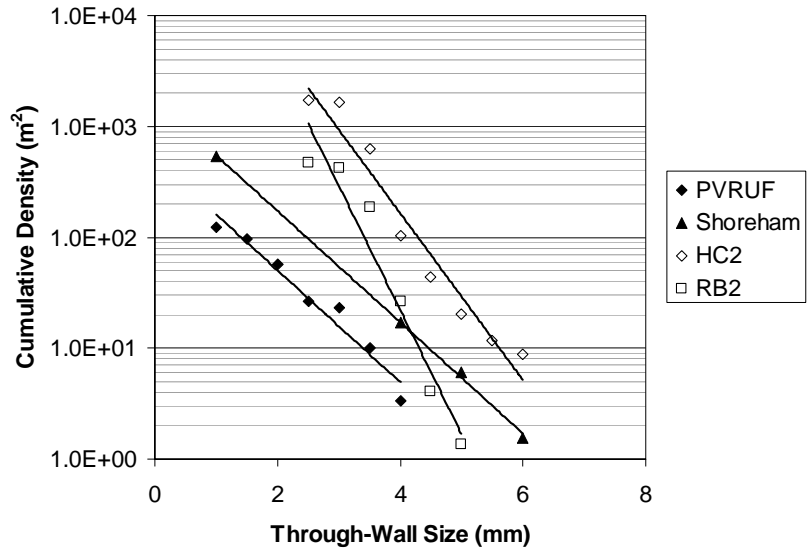
Figure ES.1   Comparison of Through-Wall Size Distribution of Cumulative Flaw Densities for Side-Wall Fusion Zones in SAW. HC2 stands for the Hope Creek Unit 2 vessel; RB2 stands for the River Bend Unit 2 vessel.

Acknowledgments

Abbreviations and Acronyms

base metal	the metal that composes the plates or forged rings of a reactor pressure vessel – the plates forming the vessel by butt-welding
BGE	Baltimore Gas & Electric Company
BWR	boiling water reactor – a nuclear reactor in which the coolant is water
CB&I	Chicago Bridge & Iron
CE	Combustion Engineering
CT	computed tomorgraphy
cumulative flaw rate	the density of flaws greater than a specified size
defect	a discontinuity or discontinuities that by nature or accumulated effect (for example, total crack length) render a part of product unable to meet minimum applicable acceptance standards or specifications – This term designates rejectability. See also *discontinuity* and *flaw* (AWS 1984).
discontinuity	an interruption of the typical structure of a weldment, such as a lack of homogeneity in the mechanical, metallurgical, or physical characteristics of the material or weldment – A discontinuity is not necessarily a defect. See also *defect* and *flaw* (AWS 1984).
EDAX	energy dispersion spectroscopy
flaw	an imperfection or unintended discontinuity in a material – a void, porosity, inclusion, lack of fusion, or crack that is physically distinct from the metallic microstructure
flaw density	the number of flaws per unit length, area, or volume
flaw depth size	see *through-wall extent*
flaw distribution	the number of flaws measured in separate categories
flaw rate	the flaw density expressed as a function of flaw through-wall extent
fusion line	one of two lines on the cross section of the weld that form the boundary between the weld metal and the base metal
indication (of a flaw)	the response or evidence of a flaw from the application of nondestructive evaluation – for ultrasonic testing, a coherent packet of (ultrasonic) energy that is characterized as originating from a flaw
inclusion	a foreign solid, (e.g., slag, scale, oxide, or nonmetallic substance) entrapped in the base metal or weld metal
laminar flaws	planar flaws that are oriented within 10 degrees of a plane parallel to the surface of the component – see ASME (1998)
Marshall Distribution	a flaw rate in the weld metal of reactor pressure vessels – see Marshall (1982)
MT	magnetic particle testing
NDE	nondestructive evaluation
near-surface zone	the first 25 mm (1.0 in.) of reactor pressure vessel material from the cladding's wetted surface

NRC	U.S. Nuclear Regulatory Commission
outside the near-surface zone	the remainder of vessel wall when the near-surface zone is excluded
planar flaw	a flat two-dimensional flaw in a plane other than parallel to the surface of the component – In this study, it includes a crack or lack of fusion that is primarily vertical in orientation in the vessel.
porosity	a group of voids located close to each other
PVRUF vessel	The Pressure Vessel Research Users' Facility vessel, at Oak Ridge National Laboratory, was a pressurized water reactor vessel from a canceled U.S. plant – see Pennel (1989).
PWR	pressurized water reactor – a nuclear reactor in which the coolant is water, maintained at such a pressure as to keep it from boiling
RPV	reactor pressure vessel
RMS	root-mean-square
RT	radiographic testing
SAFT-UT	synthetic aperture focusing technique for ultrasonic testing – see Doctor et al. (1996)
SAW	submerged arc weld
SEM	scanning electron microscope
size	see *through-wall extent*
SNR	signal-to-noise ratio
through-wall extent	the maximum dimension, normal to the surface of the component, of the rectangle circumscribing the flaw
UT	ultrasonic testing
void	a volume of gas entrapped in the vessel material
volumetric flaw	a three-dimensional flaw such as a void, porosity, or inclusion – Also includes laminar flaws.
weldment	an assembly whose component parts are joined by welding (AWS 1984)
weld metal	that portion of a weld that has been melted during welding (AWS 1984)
weld profile	the shape of the weld metal when sectioned across the weld

1. Introduction

The U.S. Nuclear Regulatory Commission (NRC) initiated a program at the Pacific Northwest National Laboratory (PNNL) with the major objective of estimating the rate of occurrence of fabrication flaws in U.S. light-water reactor pressure vessels (RPVs) (Jackson et al. 2001). PNNL's methodology for estimating the density and size distribution of fabrication flaws involves the nondestructive evaluation (NDE) of weldments from cancelled nuclear plants and the destructive validation of detected flaws. This methodology characterizes the flaws for fracture mechanics significance because the likelihood of vessel failure is sensitive to flaw location, type, size, orientation, and other flaw characterizations (Simonen and Khaleel 1995). The objective of this research is to estimate these and other relevant properties of flaws created during the fabrication of nuclear component weldments.

To meet this objective, a generalized flaw distribution is proposed because the rate of occurrence of fabrication flaws is expected to vary over product forms and over the years of component fabrication. In order to develop a generalized flaw distribution and to resolve technical issues, an expert judgment process was used. The results of this expert judgment process helped to formulate a generalized approach to fabrication flaw density and distribution (Jackson and Abramson 2000). The impaneled experts judged that the product forms and construction processes determine the fabrication flaws in weldments. So, for the ith component, the number of flaws greater than size x can be given by a sum over product forms

$$N_i(x) = \sum_j \rho_j(t_i) \cdot V_{ij} \cdot G_j(x)$$

where $\rho_j(t_i)$ is the flaw density in product form j during time interval for the construction of the ith component t_i, V_{ij} is the volume (or area) of the product form in a weldment or a region of a weldment, and $G_j(x)$ is the probability that a flaw, in product form j, has a size greater than x. PNNL data have shown that

$$G_j(x) = \exp(-\beta_j x)$$

provides a reasonable fit to the fabrication flaw data (Doctor and Schuster 2001).

This report documents the methodology that PNNL followed for estimating fabrication flaw density and distribution in reactor pressure vessel product forms. Section 2 reviews validation methods used to estimate fabrication flaw density and size distribution. Section 3 documents the development and implementation of SAFT-UT for high-resolution measurements on fabrication flaws. Section 4 shows the details of the submerged arc weld product form inspected in this study. Section 5 provides the measurement sequences for validation. The validated flaw rates for the submerged arc weld are also provided here. Findings from the overall study are summarized in Section 6.

2. Description of Measurement Methods for Fabrication Flaws

This section describes the methods used to detect and characterize fabrication flaws in reactor pressure vessel welds. The methodology involves the sectioning of the welds into test specimens of decreasing size. The methods included inspections from the clad surface of the PVRUF vessel. These measurements were made before the PVRUF vessel was cut into plates for laboratory studies. Metallographic and electron microscopy was performed on small cubes of material that were approximately 25 mm on a side.

The description of measurement methods provided in this section is introductory material for the discussion of measurement sequences provided in Section 5.1. The reader may find it helpful to skip ahead to that section and then return to this discussion. However, an overview of the PNNL strategy that was followed for the inspection of reactor pressure vessel materials involved a number of steps that are described in this section. The overall goal was to end up with the detection, characterization, and validation of all the fabrication flaws in RPV materials. It needs to be noted that the strategy that was followed evolved over time as experience and confidence increased based upon the validation of the results from the NDE techniques employed. The specific details of the process followed for material from each RPV cancelled plant is described in Section 5. In the case of PVRUF, the initial inspections were conducted from the cladding surface so that areas of interest could be identified and cut out of the RPV for further NDE work. The follow-on work for PVRUF cut-out material and for all of the other cut-out cancelled plant material had the goal to do a very thorough job but to optimize the process (in terms of time and costs) to ensure that the fabrication flaws were detected with very high reliability and that the NDE inspections provided the best information for flaw characterization and sizing. This was accomplished by cutting out the welds so that weld-normal SAFT-UT inspections could be performed. Based on the weld-normal NDE results, the next step was to remove segments in the form of slices containing indications of interest from the weld-normal pieces for use in conducting the next series of higher-resolution NDE inspections. Using all of these NDE results, 25-mm cubes were cut from the segment slices and even higher-resolution NDE was performed to further quantify the location, features, and size of the indications. In some cases, there was interest in particular flaws so metallographic analysis of cube faces was performed as the faces were systematically removed by machining exposing the flaws. In other cases, scanning electron microscopy (SEM) and energy dispersive spectroscopy (EDAX) was performed. This process may be summarized as initially applying techniques that had very high detection sensitivity to ensure that all potentially large flaws would be detected with very high reliability at the expense of probably over sizing the flaws. The following sequential steps where then intended to more accurately characterize and size the indications using higher and higher resolution NDE with the final step being validation via destructive testing.

2.1 Vessel Clad Side

The initial inspections of the PVRUF vessel were performed by using SAFT-UT from the clad inner surface as shown in Figure 2.1. Data from these inspections were analyzed and sizing rules as reported by Schuster et al. (1998) were consistently applied for two purposes. Most importantly, the material that contained the largest indications was identified for later study and validation.

In vessel examinations from the clad side, tip diffracted signals from the top and bottom of a large embedded flaws are detectable. Figure 2.2 shows typical image data from 1.5 MHz diameter 45° shear

mode ultrasound of two signals that are aligned vertically and separated by 12 mm. The analysis rules for the SAFT-UT data required that this pattern be considered as one 12-mm flaw (to ensure that no large flaws were missed). Validation research showed that the abundance of small flaws will produce most of these patterns. Because of the abundance of small flaws, tip diffracted signals from a large flaw with a small aspect ratio will be difficult to distinguish from small flaws that are vertically aligned. These two conditions were resolved by other NDE inspections and destructive validation.

2.2   Large Weld Segments

The second stage in developing validated flaw rates for RPVs used weld-normal SAFT-UT inspections with cut and machined inspection surfaces. Figure 2.3 shows large weld segments weighing up to 2000 Kg (4400 lb) prepared for inspection in the laboratory. The process for preparing the specimens is fully described in Schuster et al. (1999). Using weld-normal inspections, planar flaws in the weld's fusion zones and in the weld repairs can easily be detected and sized. Then, using these detection and sizing results, the flawed material is prioritized for additional validation testing.

The inspections were performed with a 5 MHz diameter ultrasonic probe in contact with the machined surface and coupled to the metal with mineral oil. This technique provided lateral resolution of 3 mm and a depth resolution of 1.2 mm.

Most of the flaws found were in the fusion zone of the SAW with the base metal. The SAFT-UT images from the weld-normal testing of the large weld segments removed from the Shoreham vessel can be found in Schuster et al. (1999).

2.3   Small Weld Segments

Small weld segments, such as those shown in Figure 2.4, weighed less than 200 Kg (440 lb) and fit into the PNNL immersion tank without overloading the tank's support fixtures. Immersion testing of these small weld segments permitted the use of higher resolution techniques that can accurately resolve small flaws separated by 1 mm. As described in Section 3, the technique also accurately sizes flaws 1 mm in diameter. The photo in Figure 2.5 shows a 125 Kg (275 lb) calibration block in the upper left portion of the figure. The figure also shows the SAFT-UT system and the PNNL immersion tank.

Figure 2.6 shows immersion testing data of a 5.5-mm flaw indication from the weld-normal testing of large weld segments. The flaw indication is identified in the box drawn in the SAFT-UT image on the left in the figure. The data shown here used a 10 MHz F8 immersion transducer with a depth resolution of 0.5 mm and a lateral resolution of 2.5 wavelengths or 1.5 mm. The two small flaws are resolved in depth as shown in the B-scan end view image on the right-center in the figure.

Figure 2.7 shows the same material and flaw(s) as the previous figure but with twice the resolving power. The ultrasonic immersion probe was a 10 MHz F4 and as such has a lateral resolution of 1.2 wavelength or 0.7 mm. Here the two small flaws are resolved both laterally and in depth.

Figure 2.8 shows the same material and flaw(s) as the previous two figures but with sub-wavelength resolution. The ultrasonic immersion probe was a 10 MHz F2.7 and had a lateral resolution of

0.8 wavelength or 0.5 mm. Here the two small flaws are both sized at 1 mm. See Appendix B for the metallographic results.

PNNL used all three of these transducers – F8, F4, and F2.7 – in a flaw characterization sequence. This was done to correctly identify the flaw clusters using a sequence of slowly changing images.

2.4   Weld Cross Section Plates

PNNL researchers investigated the use of radiography as a means of both characterizing the flaws for guiding the metallographic process and of validating the size and character of a larger-sized sample than possible with metallography alone. Figure 2.9 shows weld cross section plates from the PVRUF vessel. The radiographic data confirmed the presence of discontinuities on the fusion line as measured by the weld-normal ultrasonic testing.

Radiography of the PVRUF weld cross section plates was done to Westinghouse Hanford's General Radiographic Procedure (NDT-RT-4000, Rev. 3) with a Philips 450 KV X-ray machine. Required sensitivity was 2T (thickness) with a density requirement between 1.8 to 4.0 H&D units. The nominal voltage setting was 350 KV at 2.5 mA; however, it varied based on plate thickness. The film was single-loaded Fuji type 25. Image quality was based on conventional American Society of Mechanical Engineers (ASME) penetrameters.

Figure 2.10 shows a typical radiograph of a 25-mm thick plate containing some flaws. One of the flaws was located by the weld-normal ultrasonic testing and the arrow markers indicate the location of the flaw as predicted by the ultrasound. The presence of a flaw is confirmed in the location predicted.

2.5   Cubes

Figure 2.11 shows cubes containing the largest flaws from the submerged arc weld of the River Bend Unit 2 and the Hope Creek Unit 2 vessels. The flaws were all in the fusion zone of the base metal with the submerged arc (machine-made) weld metal. Immersion ultrasonic testing and film radiography were used on the flaw-bearing cubes from the submerged arc weld.

Figure 2.12 shows immersion testing data of a 6-mm flaw indication from the weld-normal testing of large weld segments. The data that are shown here used a 10 MHz F8 immersion transducer with a lateral resolution of 2.5 wavelength or 1.5 mm. At this resolution the indication appears to be one flaw. Figure 2.13 shows immersion testing data of the same 6-mm flaw indication as the previous figure. The data here used a 10 MHz F4 immersion transducer with a lateral resolution of 1.2 wavelength or 0.7 mm. The indication is starting to resolve into multiple flaws. Finally, Figure 2.14 shows immersion testing data of the flaw indication. The data that are shown here used a 10 MHz F2.7 immersion transducer with a lateral resolution of 0.8 wavelength or 0.5 mm. In this image multiple, small 1-mm flaws are resolved.

Radiographic testing was also preformed on the flaw-bearing cubes of SAW material. The testing used the same radiographic apparatus as the weld cross section plates described in Section 2.4. The radiographic test of the cubes inspected the flaws from three orthogonal directions. Results of the radiographic testing confirmed the ultrasonic testing results from the cubes (Schuster et al. 2000).

2.6   Cube Face

The analysis clad side SAFT-UT data showed that most flaws were located near the fusion zone of the weld with the base metal (Schuster et al. 2000). The metallographic results, from the small cubes, show that flaws can be planar and typically are a few microns from the heat affected zone but inside the weld metal. Figure 2.15 shows a metallograph of a flaw in the fusion zone of a weld with the base metal.

Figure 2.16 shows an image from one of PNNL's electron microscopes. A portion of a cracked weld pass was imaged using 20 keV electrons, and the magnification is shown with a 100 μ scale. The crack morphology is shown in the image to be branched and filled with segregates.

Table 2.1 shows the distribution of atomic elements in the cracked portion of the weld pass shown in Figure 2.16. The measurements were made with the electron microscope using X-ray emissions from the electron bombardment and the spectroscopic features of the microscope. The concentrations of elemental oxygen, aluminum, and silicon are evidence of metallic and nonmetallic oxides in the failed weld bead.

Table 2.1 Presence of Metallic and Nonmetallic Oxides in Failed Weld Bead

Element	Weight %	Atomic %
C	3.73	9.30
Mn	1.22	0.66
Fe	55.62	29.83
O	22.57	32.25
Al	1.65	1.84
Si	14.80	15.78
S	0.15	0.13
K	0.26	0.20

Figure 2.1 Inside View of the PVRUF Vessel during SAFT-UT Inspections
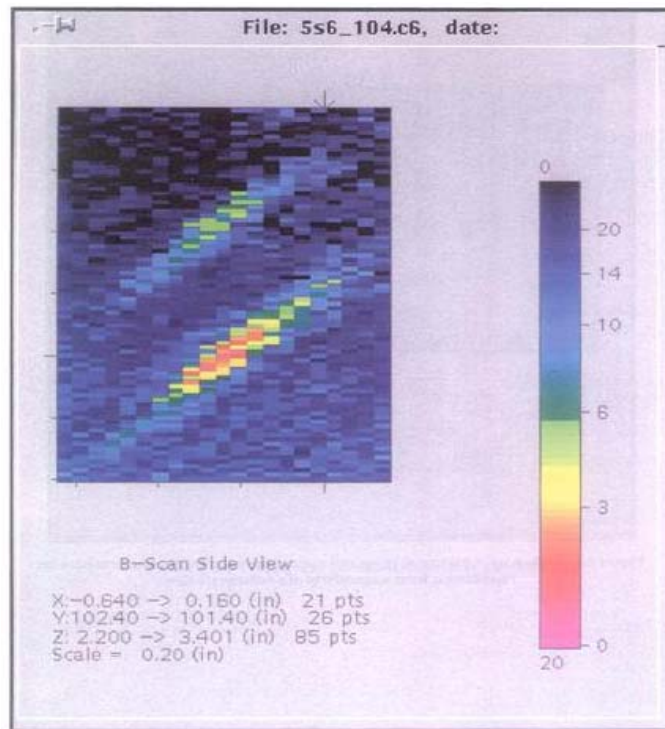
Figure 2.2 Image of Two Small Fabrication Flaws Detected by SAFT-UT from the Clad Surface of the PVRUF Vessel

Figure 2.3 Large Weld Segments from the Shoreham Vessel

Figure 2.4 Photo of Small Weld Segments from Hope Creek Unit 2 and River Bend Unit 2 Vessels for Immersion Testing

Figure 2.5 SAFT-UT Immersion Inspection of Small Weld Segments

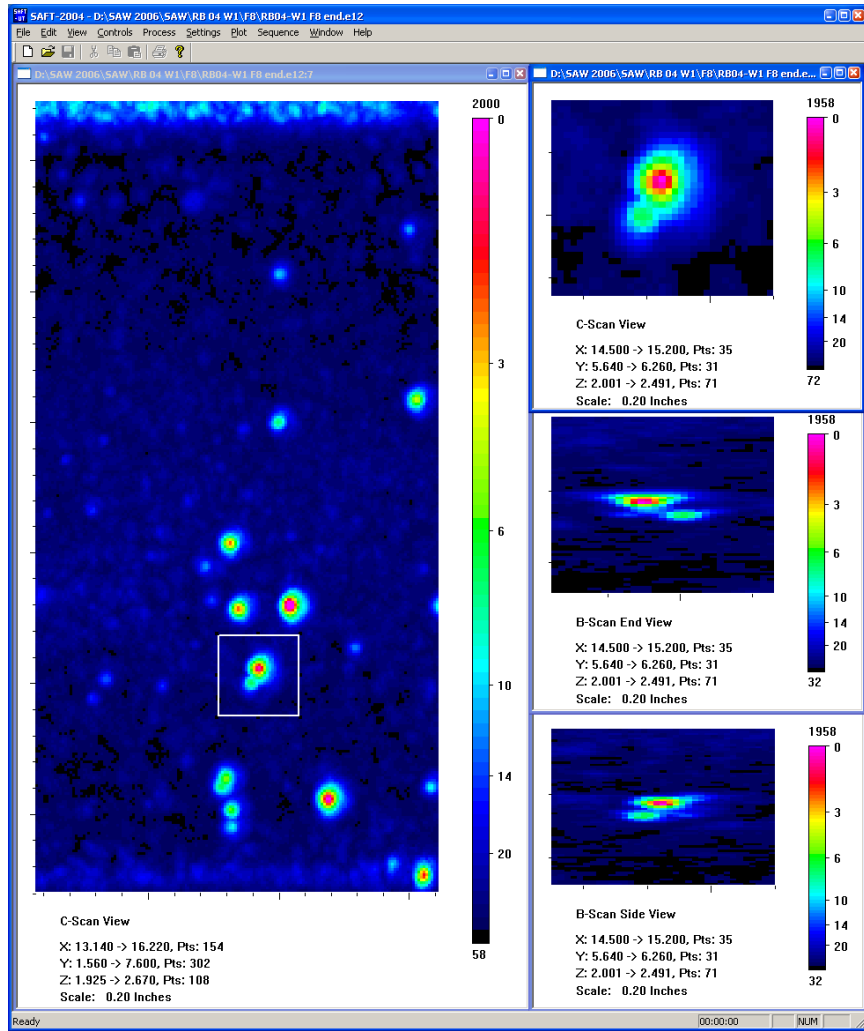**Figure 2.6 F8 Immersion Testing Images of Small Fabrication Flaw:** *RB04-5.5*
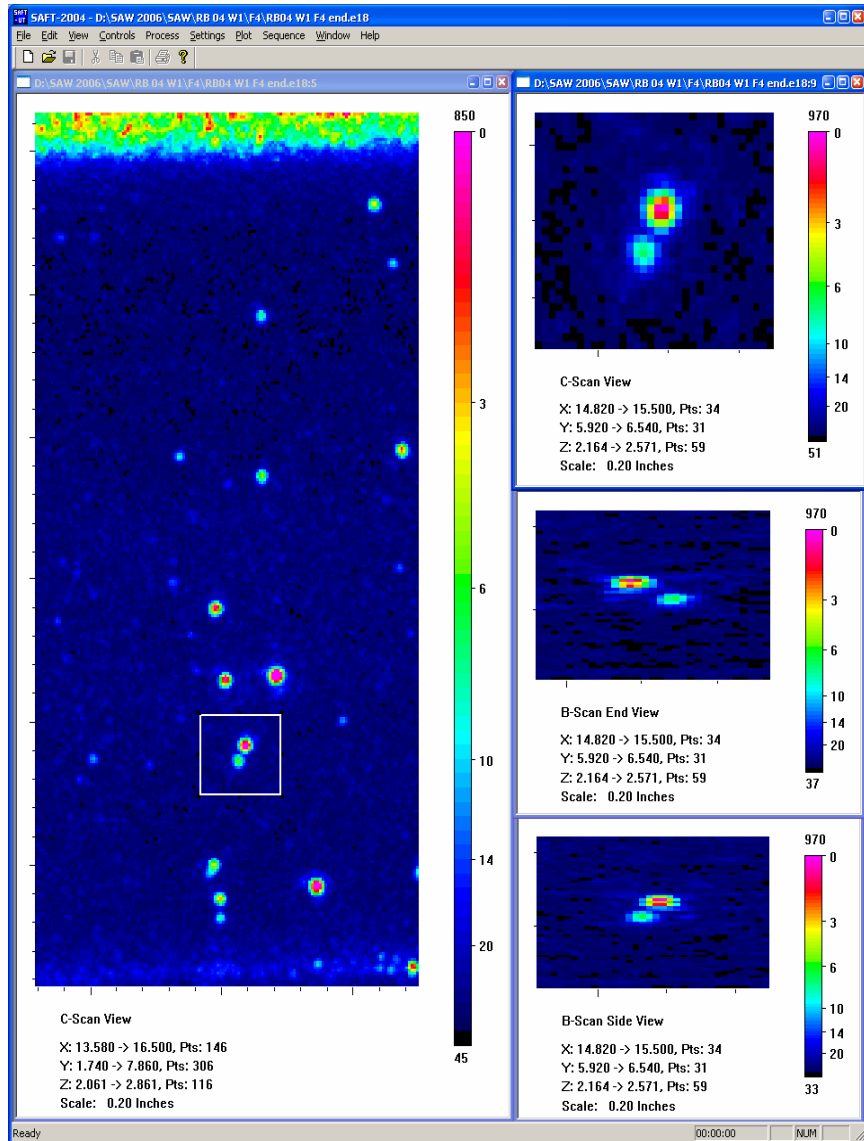
Figure 2.7 F4 Immersion Testing Images of Small Fabrication Flaw: *RB04-5.5*
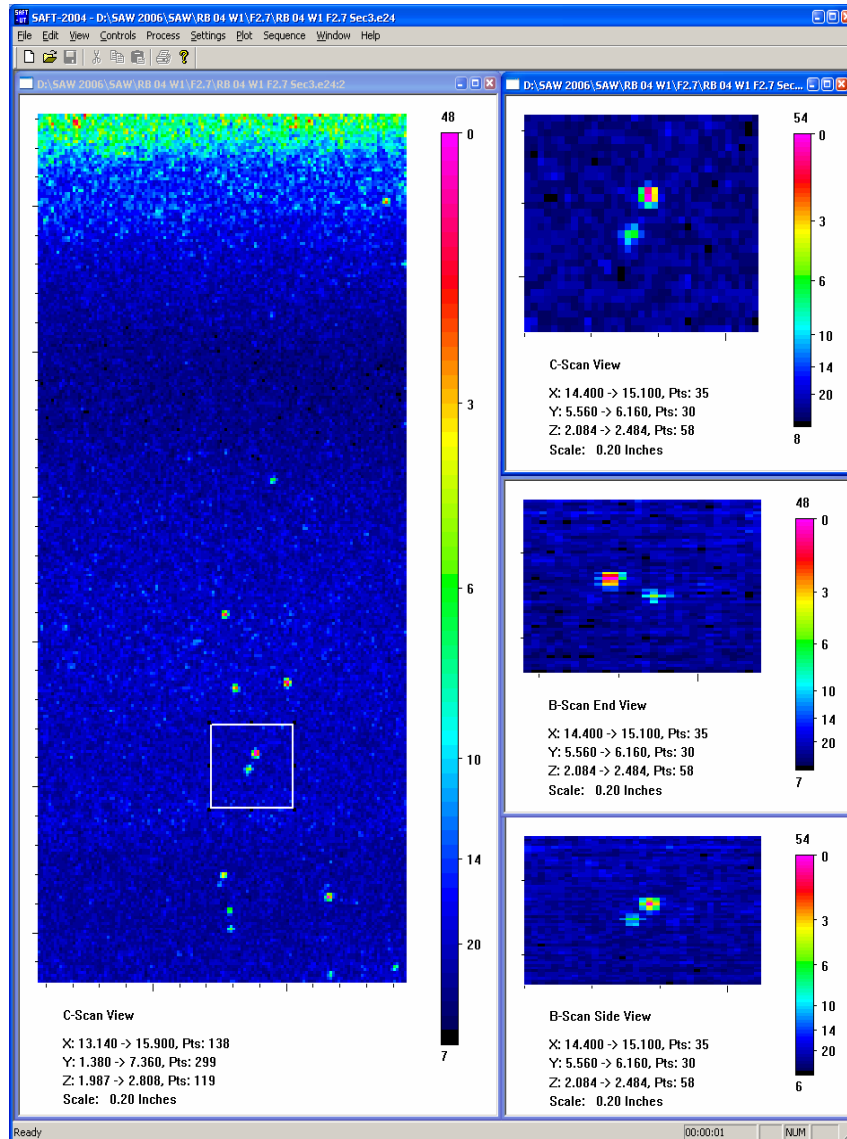
Figure 2.8 F2.7 Immersion Testing Images of Small Fabrication Flaw: *RB04-5.5*

Figure 2.9 Photo of Weld Cross Section Plates from the PVRUF Vessel
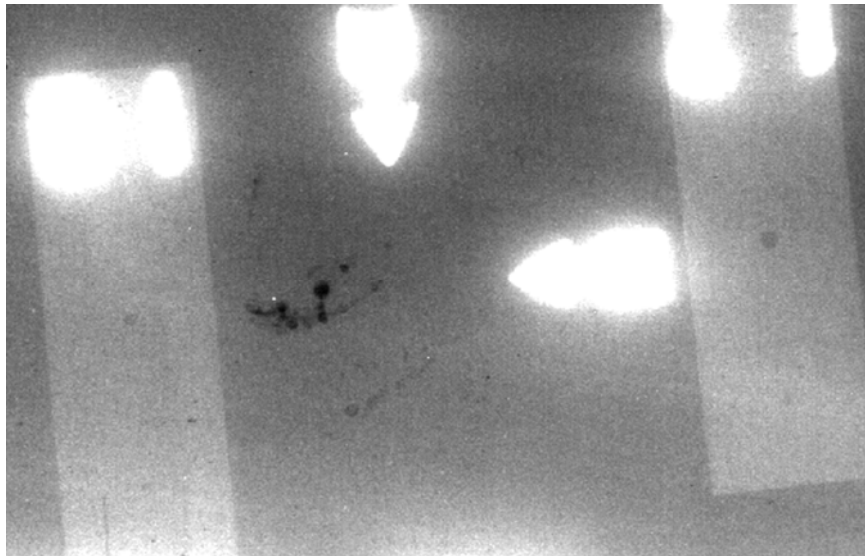
Figure 2.10 Image of Fabrication Flaw Using Film Radiography
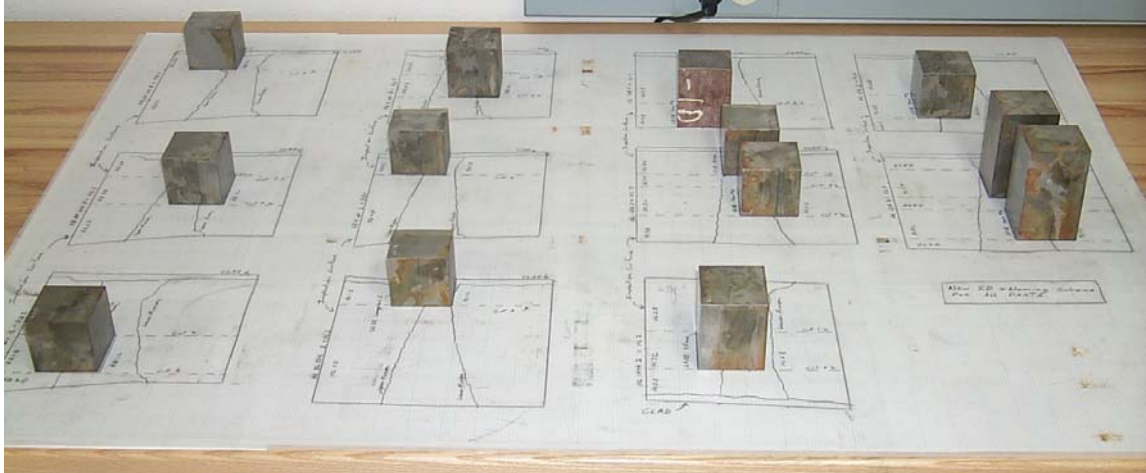
Figure 2.11 Cubes Containing the Largest Flaws from the SAW of River Bend Unit 2 and Hope Creek Unit 2 RPVs
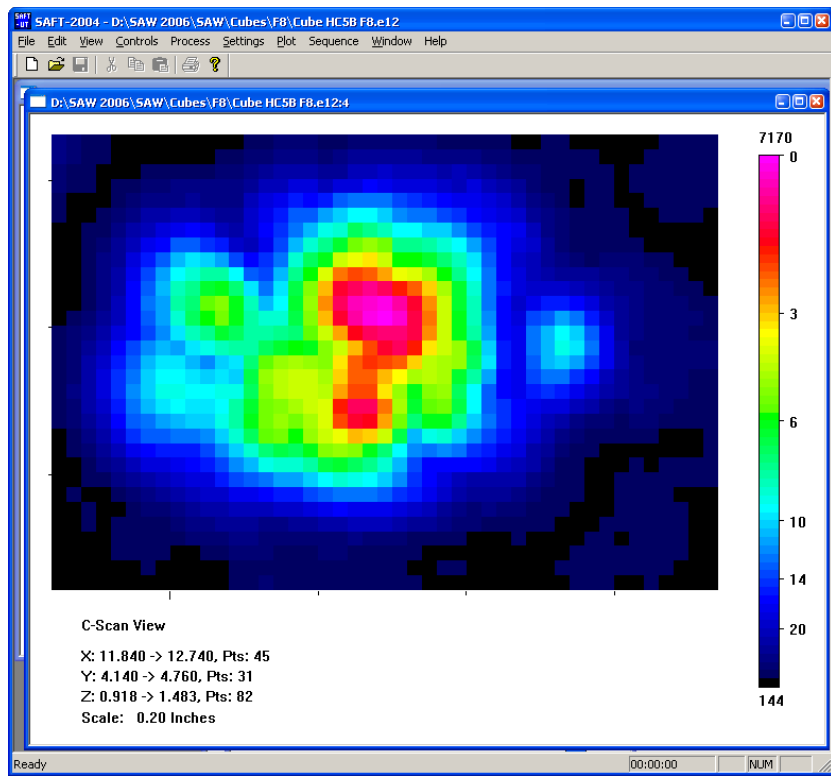
Figure 2.12 F8 Immersion UT of Fabrication Flaw in Cube: *HC5B*
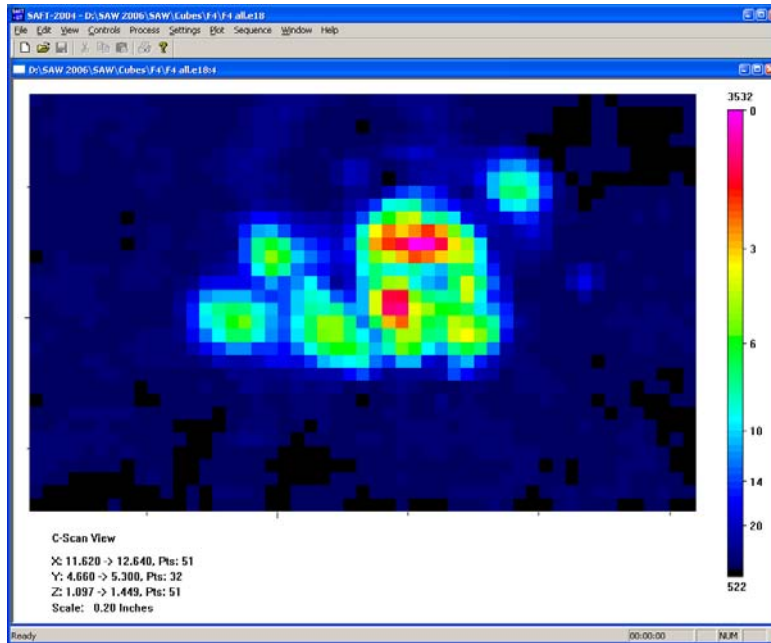
Figure 2.13 F4 Immersion UT of Fabrication Flaw in Cube: *HC5B*
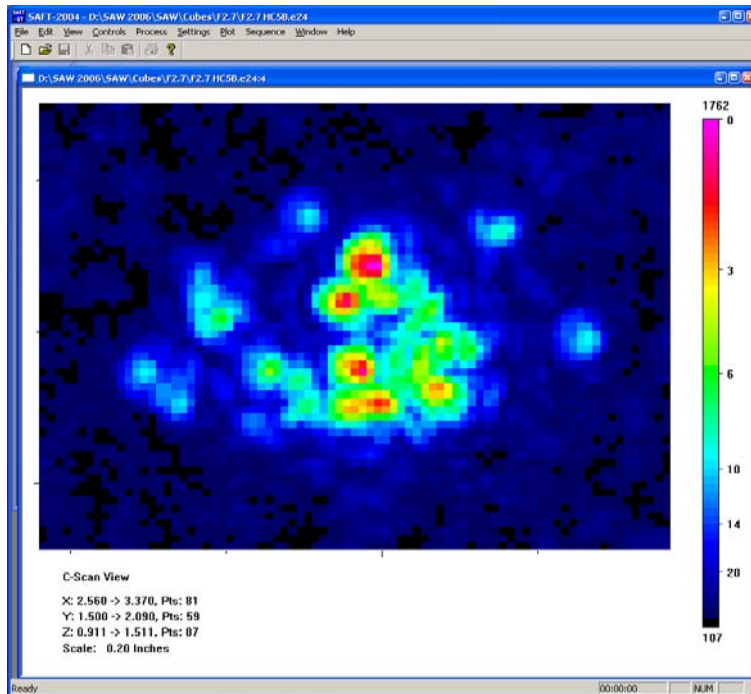
Figure 2.14 F2.7 Immersion UT of Fabrication Flaw in Cube: *HC5B*

2.13
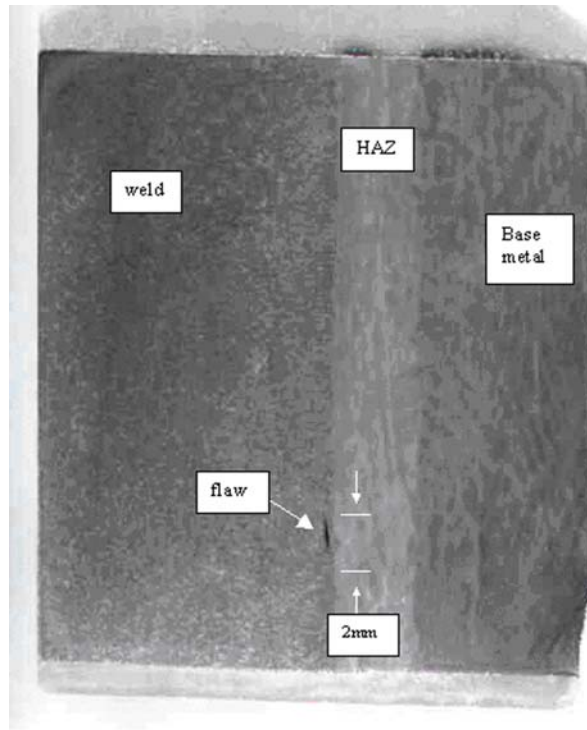
Figure 2.15 Metallograph of Flaw in the Fusion Zone of a Weld with the Base Metal
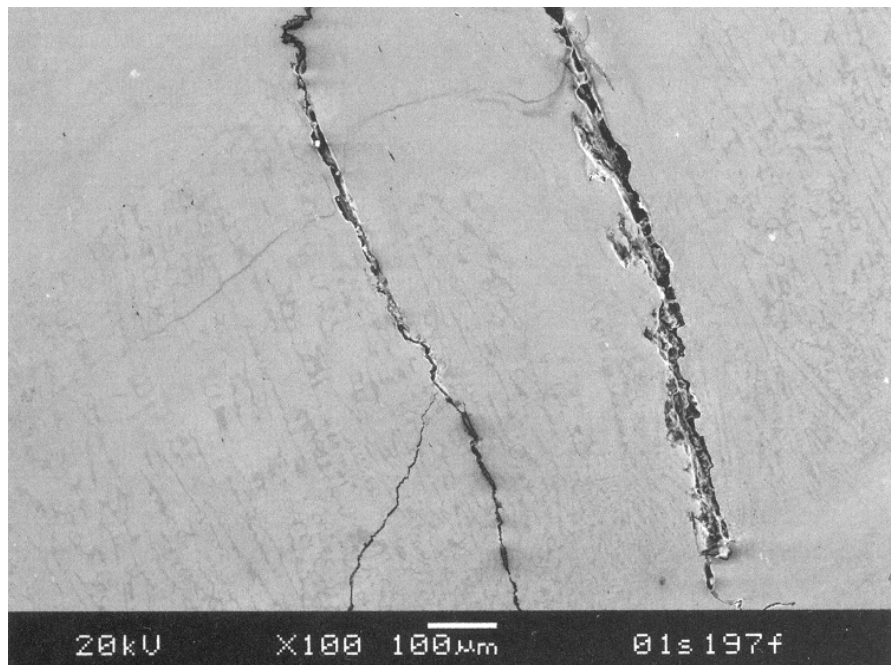
Figure 2.16 Electron Microscope Image of Cracked Weld Bead in PVRUF Vessel

3. High Resolution SAFT-UT

Because it is an important part and key step of the validation process for fabrication flaw density and distribution, this section discusses the implementation and application of ultrasonic imaging for sub-wavelength resolution on clusters of fabrication flaws. Work on the SAFT algorithm is reported that produced an improvement of three orders of magnitude in processing times. High-resolution reconstructions that took more than a day could now be completed in under a minute. This report shows how SAFT-UT images can now resolve closely spaced small flaws and more accurately size them as well. Ultrasonic imaging systems that can distinguish two objects that are separated by less than a wavelength of the ultrasound can be said to provide high-resolution images. SAFT systems have been proposed for this purpose over the years (Frederick 1979).

In the past it was argued that SAFT can provide the needed imaging for characterizing flaws in reactor pressure vessels. Generating images with sub-wavelength resolution for the vessel thickness has been the objective. The lateral resolution of a SAFT system is determined by the maxima of two separate resolution elements—the transducer's and the synthetic aperture's. In most ultrasonic applications of synthetic aperture focusing, the system resolution will be no better than the resolving power of the transducer that is used (Busse et al. 1984). In field applications of synthetic aperture focusing for NDE of welded assemblies, flat elements are used for reasons of mechanical simplicity that arise from having the element contact and follow the metal surface. For flat elements, the lateral spatial resolution is just half the diameter of the element (Schmitz 2002) and is independent of wavelength. Small contact probes, used in synthetic aperture focusing applications, typically have a 6-mm diameter that limits the system resolution to 3 mm.

Field inspections conducted with industrial systems generally use flat ultrasonic elements. In the laboratory, the use of spherical (focused) elements in ultrasonic imaging systems is widespread. For spherical elements, the transducer lateral resolution, ΔX_t, is given by

$$\Delta X_t = 1.22 \lambda_c f_L / A_t \tag{3.1}$$

where λ_c is the wavelength in the coupling material, f_L is the focal length of the transducer, A_t is the transducer aperture, and the factor of 1.22 comes from the first zero crossing of a Bessel function (Goodman 1996).

Synthetic aperture focusing permits the synthetic lens size to be chosen after the data are taken. For data processing, it is usually the intent to produce an image with shift-invariant resolution. To do this, the lens diameter is allowed to increase linearly with depth during data processing. The synthetic aperture angle, θ, describes this increasing lens diameter, and the synthetic aperture lateral resolution, ΔX_s, is given by

$$\Delta X_s = \lambda_m / 4 \tan \theta \tag{3.2}$$

where λ_m = wavelength in the metal.

Figure 3.1 is a graph of the theoretical lateral resolution for images of reflectors in carbon steel. The graph shows the synthetic aperture resolution, using Eq. (3.1), and probe resolution, using Eq. (3.2), plotted against the aperture angle and how the resolution can approach the diffraction limit of half a wavelength.
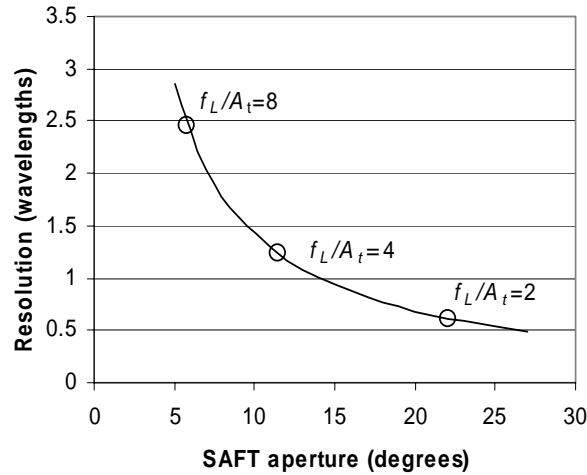
Figure 3.1 Lateral Resolution in Wavelengths

The computational complexity of the SAFT reconstruction has limited its application in the field. Initial progress with the SAFT algorithm involved lookup tables that were calculated before the focusing of the inspection volume started so that it eliminated the unnecessary repetitive calculation of temporal shifts (Ganapathy et al. 1983). In that work, the inner loop of the SAFT algorithm used a list of off-center sample positions in the synthetic aperture to fetch the temporal shift and accumulate ultrasonic responses.

The time for one iteration through the inner loop, τ, has been the limiting parameter for SAFT implementations. Some historic values for τ are given in Table 3.1. The first two values for τ in the table are taken from Ganapathy et al. (1983). They are representative of the work in the early 1980s. The third value is from PNNL's work on a SAFT real-time processor (Doctor et al. 1987). The last value is from work on a modified SAFT algorithm reported by Schuster et al. (2004).

Table 3.1 Historic SAFT Inner Loop Performance for Various Processors

Processor	T (microseconds)
D.E.C. VAX 11/780	5.5
CRAY-1	0.1
SAFT RTP (16 processors)	1.3
DELL 650 Workstation	0.001

As a part of the development, a 1-mm flat bottom hole was scanned and imaged in the qualification process for the modified SAFT algorithm. The scan used 0.25-mm lateral step sizes and produced a 200 megabyte file. The ultrasonic transducer was a spherically focused 10 MHz with a focal length of 50 mm and a diameter of 19 mm (F2.7). A SAFT system with such a transducer should be able to resolve flaws that are separated by 0.8 wavelengths or 0.5 mm. Table 3.2 reports the SAFT processing time for the 200 megabyte file on the 1-mm flat bottom hole using a DELL 650 workstation with a 3.06 GHz Pentium 4.

Table 3.2 Example of Completion Times for SAFT Reconstruction. The SAFT-UT images in this report all used 100% lens sampling.

Algorithm	Lens sampling (percent)	Time (hr:min:sec)	Sums per Voxel	Noise (counts)	Signal (counts)
By Aperture List	100	36:00:00	81729	23	725
By Cross Section	100	21:01	81729	23	743
By Cross Section	25	6:21	20432	41	739
By Cross Section	11	3:21	8990	58	769
By Cross Section	6	2:13	4904	78	694
By Cross Section	4	1:34	3269	96	714
By Cross Section	3	1:13	2452	116	767
By Cross Section	2	0:59	1635	127	712

In Table 3.2 the first row reports the time to process the file, 36 hours, for the "by aperture list" algorithm. This is the computing solution where the inner loop of the SAFT algorithm used a list of off-center sample positions in the synthetic aperture to fetch the temporal shift and accumulate ultrasonic responses. For more information on the "By Aperture List" algorithm see Ganapathy (1983). The focusing to achieve the 0.5-mm resolution required that 82,000 summations be performed per volume element (voxel) and the file had 1 million voxels.

The second line in Table 3.2 reports the results from a modified SAFT algorithm that completed the processing in 21 minutes, which is a factor of 100 improvement over "By Aperture List." The high-performance solution to the SAFT problem is obtained by minimizing the address change in the data to achieve the focusing (Schuster 2004). Instead of focusing a voxel to completion, a vector of accumulators, $\vec{s}$, can be used to sum vectors of coherent ultrasonic responses

$$\vec{s'} = \vec{s} + \vec{r^c} \qquad (3.3)$$

The vector equation forms the inner loop of the computation and the address change is 8 bytes if 32-bit integers are used. A cross section of accumulators can be used, in a similar fashion, while keeping the address change to a minimum. The solution, "By Cross Section", is fully described in Schuster et al. (2004).

Lens sampling can be used to achieve another factor of 10 or more improvement in processing time. In lens sampling, every n-1 summations are skipped in both lateral directions. So if n is set to two, every other summation is skipped in both directions and only 25% of the summations are performed – 20,432 of them as shown on the third line in Table 3.2. A 2% lens sampling finishes the test calculation in about 1 minute. It should be noted that the 6 dB drop size of the 1-mm flat bottom hole remained the same for all of the cases reported in the table – 1 mm. Of course, the average signal, about 700 counts, does not change as the sampling percentage changes because the average is performed over the same lens size. Figure 3.2 shows the signal-to-noise dependency on sums per voxel using the lens sampling algorithm described above. The dependency is fit with a power law function and the power is approximately the square root of the sums per voxel as expected.

The equation shown on the figure is:

$$y = 0.1885x^{0.4577}$$
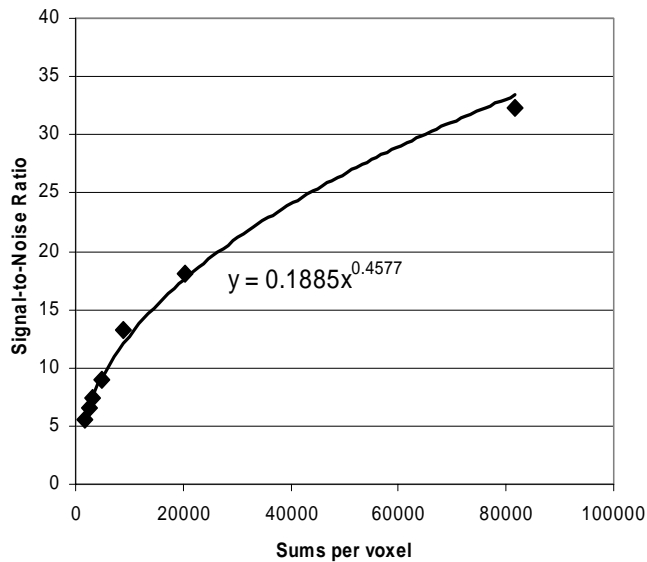
Figure 3.2 Signal-to-Noise and Sizing Performance for Lens Sampling

Sizing performance can be seen in Figure 3.3 for dual F2.7 (18 mm diameter and 50 mm focal length) transducers at 10 MHz operating in a pitch/catch mode. The steel test piece contained 1 to 8-mm diameter flat bottom holes. The results shown in Figure 3.3 required 10^5 summations per volume element. The open circles are results from using a 6-mm-diameter flat transducer in contact with the inspection sample. The error bars represent the 0.25-mm step size used for data acquisition.

Figure 3.3   Sizing Performance for Immersion F2.7 Transducer versus a 6-mm Flat Transducer in Contact with Test Specimen Containing Flat-Bottom Holes

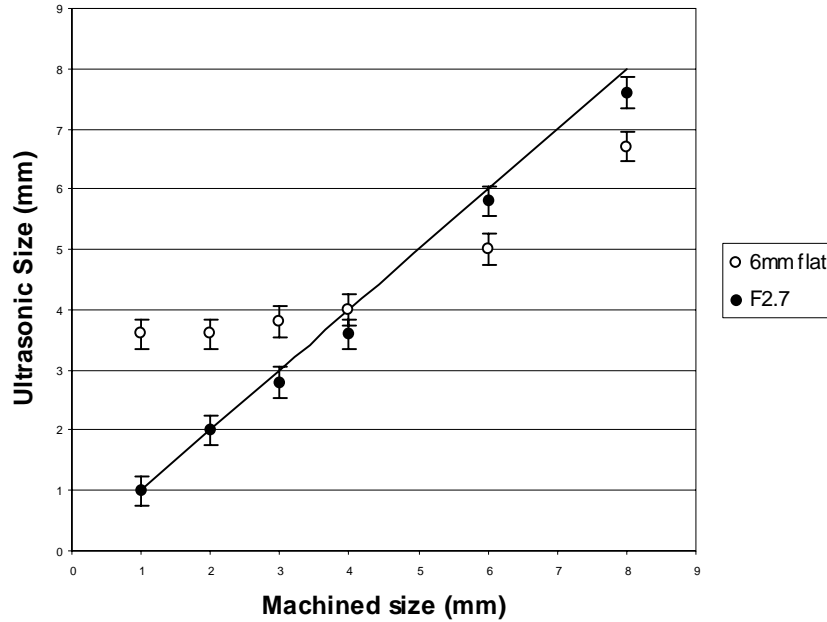The data shown in Table 3.2 and Figure 3.2 are generated from the 1-mm flat-bottom-hole response. The worst signal-to-noise value of 5.6 is from the 2% lens sampling case. Therefore, the signal-to-noise value is 5.6 (15 dB) or better for the 1-mm flat-bottom hole. Typically in flaw detection a signal-to-noise ratio (SNR) of 2 (6 dB) or better is required. The fabrication flaw data, for example in Appendix A, shows a SNR of approximately 5 (14 dB) or better except in the near-surface region where either cladding effects are detected or the near-field effects of the transducer add noise.

For further clarification, the SNR is typically used in the detection mode and a SNR of 2 or better is necessary. In the sizing mode, a flaw response is typically length-sized based on an amplitude drop or loss and for the weld-normal inspections the through-wall extent of the flaw is a length-sizing type of measurement so the same criteria is used. Either a loss of 6 dB (half amplitude) or a total loss of signal level (i.e., where the flaw response fades into the background noise level) is used.

4. Submerged Arc Weld Product Form in Reactor Pressure Vessels

Materials from four different reactor pressure vessels were selected for study. The major component manufacturers and the major reactor designs were considered in the selection of these materials. Table 4.1 gives the years of manufacture, manufacturer, and the orientation of weld seams for the vessels examined. Descriptions of the source of the welds are provided in this section. All four of these vessels were manufactured using A533B plates.

Table 4.1 Weld Material Evaluated to Generate Data on Flaw Rates

Cancelled Plant	Manufacturer	Reactor Type	Years of Construction	Seam Weld Orientations Inspected
Shoreham	CE	BWR	1968 to 1974	Axial and circumferential
Hope Creek Unit 2	CB&I	BWR	1971 to 1975	Axial and circumferential
River Bend Unit 2	CB&I	BWR	1974 to 1978	Circumferential
PVRUF Vessel	CE	PWR	1976 to 1981	Circumferential

The Shoreham vessel was assembled by Combustion Engineering in the years 1968–1974. The vessel was installed at the Shoreham Nuclear Power Station, and the BWR plant was made fully operational but did not produce electricity. When the plant was decommissioned, Baltimore Gas & Electric Company (BGE) purchased portions of the Shoreham reactor vessel, specifically the upper 5 m of the vessel plus portions of the top and bottom heads. This material includes the vessel flange, the upper shell course containing the steam outlet nozzles, and a portion of the upper-intermediate shell course. A total of about 25 m of weld was inspected.

Material from the Hope Creek Unit 2 RPV was from a BWR design. The base metal is A533B bent plate, 15 cm thick. The specimen contained a circumferential seam weld and an axial seam weld for a total of 2.3 m of weld. The inspection of the welds in the PNNL specimen from the Hope Creek Unit 2 RPV was conducted from a cut and machined surface.

PNNL acquired 15 m of girth weld from the River Bend Unit 2 reactor pressure vessel. Chicago Bridge & Iron manufactured the vessel for the River Bend Nuclear Plane Unit 2. Unit 2 was a BWR 6 design but was cancelled. The vessel was dismantled in 1996. The PNNL weld specimens contained a portion of a circumferential seam weld.

The PVRUF pressure vessel was assembled by Combustion Engineering in the years 1976 through 1981 for a nuclear power plant that was cancelled. The pressure vessel was 4.39 m in diameter, 13.34 m high, and made of A533B material. The wall thickness varies from one region to the next, but within 25 cm of the beltline weld it was 22 cm thick. PNNL inspected about 20 m of weldment at Oak Ridge National Laboratory but only 15 m was cut out and provided to PNNL for further studies.

A cross section of an examined circumferential weld of the PVRUF Vessel is shown in Figure 4.1. The cladding is shown at the bottom of the figure as the dark region below the notation in the figure denoting the first 4 to 5 layers of weld passes. This 1.6-cm deep region near the vessel ID is filled with shielded metal arc weld metal that was manually applied. The remainder of the weld is filled with submerged arc weld metal that was machine made. The macro etch was made at PNNL and provides sufficient detail to allow the weld passes to be counted and sized.
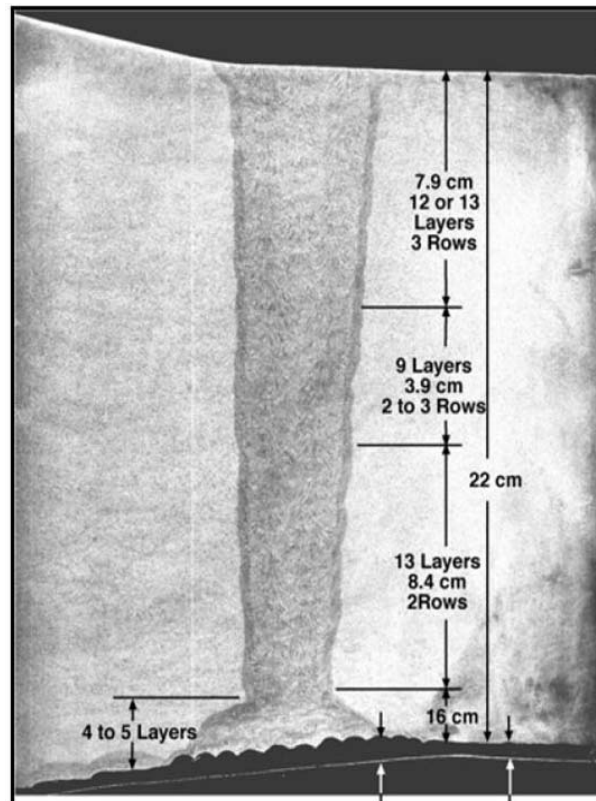

Figure 4.1 Metallographic Cross Section of a Circumferential Weld from PVRUF Vessel Showing Adjacent Regions of Base Metal and Cladding

Table 4.2 shows the amount of material inspected and analyzed in the specimens including those from Hope Creek Unit 2 and River Bend Unit 2 Reactor Pressure Vessels. The six fusion zone amounts are given as areas with units of square meters. The side-wall planes are the surfaces of the base metal with the weld metal and run the length of the weld following the weld profile. The inter-run planes are the surfaces between the weld passes and run vertically or horizontally along and within the weld.

A discussion of the product forms in the U.S. operating reactors can be found in Jackson and Abramson (2000). The report discusses field vs. shop fabrication, weld procedure, and other topics that affected flaw rates. Appendix A in that report lists the welding and cladding processes for domestic reactor pressure vessels.

Table 4.2 Inspection Volumes and Areas for SAW Product Form

Vessel	Fusion Zone	Surface Area (m^2)
Shoreham	side-wall	7.1
Hope Creek Unit 2	side-wall	0.34
Hope Creek Unit 2	inter-run	1.3
River Bend Unit 2	side-wall	3.7
River Bend Unit 2	inter-run	14.7
PVRUF, thin plates	side-wall	0.30

NUREG/CR-6471, Volume 3 provides all of the detailed work that was conducted on the fabrication flaws located in the welds from the Shoreham vessel. Section 6 of that report addresses the comparison of fabrication flaws in axial and circumferential welds. It was shown that the results were very similar for both weld orientations and this forms the basis for using the developed distributions for both axial and circumferential welds.

5. Measurement Sequences and Validated Flaw Rates for SAW

This section reports the sequences in measurements used on the weldments from the four vessels examined. The inspection, detection, analysis, and validation process evolved as the work progressed principally for two reasons: to take advantage of new knowledge about the flaws and because of improvement in the measurement methods. Validated flaw rates are given in this section for the submerged arc weld in the four vessels. A separate analysis is presented for side-wall lack of fusion and inter-run lack of fusion.

5.1 Sequences of Measurements for Estimating Flaw Density and Distribution

Table 5.1 provides a sequential list of the measurement methods for fabrication flaw density and size distribution. The table defines a numbering system for the measurement methods on components and inspection surfaces. Figure 5.1 shows the PVRUF vessel measurement sequence. Documenting the measurement methods and their deployment in sequences is the purpose of this NUREG/CR report. The sequence used on the PVRUF fabrication flaws started with the SAFT-UT inspections from the inside, clad surface of the vessel.

Figure 5.2 shows the Shoreham vessel measurement sequence. The sequence used on the Shoreham vessel fabrication flaws did not have SAFT-UT inspections from the inside, clad surface of the vessel. The weld normal inspections provided much better and more reliable detection data to insure that all flaws with through wall sizes of interest were reliably detected and as a result the clad inspections were not used further (this was based on the PVRUF experience). Measurement with film radiography was also not made because once the ultrasonic responses were understood to be from real weld discontinuities in the fusion zone of the weld with the side wall of the base metal (based on PVRUF validated results), the need for confirmatory film radiography was determined to not be needed since it added no new information.

Figure 5.3 shows the River Bend Unit 2 and Hope Creek Unit 2 vessel measurement sequence. The sequence used on the River Bend Unit 2 and Hope Creek Unit 2 vessels is the same as that for the Shoreham vessel except for the addition of immersion UT on small weld segments less than 500 lbs. The progress on high resolution SAFT-UT, reported in Section 3, allowed more accurate characterization of clusters of small flaws.

In summary, examination from the clad surface could be discontinued because weld-normal UT could detect and characterize all the flaws with a very high sensitivity and high SNR. Film radiography could be discontinued once the flaw indications were understood as lack of fusion in the side wall of the weld with the base metal. Higher-resolution SAFT-UT was useful once flaw clusters were expected. The inspection process changed over time because of these lessons learned on how to conduct the work. Although some of the measurements were determined to be redundant, the process always had closure in the sense that there should be no surprises in flaws selected for destructive testing and the best UT sizing data. If there would have been surprises during the destructive testing, then complementary NDE such as radiography would have been added back into the process.

Table 5.1 Summary of Measurement Methods for Fabrication Flaw Density and Size Distribution

Measurement Sequence No.	Component Shape or Description	Inspection Surface	Measurement
1	Vessel (whole)	Clad surface	Contact Ultrasound
2	Large weld segments (greater than 500 lbs.)	Cut face parallel to weld	Contact Ultrasound
3	Small weld segments (less than 500 lbs.)	Cut face parallel to weld	Immersion UT
4	Plates (25-mm thick)	Weld cross section	Film Radiography
5A	Cube	Parallel to flaw	Immersion UT
5B	Cube	Perpendicular to flaw	Film Radiography
5C	Cube	Four faces around flaw	X-Ray CT
6A	Cube face	Perpendicular to flaw	Metallography
6B	Cube face	Perpendicular to flaw	Electron Microscopy
6C	Cube face	Perpendicular to flaw	X-Ray spectroscopy

5.2   Validated Flaw Rates for SAW

Validated flaw density and distribution was estimated for the side-wall lack of fusion for four vessels: Shoreham, Hope Creek Unit 2, River Bend Unit 2, and PVRUF. Validated flaw density and distribution is provided for inter-run lack of fusion in the submerged arc weld for Hope Creek Unit 2 and River Bend Unit 2.

Tables 5.2 through 5.7 document the validated size distribution for flaws in submerged arc weld. The cumulative frequency is the number of flaws greater than or equal to the size given at the top of columns in the tables. The density is the cumulative frequency divided by the amount of material inspected from Table 4.2.

Figure 5.4 shows the flaw density and distribution in the side-wall and inter-run fusion zones of the submerged arc weld of specimens removed from Hope Creek Unit 2 and River Bend Unit 2 reactor pressure vessels. For flaws greater than or equal to 5 mm, there are 10 times more flaws per unit area of fusion zone for side-wall compared to inter-run lack of fusion.

Figure 5.5 compares the flaw density and distribution for the side-wall lack of fusion for the four vessels. Table 5.8 gives the parametric fit results for the un-validated through-wall size distributions for fabrication flaws in the weld specimens removed from the four vessels. An exponential fit was performed where x is the through-wall size in mm, y is the flaw density as a function of through-wall size, and α and β are the fit parameters given in the table.

The Combustion Engineering (CE) vessels, Shoreham and PVRUF, have a similar through-wall size dependence and a factor of three difference in overall density. The vessels by Chicago Bridge and Iron do not share the same through-wall size dependence as the vessels by CE. The slope is much greater as show, in the figure. For flaws greater than 4 mm, the cumulative flaw density is a factor of 10 less for River Bend Unit 2 than for Hope Creek Unit 2 showing the change in flaw rate over the years on vessel construction.

Table 5.2 Size Distribution of Small Flaws in the SAW of the PVRUF Vessel

Through-Wall Dimension	1 mm	1.5 mm	2 mm	2.5 mm	3 mm	3.5 mm	4 mm
Frequency	8	12	9	1	4	2	1
Cum. Freq.	37	29	17	8	7	3	1
Density(m^{-2})	123	97	57	27	23	10	3

Table 5.3 Size Distribution of Flaws in the SAW of the Shoreham Vessel

Through-Wall Dimension	<3.5 mm	4 mm	5 mm	6 mm
Frequency	8	12	9	1
Cum. Freq.	30	22	10	1
Density (m^{-2})	535.2	17.2	6.1	1.5

Table 5.4 Size Distribution of Flaws in the Weld Side-Wall of the Hope Creek Unit 2 Vessel

Through-Wall Dimension	<2.5 mm	3 mm	3.5 mm	4 mm	4.5 mm	5 mm	5.5 mm	6 mm
Frequency	19	350	180	20	8	3	1	3
Cum. Freq.	584	565	215	35	15	7	4	3
Density (m^{-2})	1711	1655	630	103	44	21	12	9

Table 5.5 Size Distribution of Flaws in the Weld Inter-Run Planes of the Hope Creek Unit 2 Vessel

Through-Wall Dimension	<2.5 mm	3 mm	3.5 mm	4 mm	4.5 mm
Frequency	17	76	50	9	2
Cum. Freq.	154	137	61	11	2
Density (m^{-2})	118.5	105.4	46.9	8.5	1.5

Table 5.6 Size Distribution of Small Flaws in the SAW of the PVRUF Vessel

Through-Wall Dimension	<2.5 mm	3 mm	3.5 mm	4 mm	4.5 mm	5 mm
Frequency	152	871	596	82	10	5
Cum. Freq.	1716	1564	693	97	15	5
Density (m^{-2})	467.6	426.2	188.8	26.4	4.1	1.4

Table 5.7 Size Distribution of Flaws in the Weld Inter-run Fusion Zone of the River Bend Unit 2 Vessel

Through-Wall Dimension	<2.5 mm	3 mm	3.5 mm	4 mm	4.5 mm	5 mm	5.5 mm
Frequency	99	371	130	10	1	0	1
Cum. Freq.	612	513	142	12	2	1	1
Density (m^{-2})	41.73	34.98	9.68	0.82	0.14	0.07	0.07

Table 5.8 Exponential Fit Results for Through-Wall Size

	Fusion zone	α	β
Shoreham side-wall	Side-wall	1.7 E03 m^{-2}	1.2 mm^{-1}
Hope Creek Unit 2	Side-wall	1.7 E05 m^{-2}	1.7 mm^{-1}
Hope Creek Unit 2	Inter-run	6.6 E05 m^{-2}	2.5 mm^{-1}
River Bend Unit 2	Side-wall	6.1 E04 m^{-2}	2.2 mm^{-1}
River Bend Unit 2	Inter-run	1.3 E05 m^{-2}	2.9 mm^{-1}
PVRUF vessel	Side-wall	5.1 E02 m^{-2}	1.2 mm^{-1}

```
┌─────────────────────┐      start
│ 1. Vessel clad side │       │
│    contact UT       │       │
└─────────────────────┘       │
┌─────────────────────┐       │
│ 2. Large weld       │       │
│    segments         │       │
│    contact UT       │       │
└─────────────────────┘       │
┌─────────────────────┐       │
│ 4. Plates           │       │
│    film radiography │       │
└─────────────────────┘       │
┌─────────────────────┐       │   PVRUF vessel
│ 5A. Cubes           │       │   Measurement
│     immersion UT    │       │   Sequence
└─────────────────────┘       │
┌─────────────────────┐       │
│ 5B. Cubes           │       │
│     film radiography│       │
└─────────────────────┘       │
┌─────────────────────┐       │
│ 5C. Cubes           │       │
│     X-ray CT        │       │
└─────────────────────┘       │
┌─────────────────────┐       │
│ 6A. Cube face       │       │
│     Metallography   │       │
└─────────────────────┘       │
┌─────────────────────┐       │
│ 6B. Cube face       │       │
│     SEM             │       │
└─────────────────────┘       │
┌─────────────────────┐       ▼
│ 6C. Cube face       │      end
│     EDAX            │
└─────────────────────┘
```
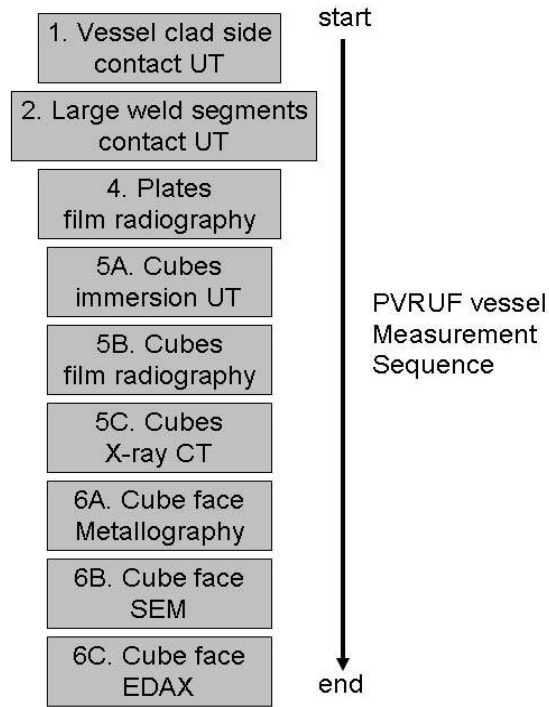
Figure 5.1 PVRUF Vessel Measurement Sequence

```
┌─────────────────────┐      start
│ 2. Large weld       │       │
│    segments         │       │
│    contact UT       │       │
└─────────────────────┘       │
┌─────────────────────┐       │
│ 5A. Cubes           │       │
│     immersion UT    │       │
└─────────────────────┘       │   Shoreham vessel
┌─────────────────────┐       │   Measurement
│ 6A. Cube face       │       │   Sequence
│     Metallography   │       │
└─────────────────────┘       │
┌─────────────────────┐       │
│ 6B. Cube face       │       │
│     SEM             │       │
└─────────────────────┘       │
┌─────────────────────┐       ▼
│ 6C. Cube face       │      end
│     EDAX            │
└─────────────────────┘
```
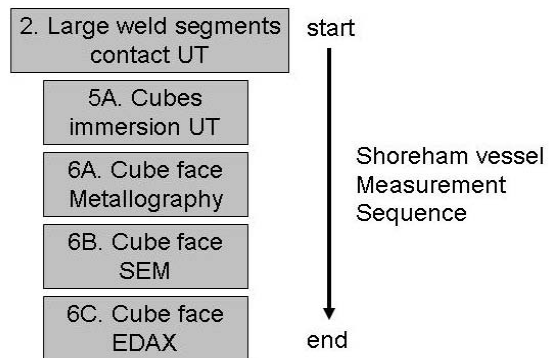
Figure 5.2 Shoreham Vessel Measurement Sequence
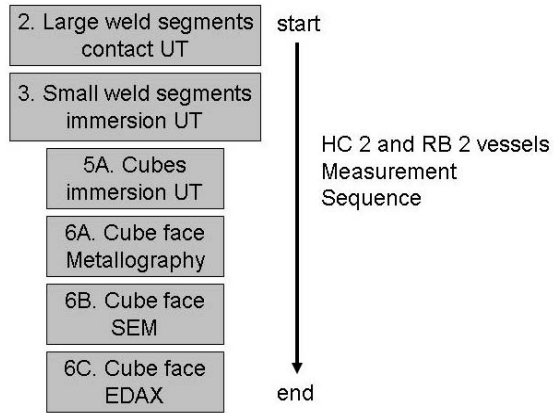
Figure 5.3 River Bend Unit 2 and Hope Creek Unit 2 Vessel Measurement Sequence
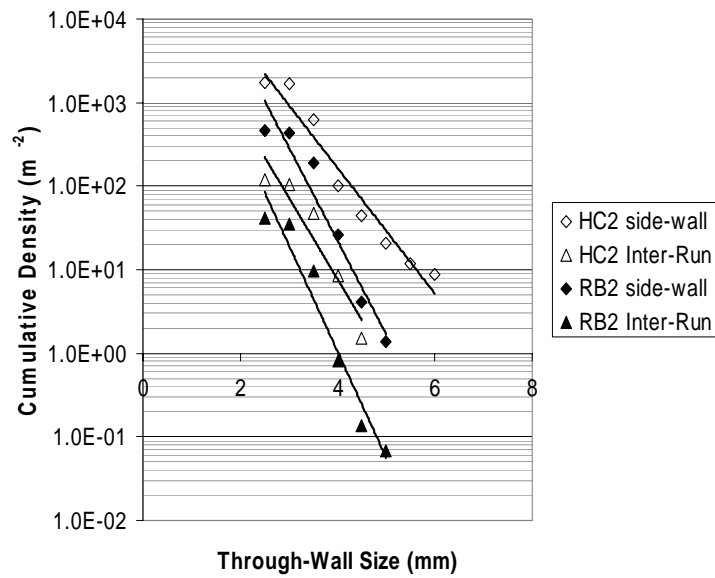
Figure 5.4 Comparison of Through-Wall Size Distribution of Cumulative Flaw Densities for Side-Wall and Inter-Run Fusion Zones
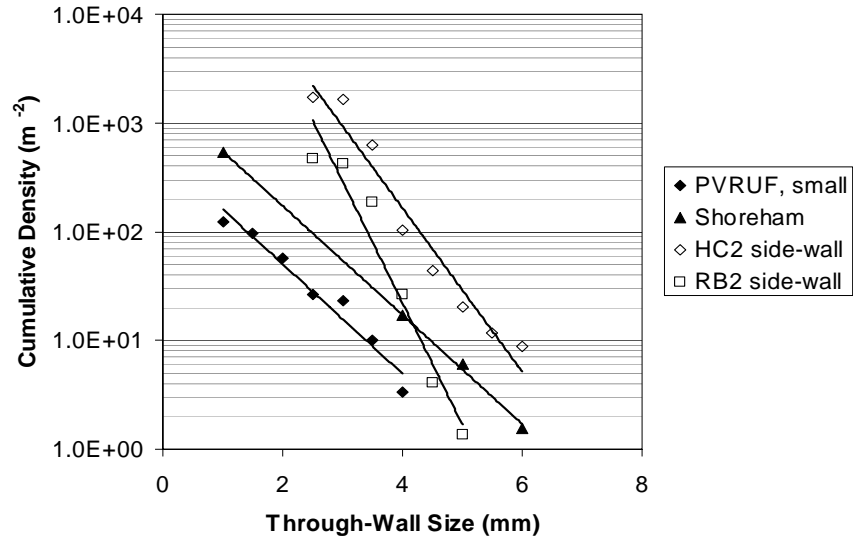
Figure 5.5 Comparison of Through-Wall Size Distribution of Cumulative Flaw Densities for Side-Wall Fusion Zones in SAW

6. Summary

Pacific Northwest National Laboratory found many fabrication flaws in the machine made weld passes, and the data were analyzed for density and distribution. Descriptions of the source of the welds are provided in the report. An estimate of flaw density and distribution was made, and the results for through-wall size distribution are given in Section 5. The Combustion Engineering (CE) vessels, Shoreham and PVRUF, have a similar through-wall size dependence and a factor of three difference in overall density. The vessels by Chicago Bridge and Iron (CB&I) do not share the same through-wall size dependence as the vessels by CE. The slope for the cumulative flaw density vs. size curve is much greater for CB&I vessels compared to CE vessels. For flaws greater than 4 mm, the cumulative flaw density is a factor of 10 less for River Bend Unit 2 than for Hope Creek Unit 2, showing the change in flaw rate over the years of vessel construction.

The report describes the changes in methodology based on lessons learned that was used by PNNL to produce flaw rates. These changes were made to take advantage of PNNL's work on fabrication flaw morphology as it progressed. Flaws in weld segments can now be accurately characterized using high-resolution SAFT-UT. Work on the SAFT algorithm is reported that produced an improvement of three orders of magnitude in processing times. High-resolution reconstructions that previously required greater than 24 hours can now be completed in under a minute. The refined SAFT-UT was shown to resolve closely spaced small flaws and more accurately size them as well.

To address concerns with the fracture behavior of complex flaws in vessel welds such as those that were observed in the vessel repairs, the NRC and PNNL have initiated further study. Factors of concern are flaws with off-axis orientations, interactions of closely spaced flaws, flaws that are only partially crack-like in nature, and flaws along weld fusion lines with compositions and microstructures differing from the adjacent base metal and weld materials. In-service inspection data will be used for estimating fabrication flaw density and distribution in existing nuclear power plant vessels and also to assess the concerns raised relative to repairs.

7.   References

American Society of Mechanical Engineers (ASME). 1998. "Section XI Rules for Inservice Inspection of Nuclear Power Plant Components." In *ASME Boiler and Pressure Vessel Code*. American Society of Mechanical Engineers, New York.

American Welding Society, Inc. (AWS). 1984. *Standard Welding Terms and Definitions*, ANSI/AWS A3.0-85. American Welding Society, Inc., Miami, Florida.

Busse LJ, HD Collins and SR Doctor. 1984. *Review and Discussion of the Development of Synthetic Aperture Focusing Technique for Ultrasonic Testing, SAFT-UT*. NUREG/CR-3625, PNL-4957, U.S. Nuclear Regulatory Commission, Washington, D.C.

Chapman OJV and FA Simonen. 1998. *RR-PRODIGAL – A Model for Estimating the Probabilities of Defects in Reactor Pressure Vessel Welds*. NUREG/CR-5505, PNNL-11898, U.S. Nuclear Regulatory Commission, Washington, D.C.

Dickson TL. 1994. *FAVOR: A Fracture Mechanics Analysis Code for Nuclear Reactor Pressure Vessels, Release 9401*. ORNL/NRC/LTR/94/1, Martin Marietta Energy Systems, Inc., Oak Ridge National Laboratory, Oak Ridge, Tennessee.

Doctor SR, TE Hall, LD Reid, SL Crawford, RJ Littlefield and RW Gilbert. 1987. *Development and Validation of a Real-Time SAFT-UT System for the Inspection of Light Water Reactor Components*. NUREG/CR-4583, PNL-5822, Vol. 2, U.S. Nuclear Regulatory Commission, Washington, D.C.

Doctor SR, GJ Schuster, LD Reid and TE Hall. 1996. *Real-Time 3-D SAFT-UT Evaluation and Validation*. NUREG/CR-6344, PNNL-10571, U.S. Nuclear Regulatory Commission, Washington, D.C.

Doctor SR and GJ Schuster. 2001. "Destructive Validation Methodology and Results for the Characterization of Flaws in Nuclear Reactor Pressure Vessels." Presented to the 3rd International Conference of NDE in Relation to Structural Integrity for Nuclear and Pressurized Components, November 14-16, 2001, Seville, Spain.

Frederick JR, C Vanden Broek, S Ganapathy, M Elzinga, W De Vries, D Papworth and N Hamano. 1979. *Improved Ultrasonic Nondestructive Testing of Pressure Vessels*. NUREG/CR-0909, U.S. Nuclear Regulatory Commission, Washington, D.C.

Ganapathy S, B Schmult, WS Su, N Hamano and D Bristor. 1983. *Investigation of Special Purpose Processors for Real-Time Synthetic Aperture Focusing Techniques for Nondestructive Evaluation of Nuclear Reactor Vessels and Piping Components*. NUREG/CR-2703, U.S. Nuclear Regulatory Commission, Washington, D.C.

Goodman JW. 1996. *Introduction to Fourier Optics*. McGraw-Hill, p. 77.

Jackson DA and L Abramson. 2000. *Report on the Preliminary Results of the Expert Judgment Process for the Development of a Methodology for a Generalized Flaw Size and Distribution for Domestic Reactor Pressure Vessels.* MEB-00-01, PRAB-00-01, U.S. Nuclear Regulatory Commission, Washington, D.C.

Jackson DA, SR Doctor, GJ Schuster and FA Simonen. 2001. "Developing a generalized flaw distribution for reactor pressure vessels." *Nuclear Engineering and Design* **208**:123-131.

Marshall W. 1976. *An Assessment of the Integrity of PWR Pressure Vessels, Summary Report.* Report of a study group under the Chairmanship of Dr. Walter Marshall, CBE FRS, United Kingdom Atomic Energy Authority, London.

Pennel WE. 1989. *Mission Survey for the Pressure Vessel Research Users' Facility (PVRUF).* NUREG/CR-5350, prepared by Oak Ridge National Laboratory, Oak Ridge, Tennessee, for the U.S. Nuclear Regulatory Commission, Washington, D.C.

Schmitz V. 2002. "Nondestructive Acoustic Imaging Techniques, Imaging of Complex Media with Acoustic and Seismic Waves," *Topics in Applied Physics*, **84**:167-189.

Schuster GJ, SR Doctor and PG Heasler. 1998. *Characterization of Flaws in U.S. Reactor Pressure Vessels: Density and Distribution of Flaw Indications in PVRUF.* NUREG/CR-6471, PNNL-11143, Vol. 1, U.S. Nuclear Regulation Commission, Washington, D.C.

Schuster GJ, SR Doctor, SL Crawford and AF Pardini. 1999. *Characterization of Flaws in U.S. Reactor Pressure Vessels: Density and Distribution of Flaw Indications in the Shoreham Vessel.* NUREG/CR-6471, PNNL-11143, Vol. 3, U.S. Nuclear Regulatory Commission, Washington, D.C.

Schuster GJ, SR Doctor, AF Pardini and SL Crawford. 2000. *Characterization of Flaws in U.S. Reactor Pressure Vessels: Validation of Flaw Density and Distribution in the Weld Metal of the PVRUF Vessel.* NUREG/CR-6471, PNNL-11143B, Vol. 2, U.S. Nuclear Regulatory Commission, Washington, D.C.

Schuster GJ, SR Doctor and LJ Bond. 2004. "A System for High-Resolution, Nondestructive, Ultrasonic Imaging of Weld Grains." *IEEE Transactions on Instrumentation and Measurement*, **53**(6):1526-1532.

Simonen FA and MA Khaleel. 1995. "A Model for Predicting Vessel Failure Probabilities Due to Fatigue Crack Growth." In *Pressure Vessel and Piping Conference*. Fatigue and Fracture Mechanics, PVP-Vol. 304, pp. 401-416. American Society of Mechanical Engineers, New York.

Appendix A

Immersion Ultrasound

Appendix A
Immersion Ultrasound

This appendix contains the high resolution ultrasonic images of the largest flaw indications from the un-validated data from the submerged arc weld metal of both the Hope Creek Unit 2 and River Bend Unit 2 vessels. All of the flaw indications reported here are confirmed to be separate small flaws that are less than 2.5 mm in through wall size. Appendix B on metallography confirms the results of this appendix on one flaw for each of the two vessels.

The figures in this appendix show the increasing resolution of the separate small flaws in groups of three images. The figures analyze only one flaw indication that is centered in the white box in the left pane. The flaw outside the box may be saturated and as such appear artificially large. Figure "a" shows F8 data with the lowest resolution. Figure "b" shows intermediate resolution and new and improved sizing results in the figure caption. The last figure in the sequence, Figure "c", gives the high resolution results with final sizes for the separate small flaws.
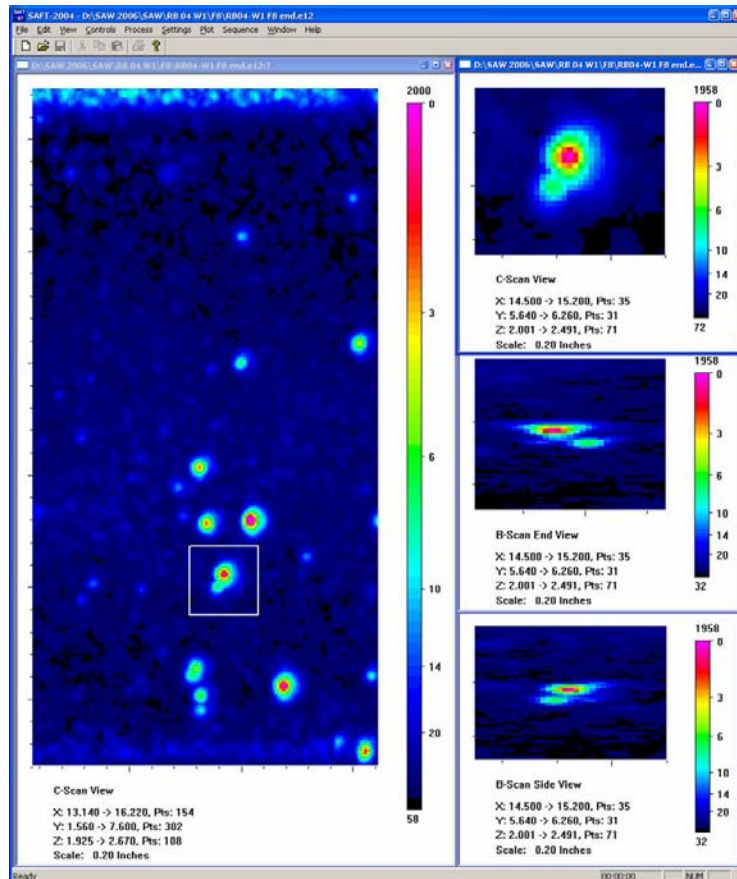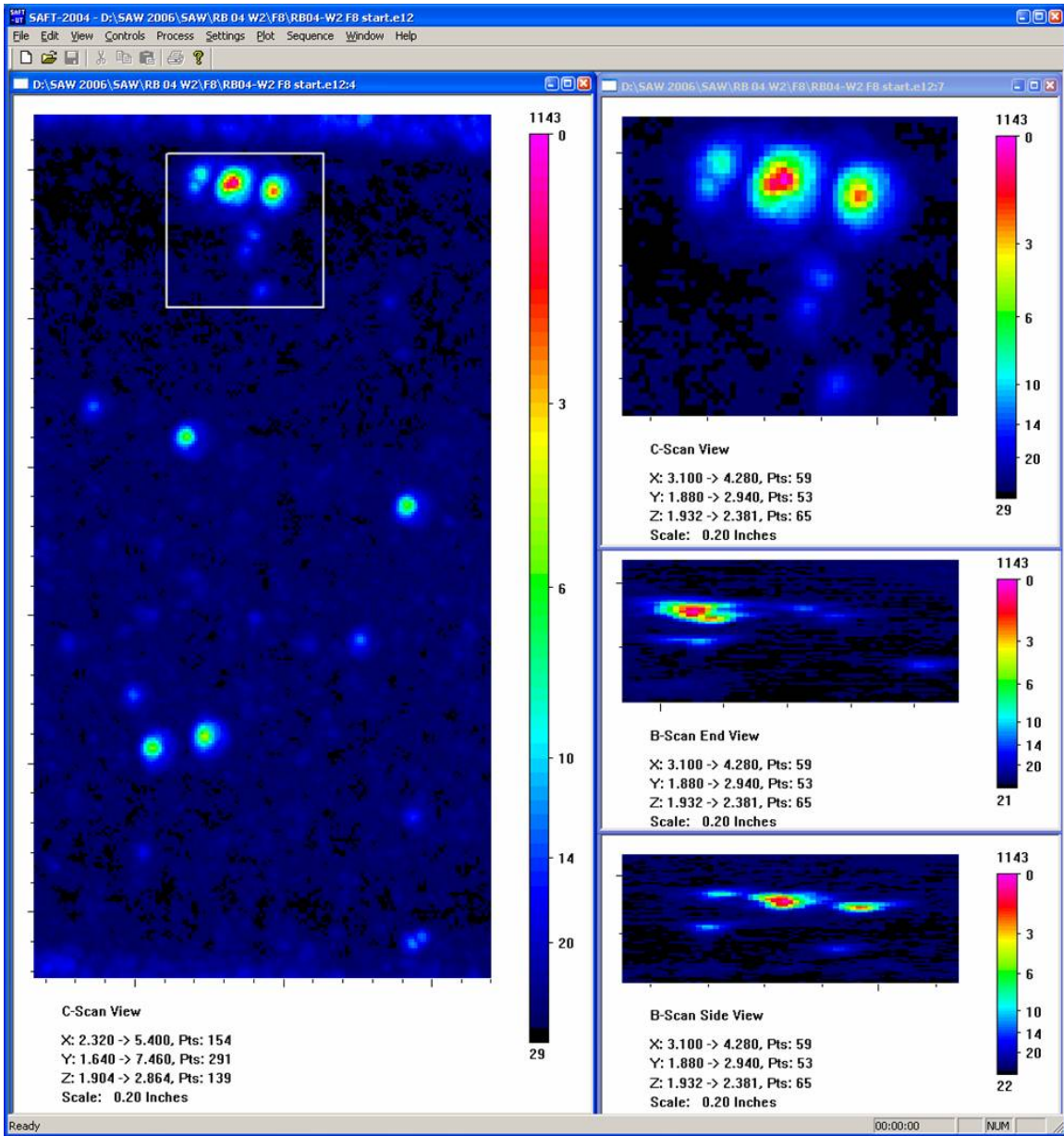

Figure A.1.a 10 MHz F8 Immersion Testing Images of Small Fabrication Flaw: *RB1A*. This figure shows immersion testing data of a 5.5-mm flaw indication from the weld-normal testing of large weld segments. The flaw indication is identified in the box drawn in the SAFT-UT image on the left in the figure. A close up of the flaw in the C-scan view (top right) shows 2 unresolved flaws.
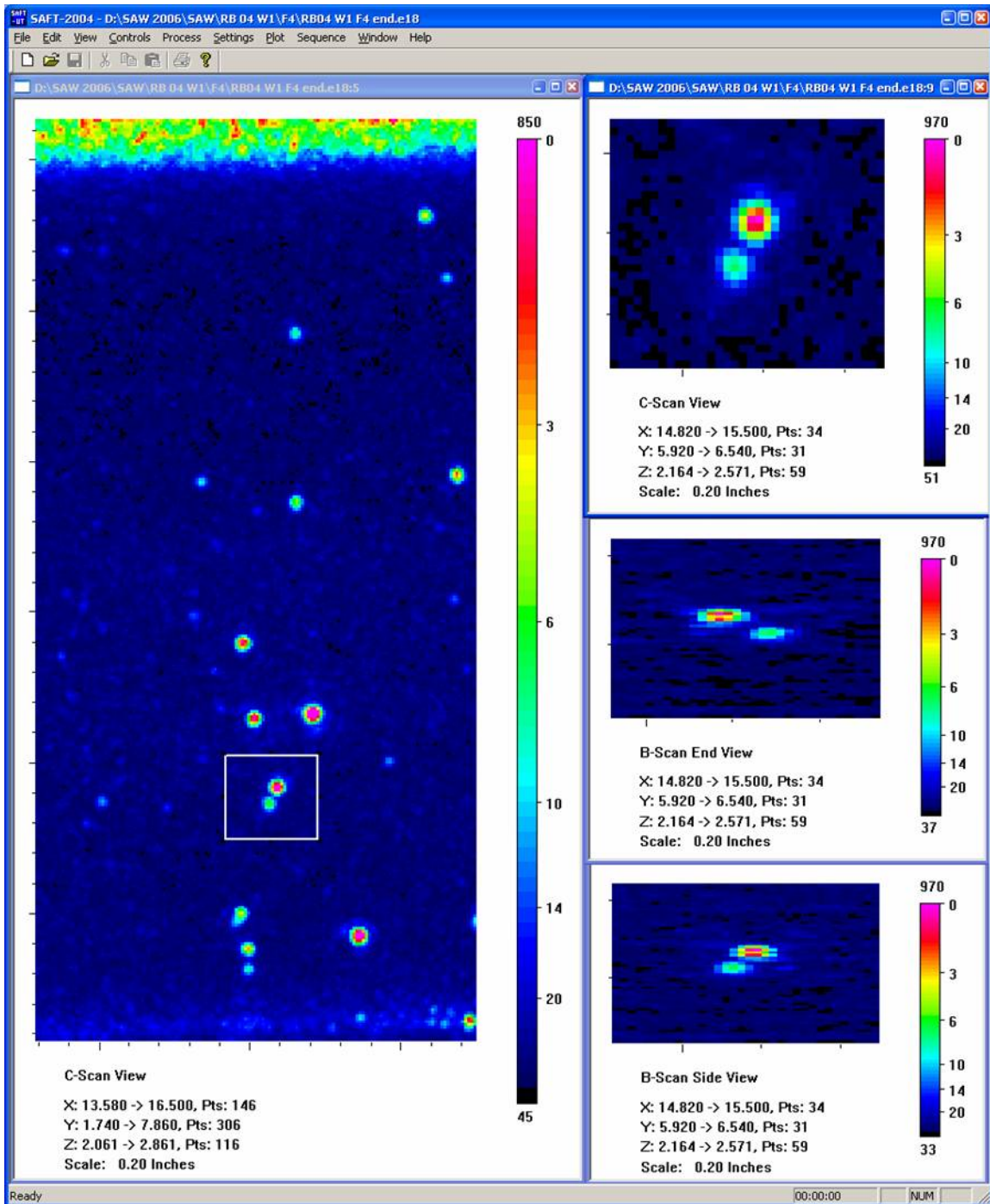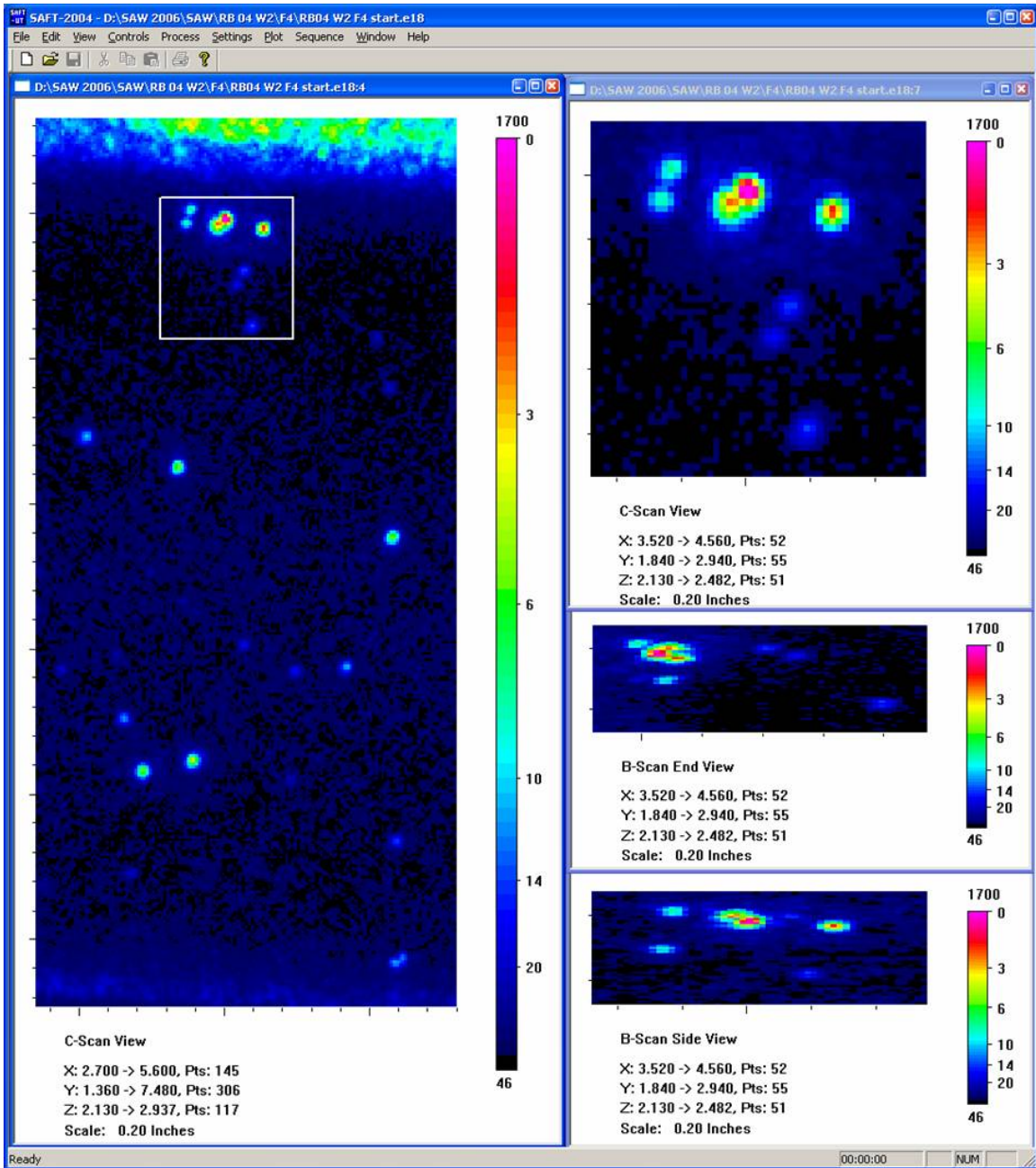
Figure A.1.b F4 Immersion Testing Images of Small Fabrication Flaw: *RB1A*. **This figure shows the same material and flaw(s) as the previous figure but with twice the resolving power. The ultrasonic immersion probe was a 10 MHz F4 and as such has a lateral resolution of 1.2 wavelength or 0.7 mm. Here the two flaws are resolved both laterally and in depth. The through-wall sizes are 2.0 mm and 1.0 mm.**
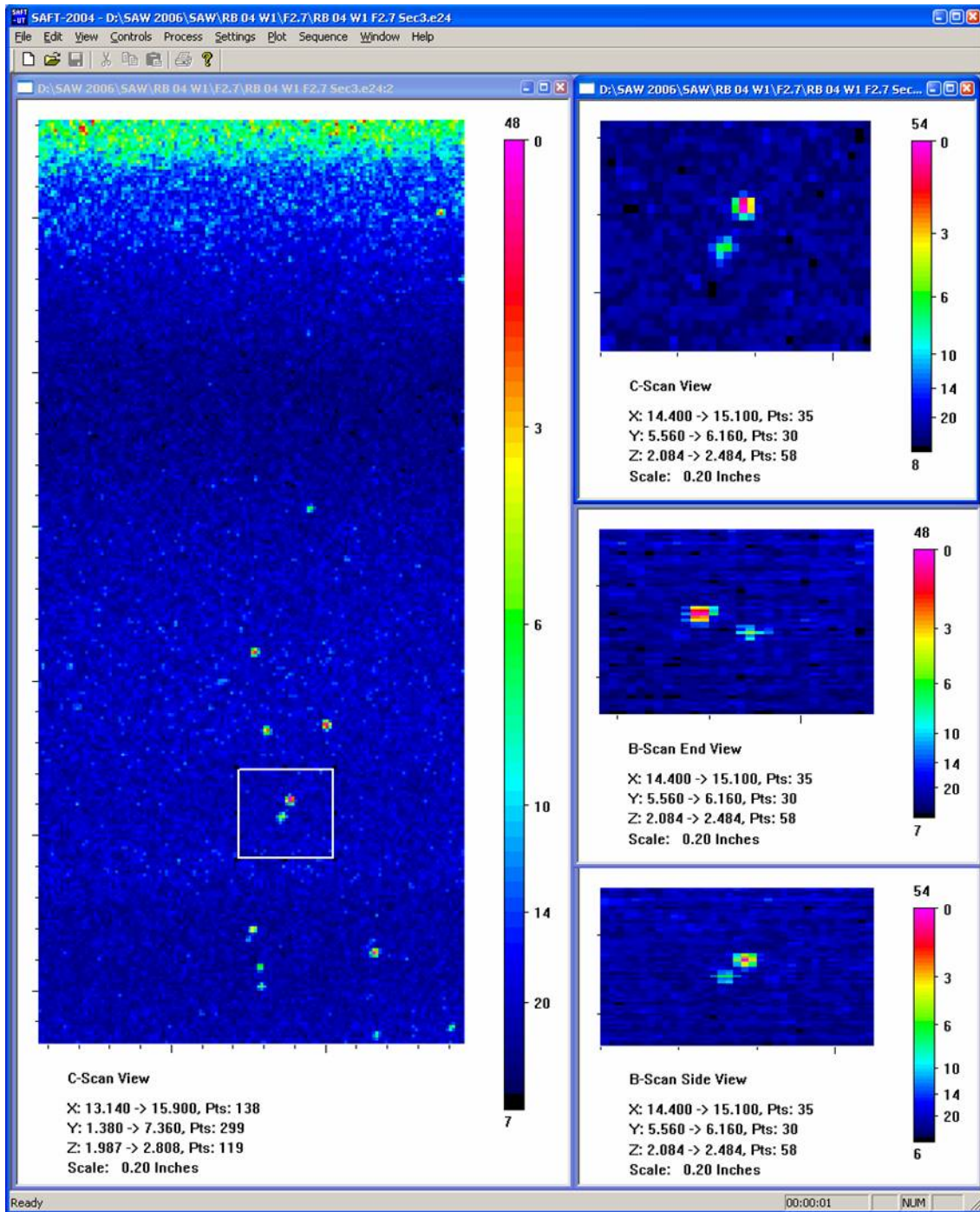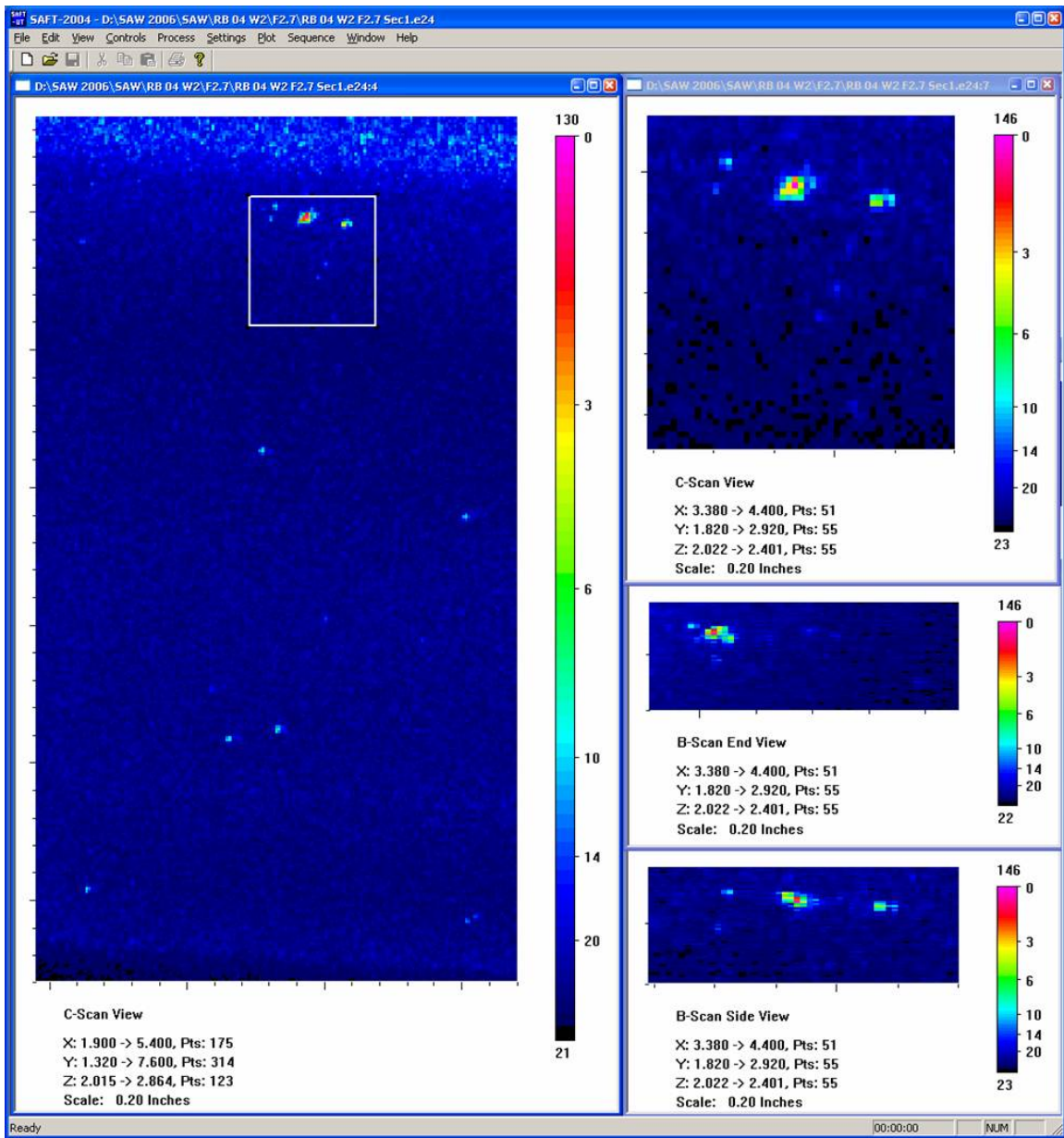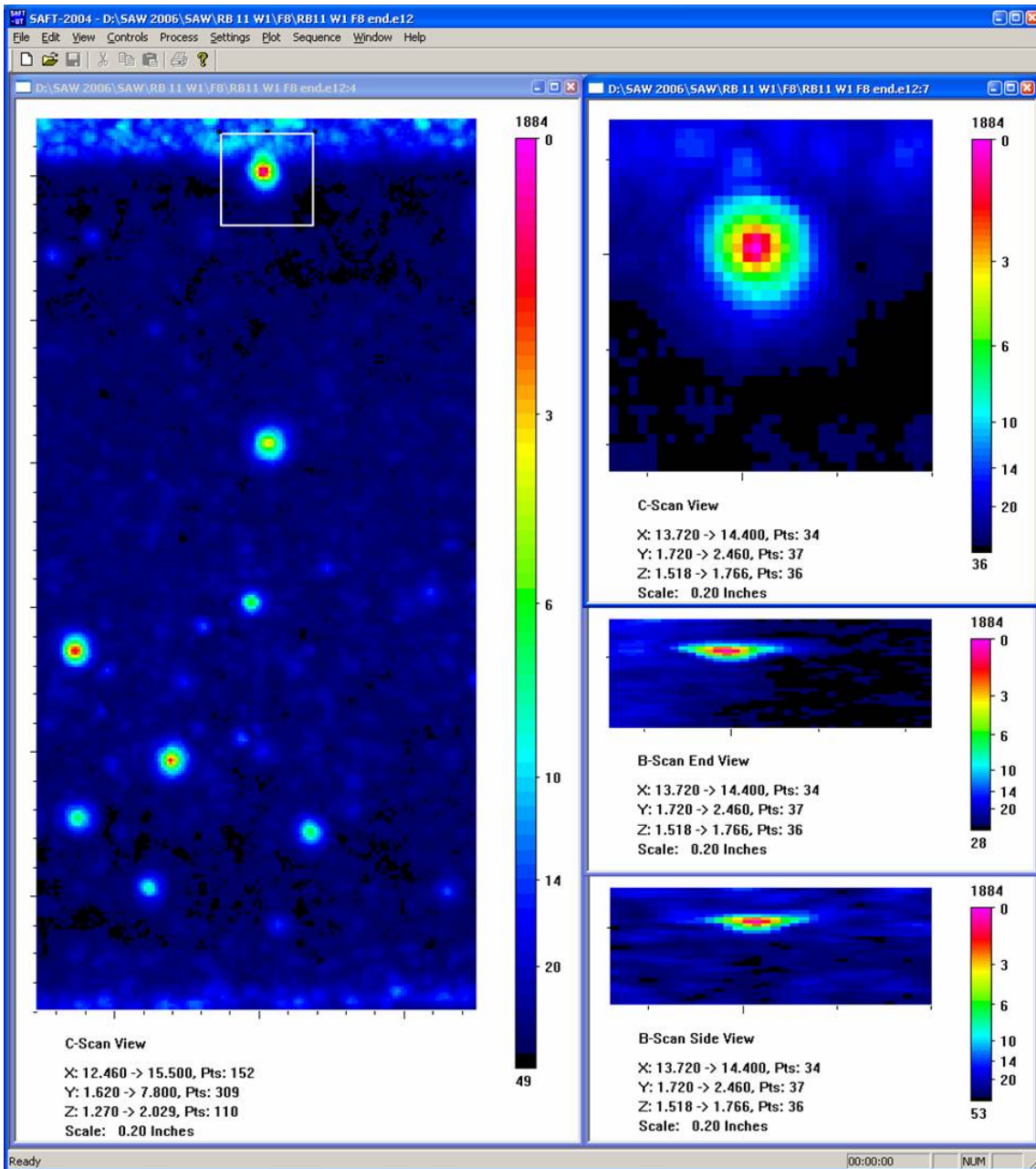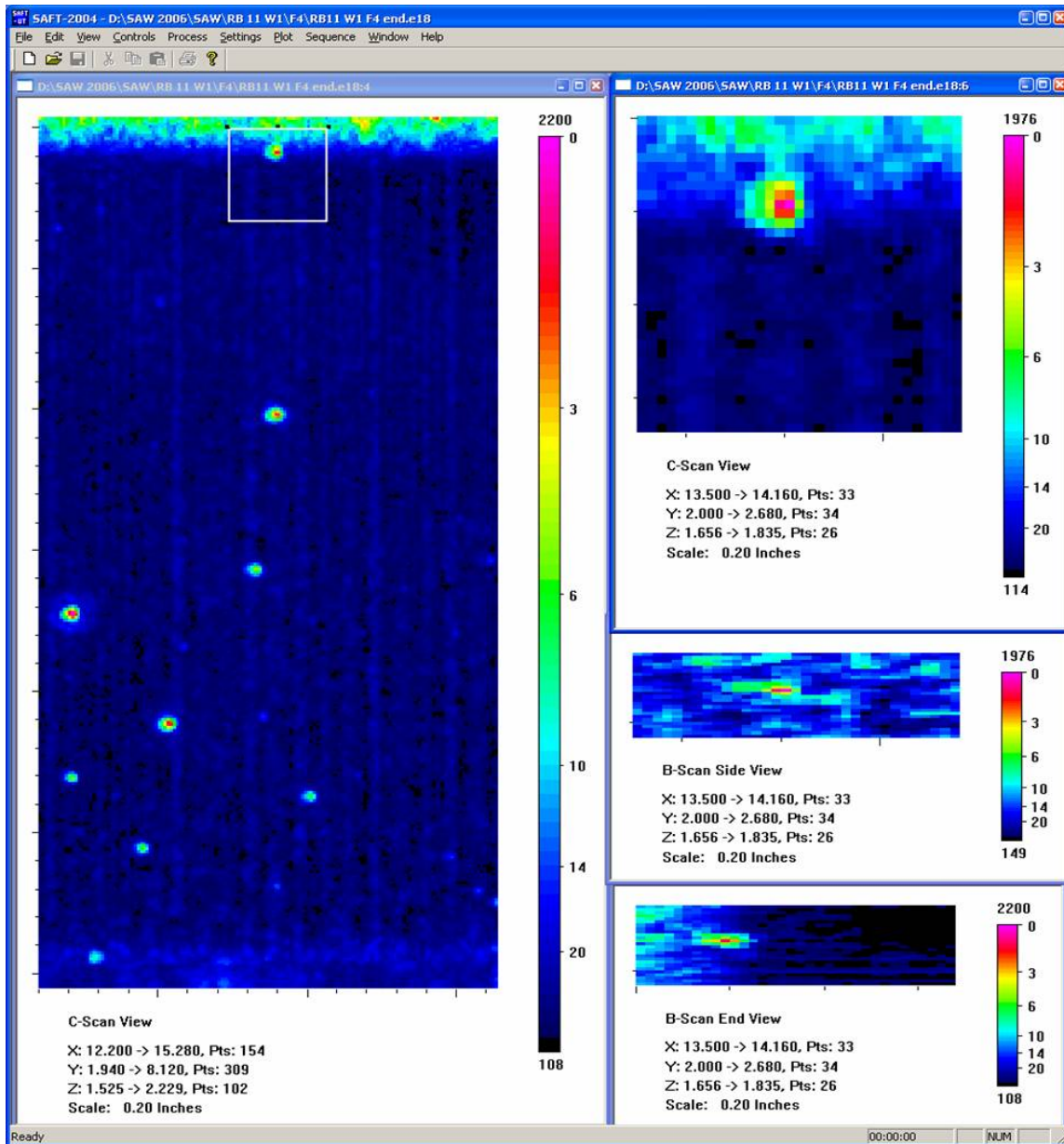
Figure A.1.c F2.7 Immersion Testing Images of Small Fabrication Flaw: *RB1A*. **This figure shows the same material and flaw(s) as the previous figures. Here the two flaws are resolved to through-wall sizes of 1.0 mm and 0.5 mm.**
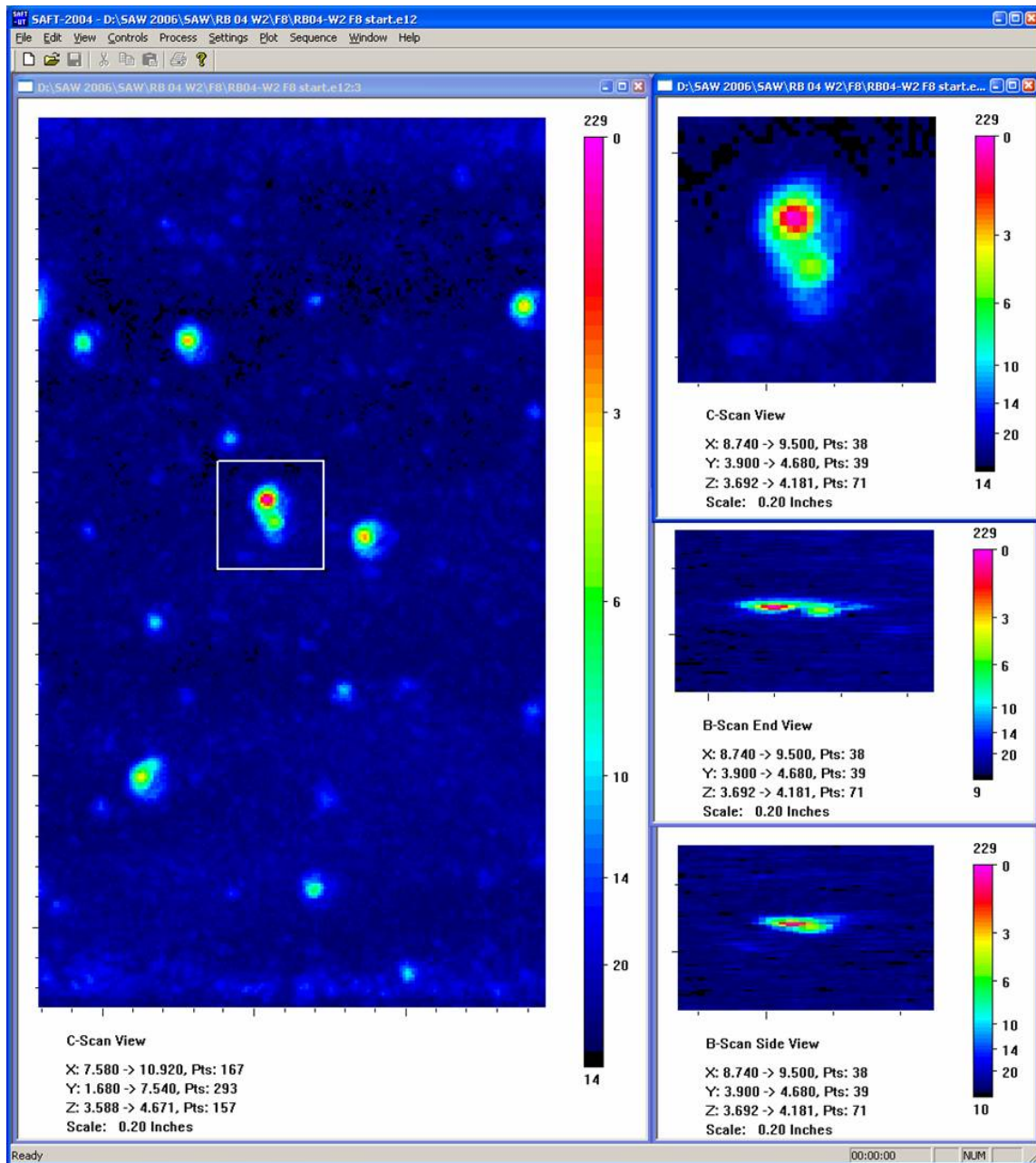
Figure A.2.a 10 MHz F8 Immersion Testing Images of Small Fabrication Flaw: *RB2A*. **This figure shows immersion testing data of a 5.5-mm flaw indication from the weld-normal testing of large weld segments. The flaw indication is identified in the box drawn in the SAFT-UT image on the left in the figure. A close up of the flaw in the C-scan view (top right) shows 2 unresolved flaws.**
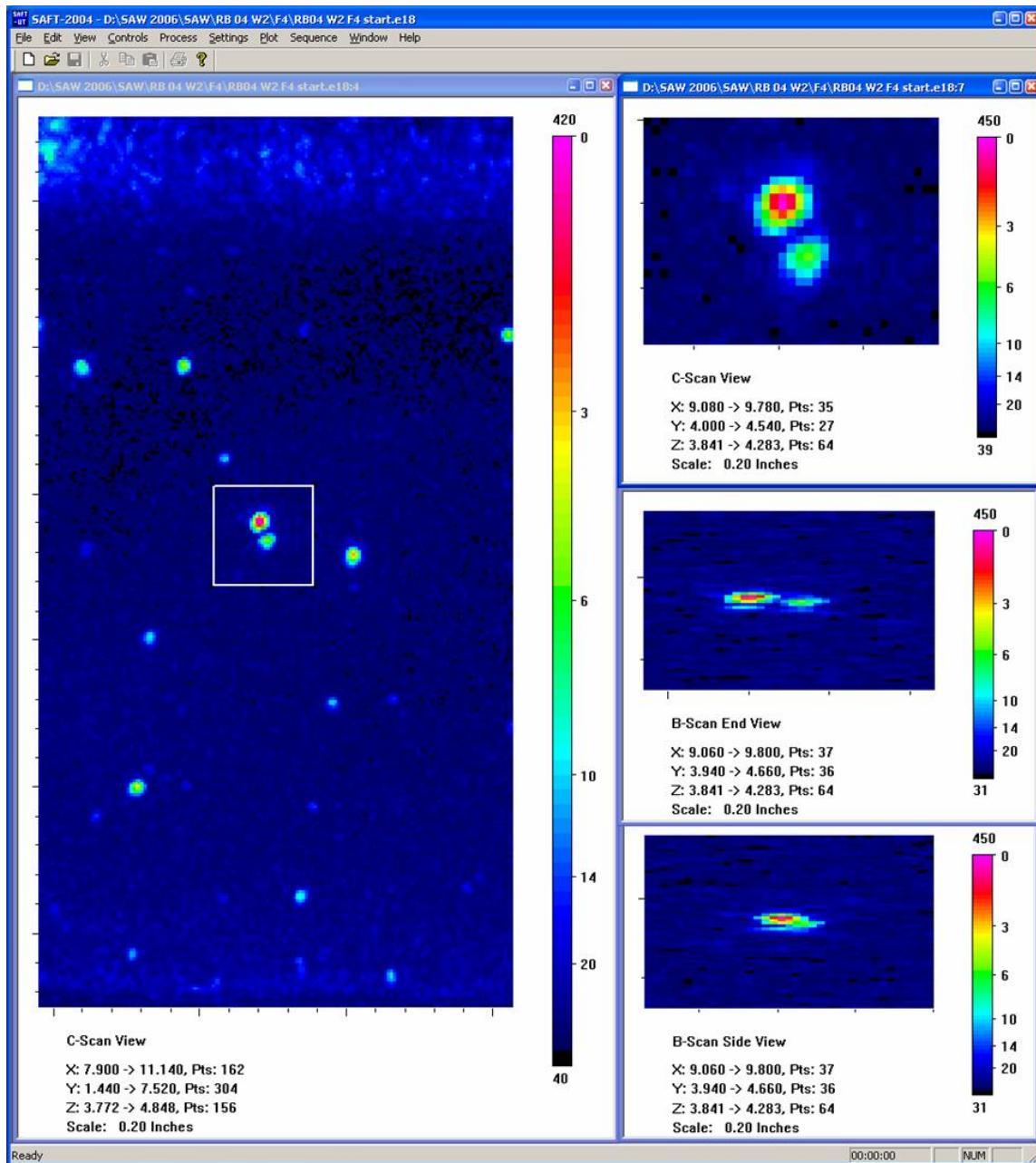
Figure A.2.b F4 Immersion Testing Images of Small Fabrication Flaw: *RB2A*. **This figure shows the same material and flaw(s) as the previous figure but with twice the resolving power. The ultrasonic immersion probe was a 10 MHz F4 and as such has a lateral resolution of 1.2 wavelength or 0.7 mm. Here the two flaws are resolved both laterally and in depth. The through-wall sizes are 2.5 mm and 1.5 mm.**
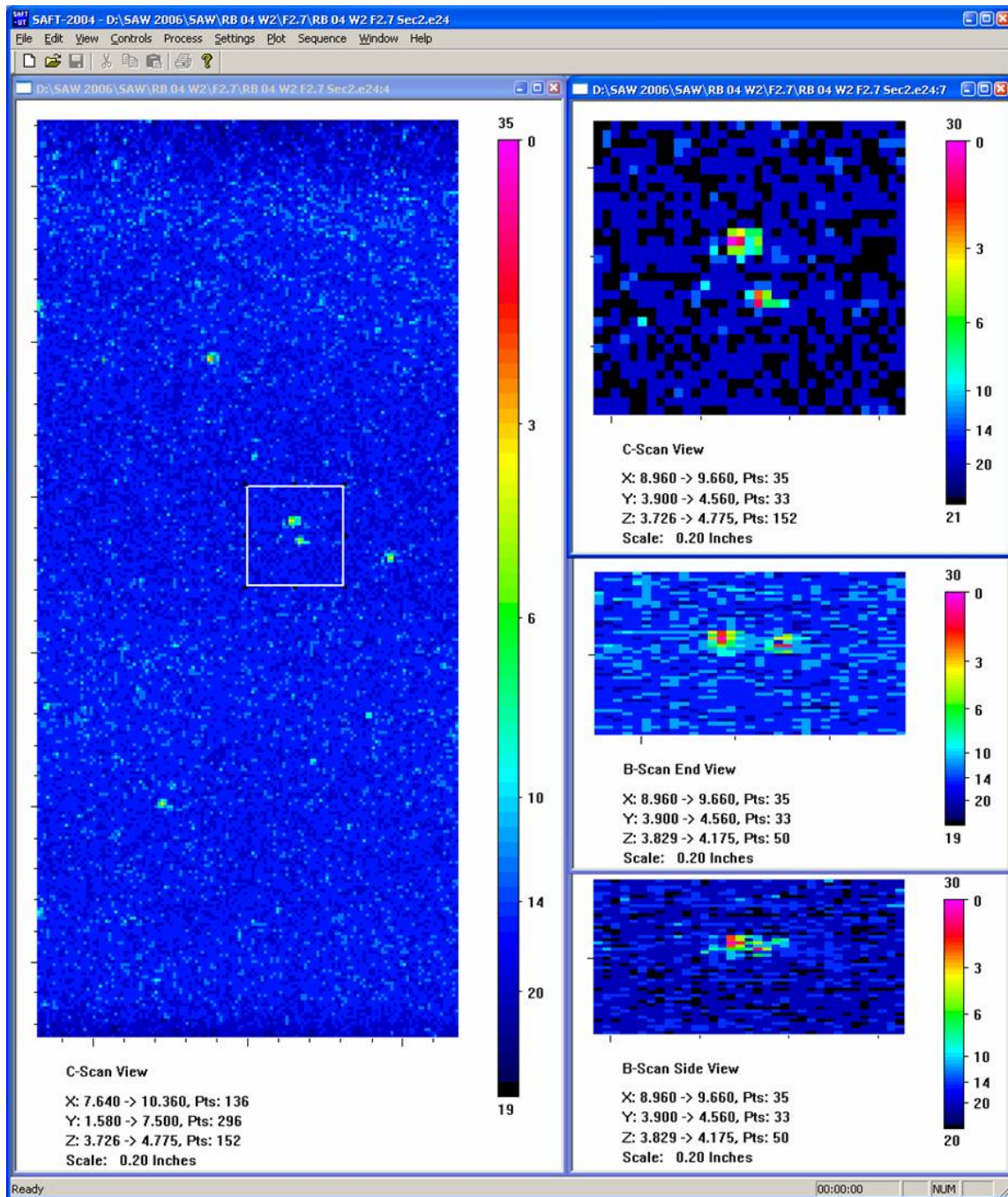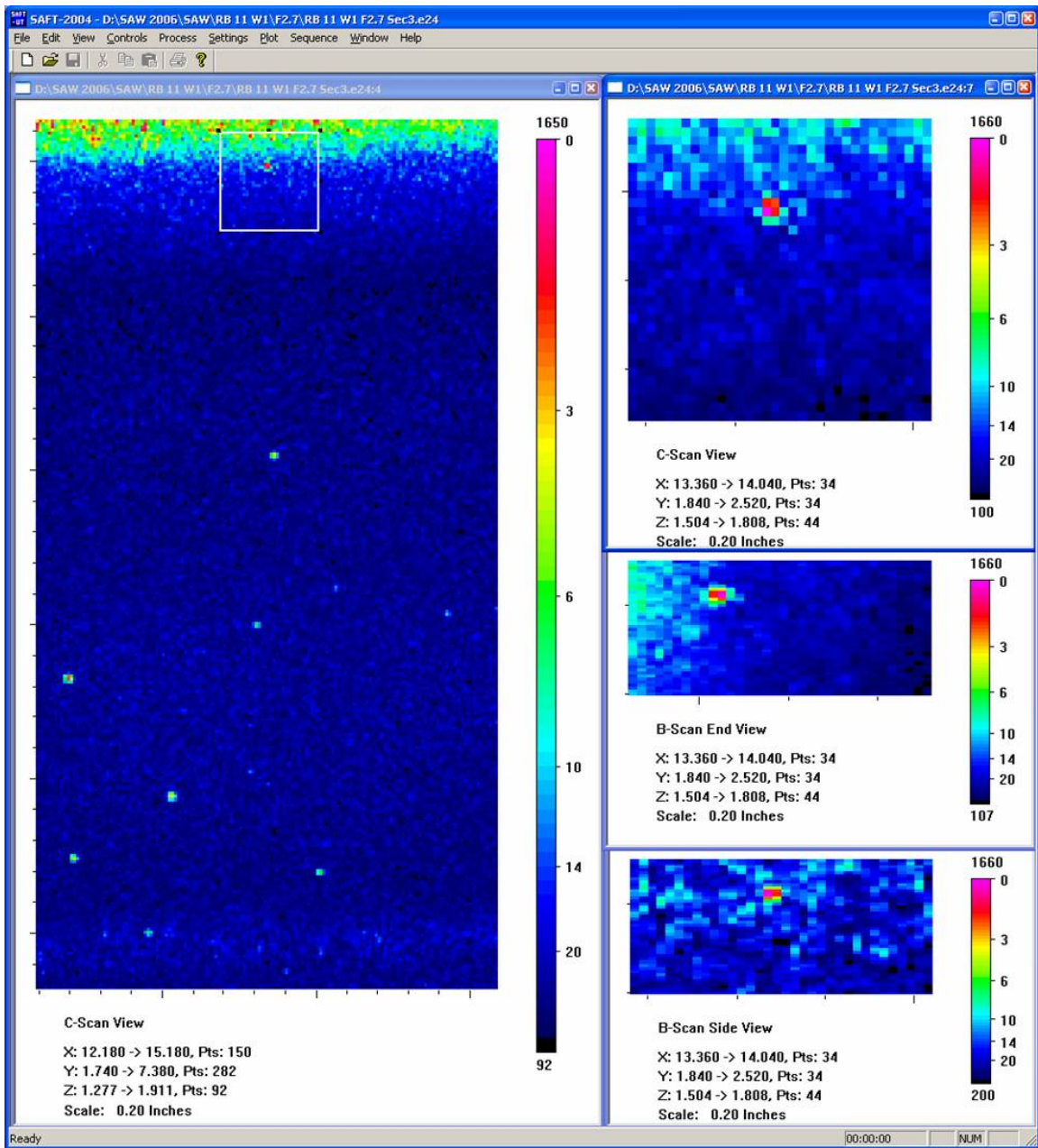
Figure A.2.c F2.7 Immersion Testing Images of Small Fabrication Flaw: *RB2A*. **This figure shows the same material and flaw(s) as the previous figures. Here the two flaws are resolved to through-wall sizes of 1.5 mm and 1.0 mm.**
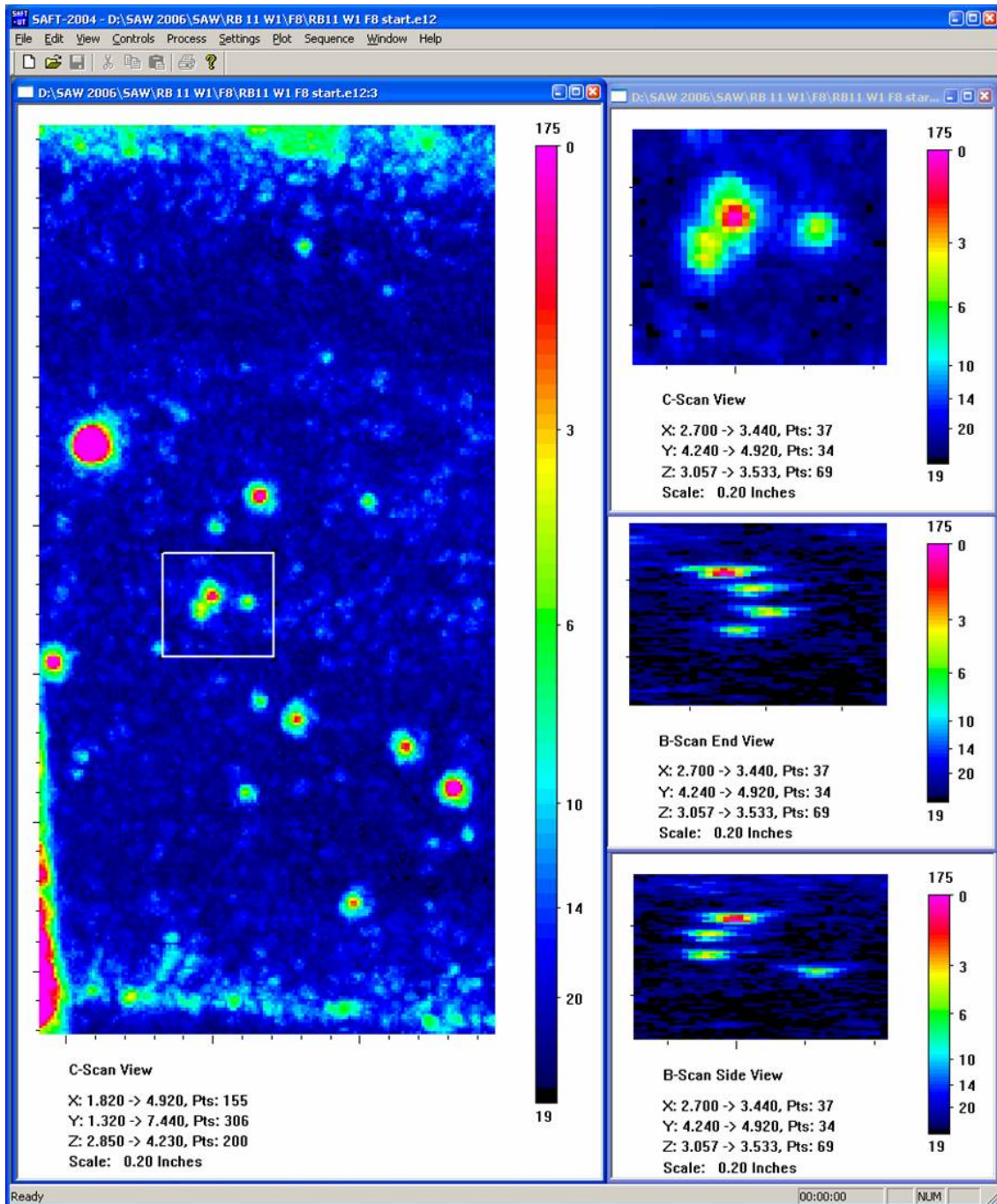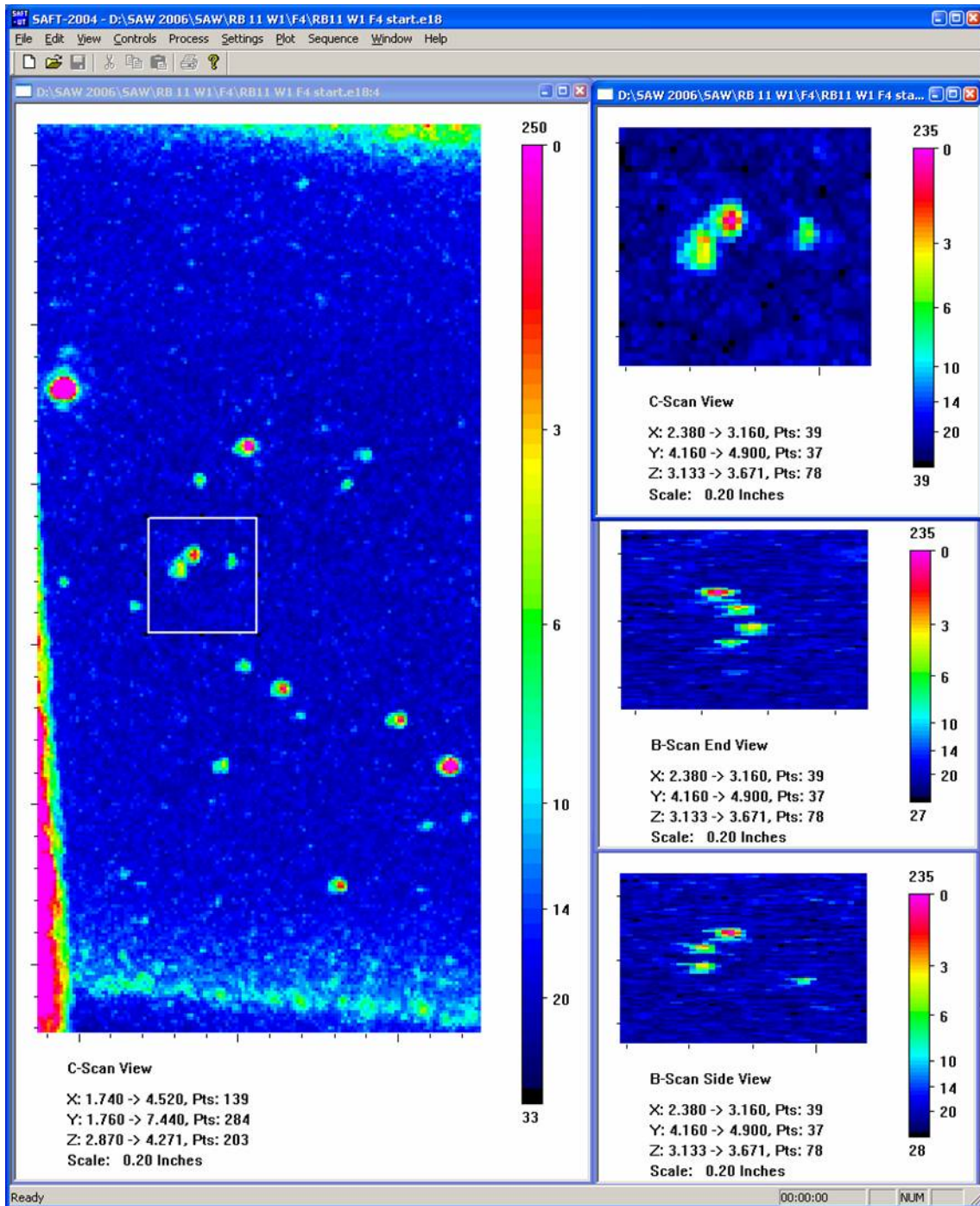
Figure A.3.a 10 MHz F8 Immersion Testing Images of Small Fabrication Flaw: *RB3A*. **This figure shows immersion testing data of a 6-mm flaw indication from the weld-normal testing of large weld segments. The flaw indication is identified in the box drawn in the SAFT-UT image on the left in the figure.**

Figure A.3.b F4 Immersion Testing Images of Small Fabrication Flaw: *RB3A*. **This figure shows the same material and flaw(s) as the previous figure but with twice the resolving power. The ultrasonic immersion probe was a 10 MHz F4 and as such has a lateral resolution of 1.2 wavelength or 0.7 mm. Here the flaw is resolved both laterally and in depth. The through-wall size is 2.5 mm.**
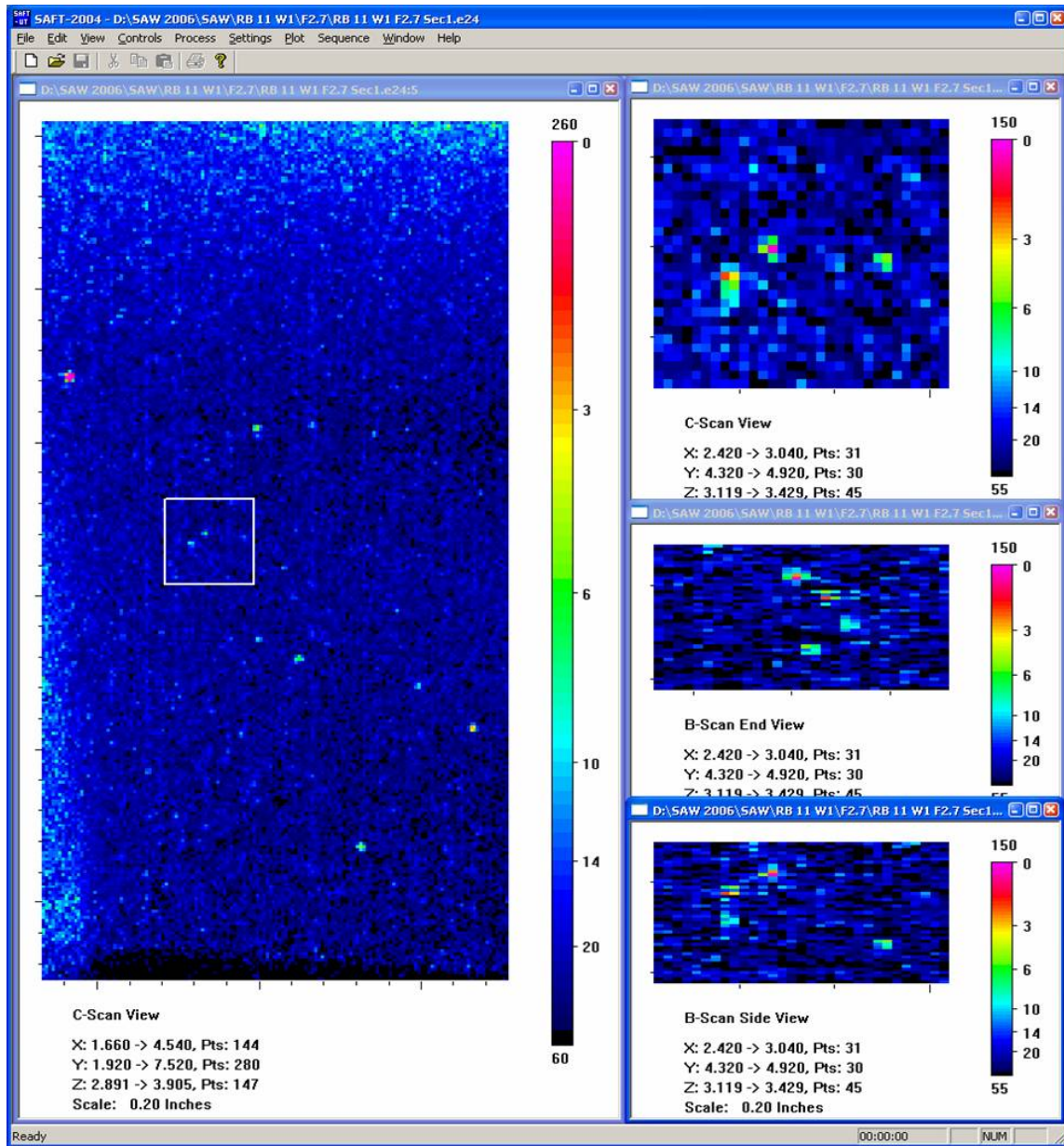
Figure A.3.c F2.7 Immersion Testing Images of Small Fabrication Flaw: *RB3A*. **This figure shows the same material and flaw as the previous figures. Here the flaw is resolved to a through-wall size of 1.5 mm.**
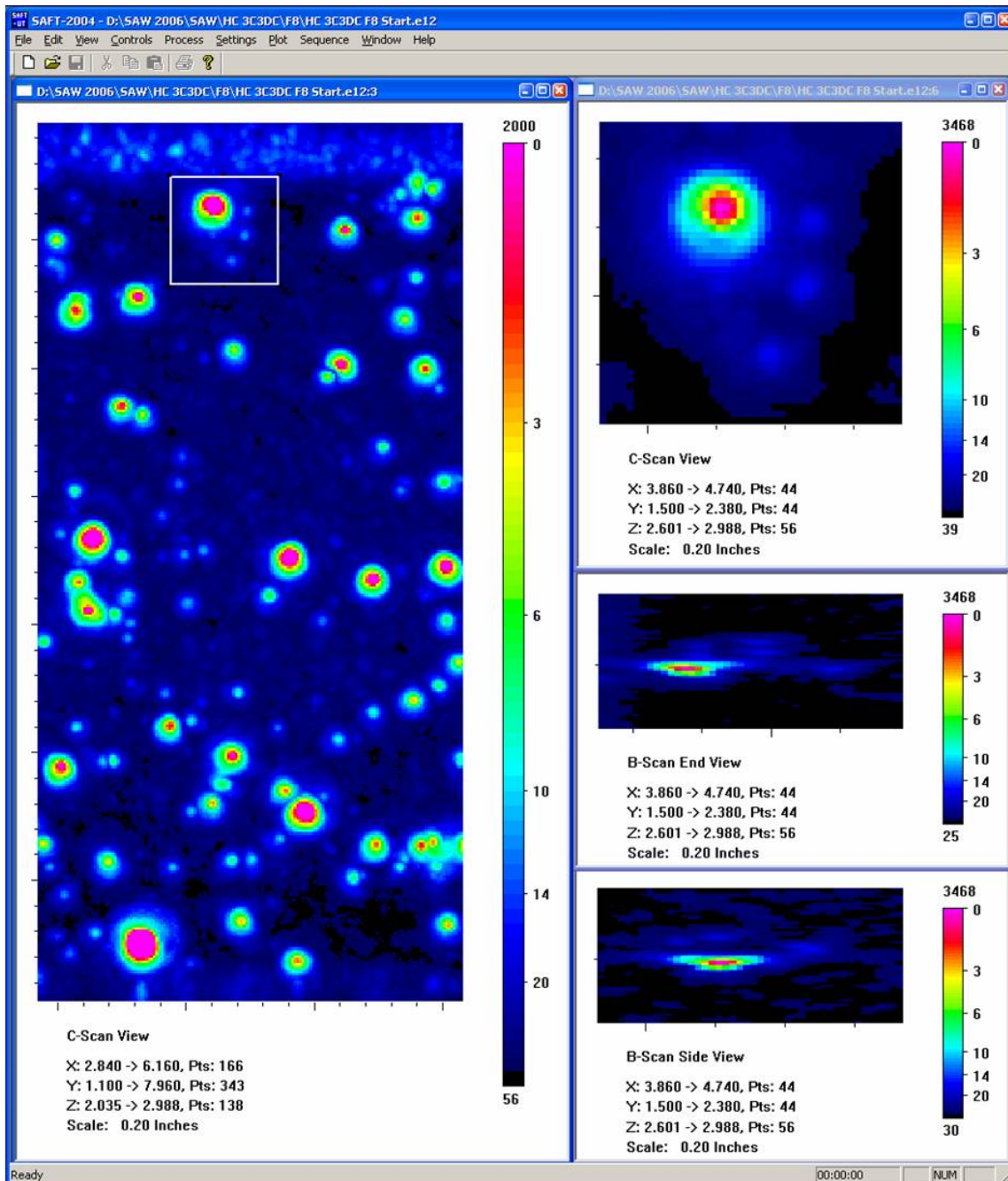
Figure A.4.a 10 MHz F8 Immersion Testing Images of Small Fabrication Flaw: *RB4A***. This figure shows immersion testing data of a 6-mm flaw indication from the weld-normal testing of large weld segments. The flaw indication is identified in the box drawn in the SAFT-UT image on the left in the figure.**
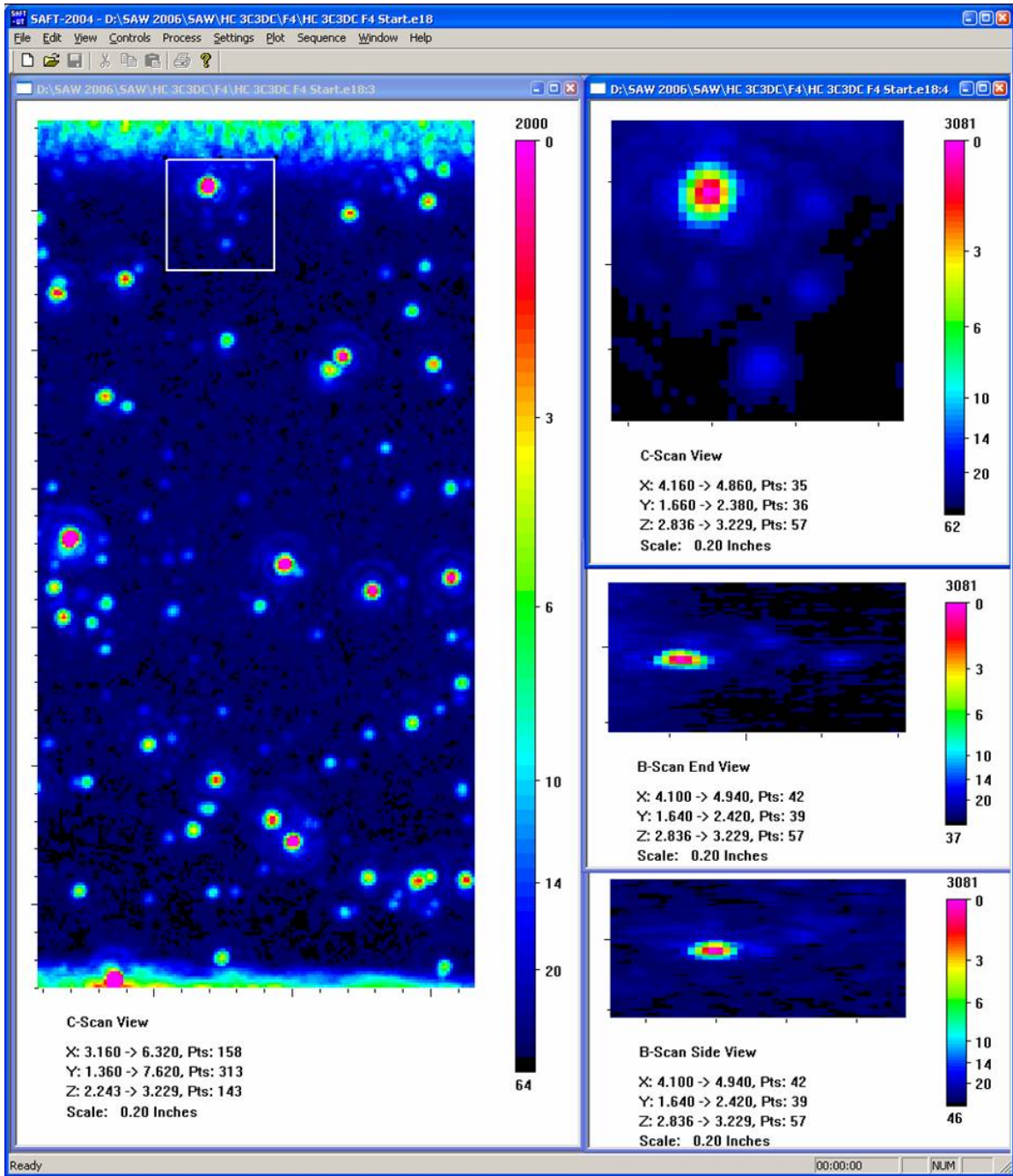
A.10

Figure A.4.b F4 Immersion Testing Images of Small Fabrication Flaw: *RB4A*. **This figure shows the same material and flaw(s) as the previous figure but with twice the resolving power. The ultrasonic immersion probe was a 10 MHz F4 and as such has a lateral resolution of 1.2 wavelength or 0.7 mm. Here the flaw is resolved both laterally and in depth. The through-wall size is 2.5 mm.**
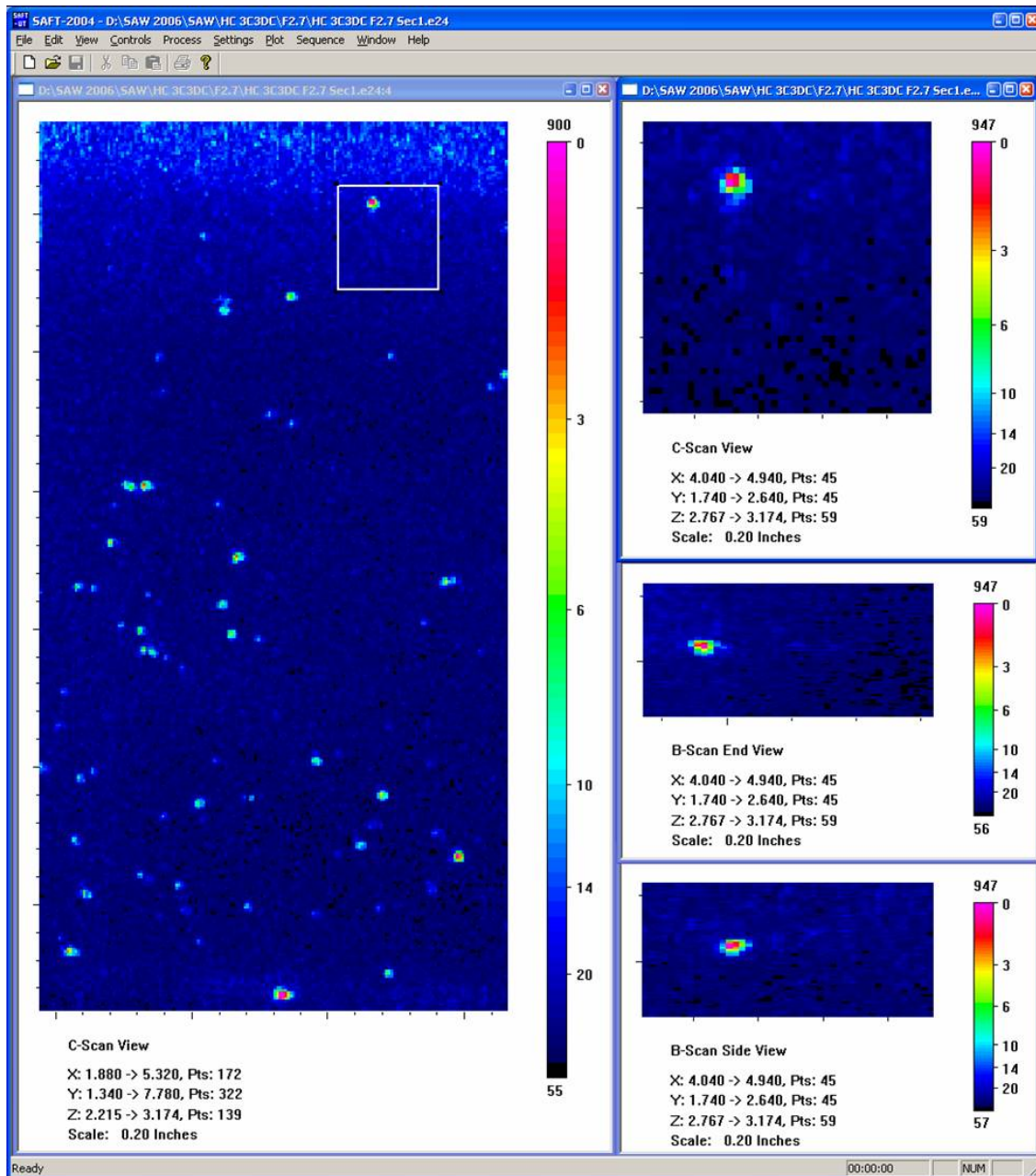
Figure A.4.c F2.7 Immersion Testing Images of Small Fabrication Flaw: *RB4A*. **This figure shows the same material and flaw as the previous figures. Here the flaw is resolved to a through-wall size of 1.0 mm.**
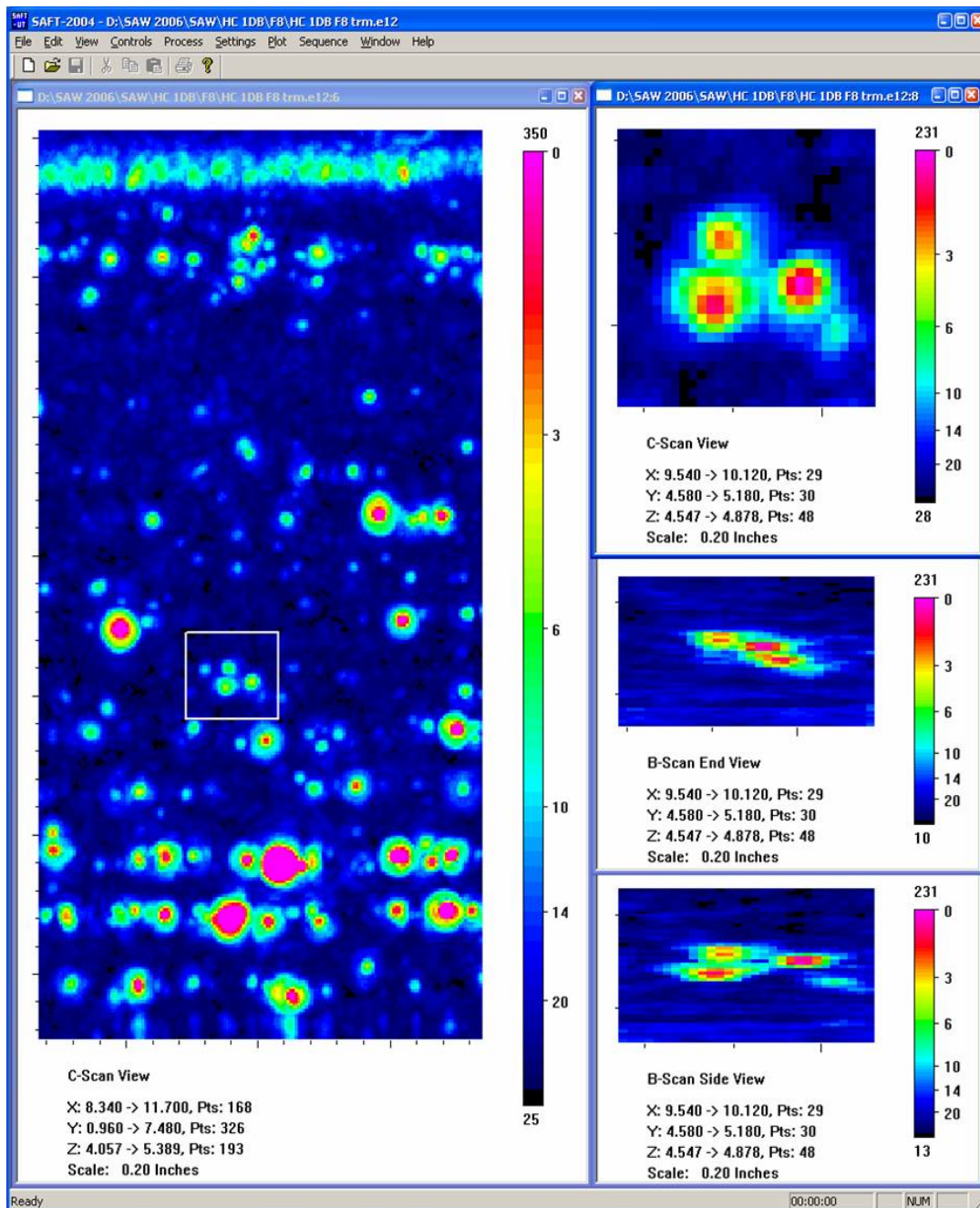
Figure A.5.a 10 MHz F8 Immersion Testing Images of Small Fabrication Flaw: *RB5A*. **This figure shows immersion testing data of a 5.5-mm flaw indication from the weld-normal testing of large weld segments. The flaw indication is identified in the box drawn in the SAFT-UT image on the left in the figure. A close up of the flaw in the C-scan view (top right) shows 2 unresolved flaws.**

A.13

Figure A.5.b F4 Immersion Testing Images of Small Fabrication Flaw: *RB5A***. This figure shows the same material and flaw(s) as the previous figure but with twice the resolving power. The ultrasonic immersion probe was a 10 MHz F4 and as such has a lateral resolution of 1.2 wavelength or 0.7 mm. Here the two flaws are resolved both laterally and in depth. The through-wall sizes are 2.5 mm and 3.0 mm.**

Figure A.5.c F2.7 Immersion Testing Images of Small Fabrication Flaw: *RB5A*. **This figure shows the same material and flaw(s) as the previous figures. Here the two flaws are resolved to through-wall sizes of 1.0 mm and 1.5 mm.**

Figure A.6.a 10 MHz F8 Immersion Testing Images of Small Fabrication Flaw: HC1A. This figure shows immersion testing data of a complex flaw indication from the weld-normal testing of large weld segments. The flaw indication is identified in the box drawn in the SAFT-UT image on the left in the figure. A close up of the flaw in the C-scan view (top right) shows 1 flaw 3.5-mm long in through-wall direction.
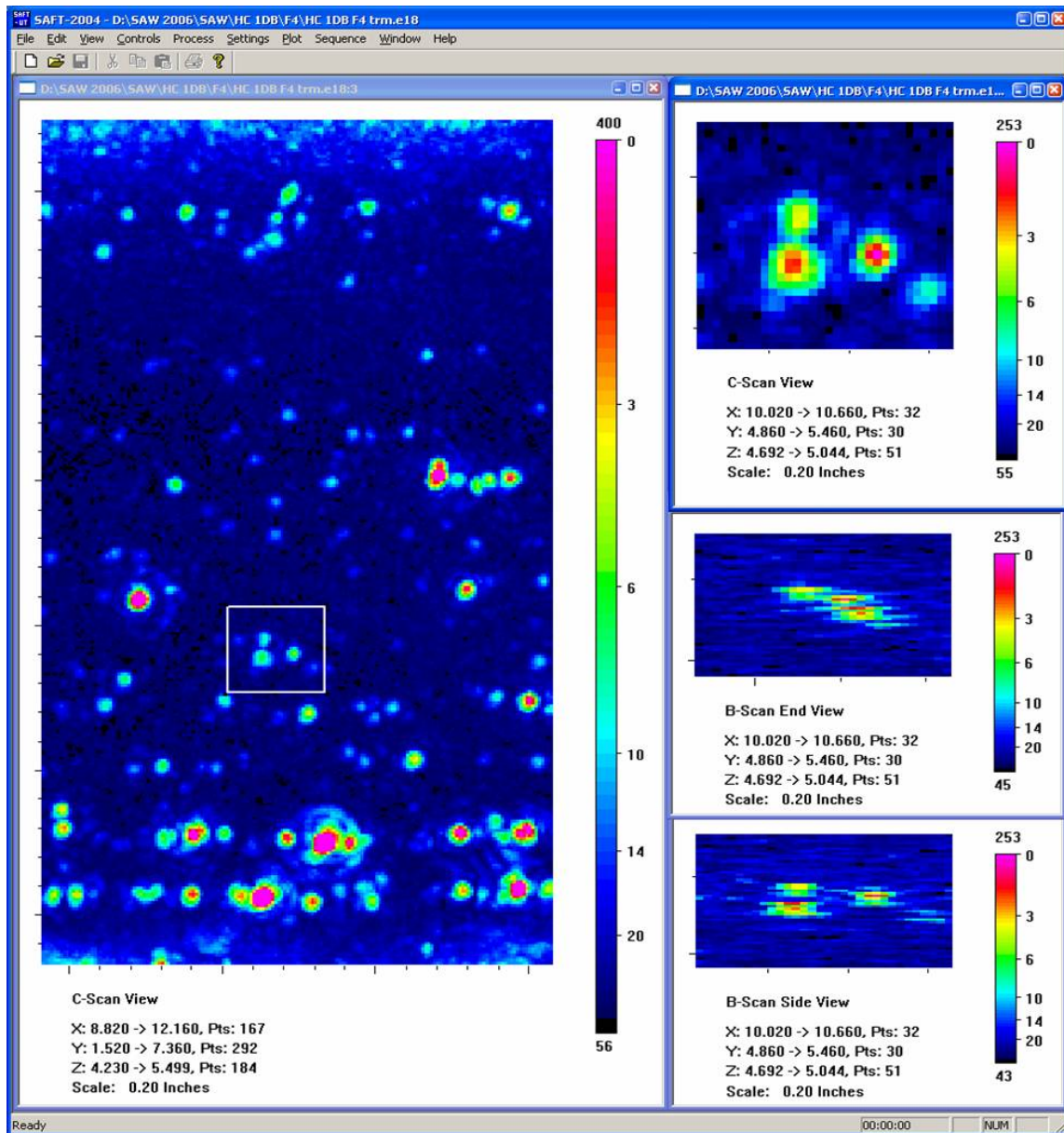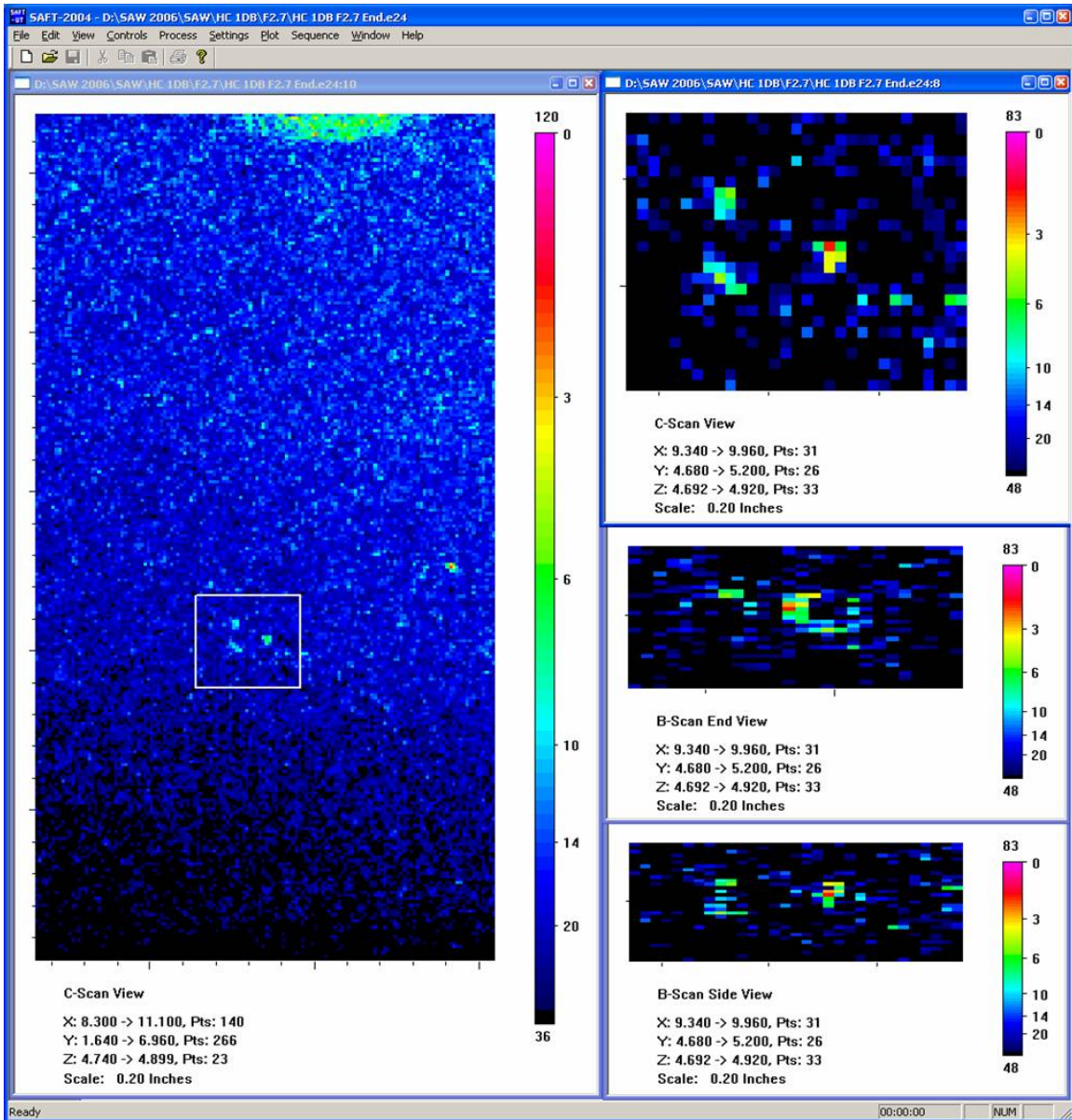
Figure A.6.b F4 Immersion Testing Images of Small Fabrication Flaw: *HC1A*. **This figure shows the same material and flaw(s) as the previous figure but with twice the resolving power. The ultrasonic immersion probe was a 10 MHz F4 and as such has a lateral resolution of 1.2 wavelength or 0.7 mm. Here the flaw is resolved both laterally and in depth with a through-wall size of 2.5 mm.**

Figure A.6.c F2.7 Immersion Testing Images of Small Fabrication Flaw: *HC1A*. **This figure shows the same material and flaw as the previous figures. Here the flaw is resolved to a through-wall size of 1.5 mm.**
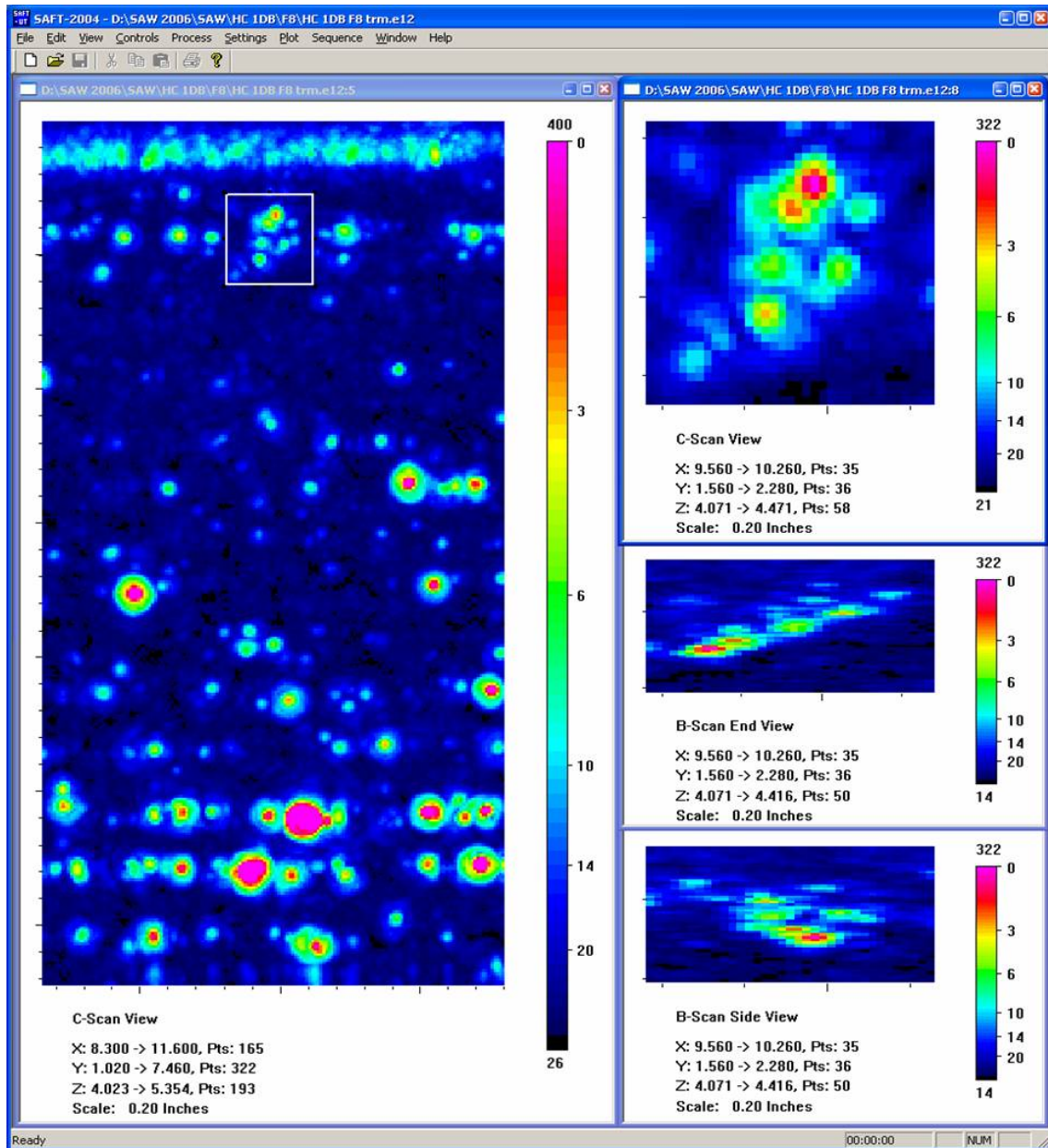
Figure A.7.a 10 MHz F8 Immersion Testing Images of Small Fabrication Flaw: *HC3A*. **This figure shows immersion testing data of a 7-mm flaw indication from the weld-normal testing of large weld segments. The flaw indication is identified in the box dr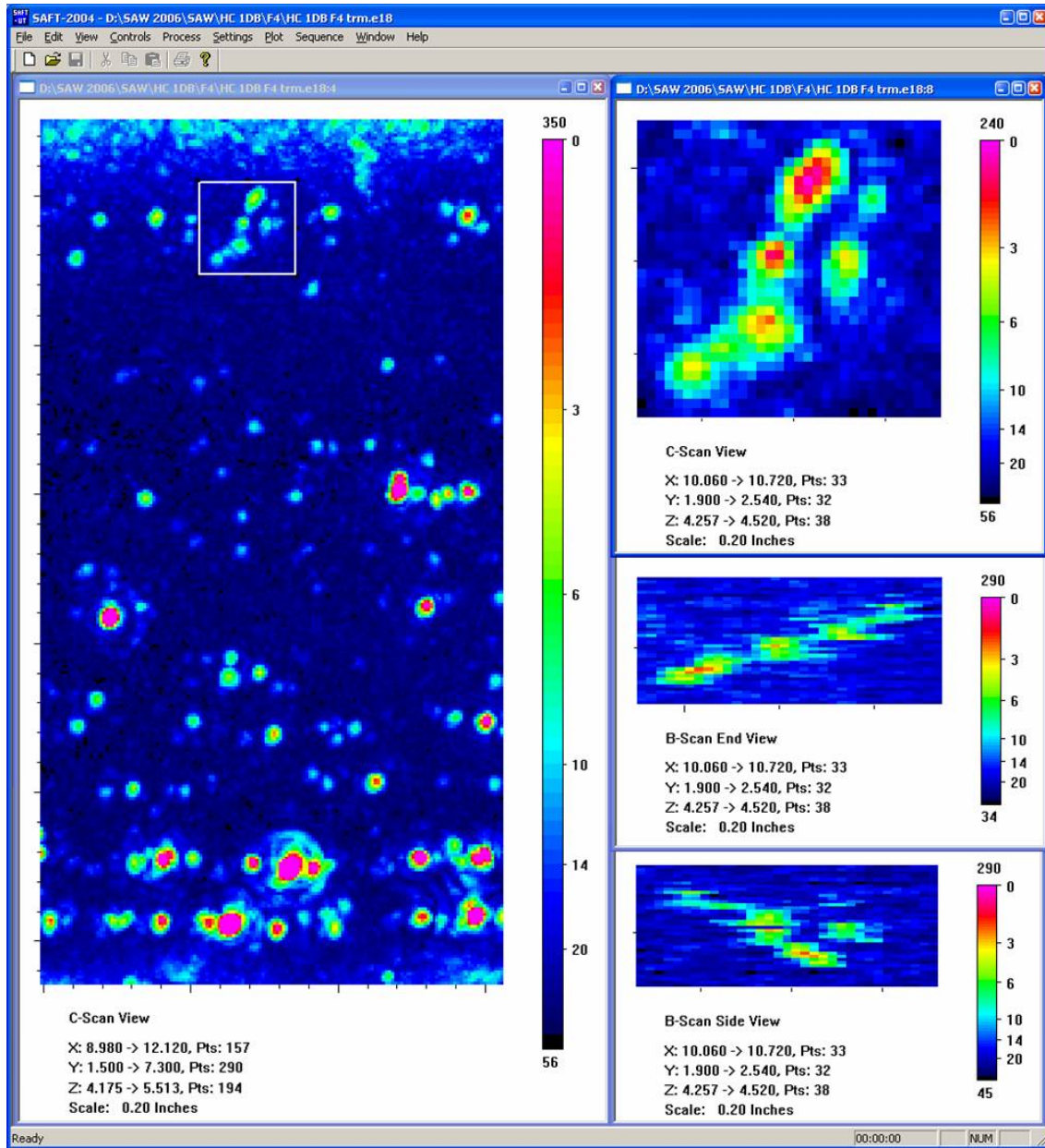awn in the SAFT-UT image on the left in the figure. A close up of the flaw in the C-scan view (top right) shows 3 unresolved flaws.**

Figure A.7.b F4 Immersion Testing Images of Small Fabrication Flaw: *HC3A*. **This figure shows the same material and flaw(s) as the previous figure but with twice the resolving power. The ultrasonic immersion probe was a 10 MHz F4 and as such has a lateral resolution of 1.2 wavelength or 0.7 mm. Here the 2 flaws are resolved to 3 flaws both laterally and in depth. Through-wall sizes are 3.0 mm, 2.5 mm and 2.5 mm.**

Figure A.7.c F2.7 Immersion Testing Images of Small Fabrication Flaw: *HC3A*. **This figure shows the same material and flaw(s) as the previous figures. Here the flaws are resolved to through-wall sizes of 2.0 mm, 1.5 mm, and 1.5 mm.**

A.21

Figure A.8.a 10 MHz F8 Immersion Testing Images of Small Fabrication Flaw: *HC3B (HC 1DB-3 / 1D1E 14.0 mm)*. This figure shows immersion testing data of a 14-mm flaw indication from the weld-normal testing of large weld segments. The flaw indication is identified in the box drawn in the SAFT-UT image on the left in the figure.
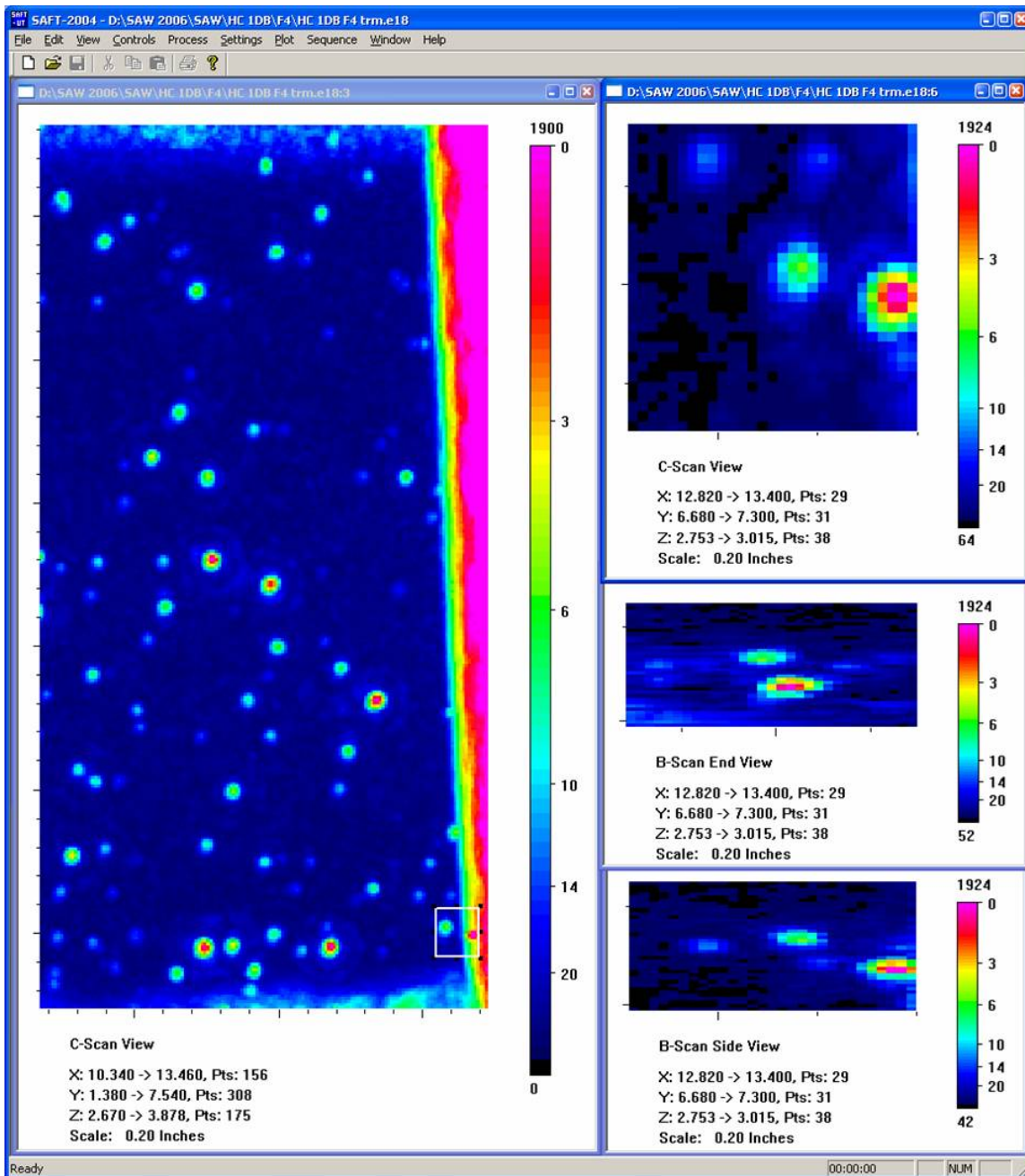
Figure A.8.b F4 Immersion Testing Images of Small Fabrication Flaw: *HC3B (HC 1DB-3 / 1D1E 14.0mm).* **This figure shows the same material and flaw(s) as the previous figure but with twice the resolving power. The ultrasonic immersion probe was a 10 MHz F4 and as such has a lateral resolution of 1.2 wavelength or 0.7 mm.**
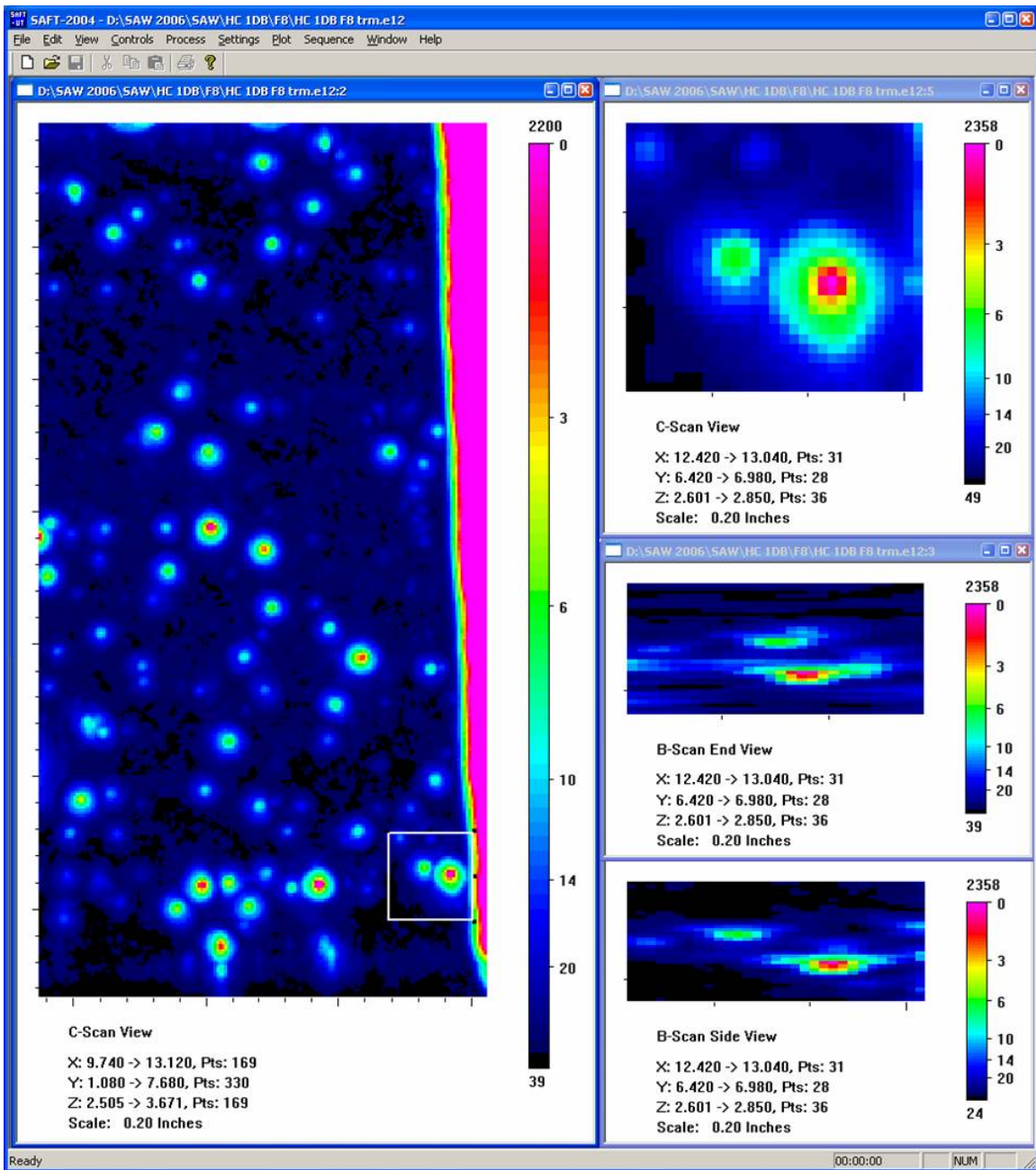
Figure A.9.a 10 MHz F8 Immersion Testing Images of Small Fabrication Flaw: *HC4A*. **This figure shows immersion testing data of a 7-mm flaw indication from the weld-normal testing of large weld segments. The flaw indication is identified in the box drawn in the SAFT-UT image on the left in the figure.**
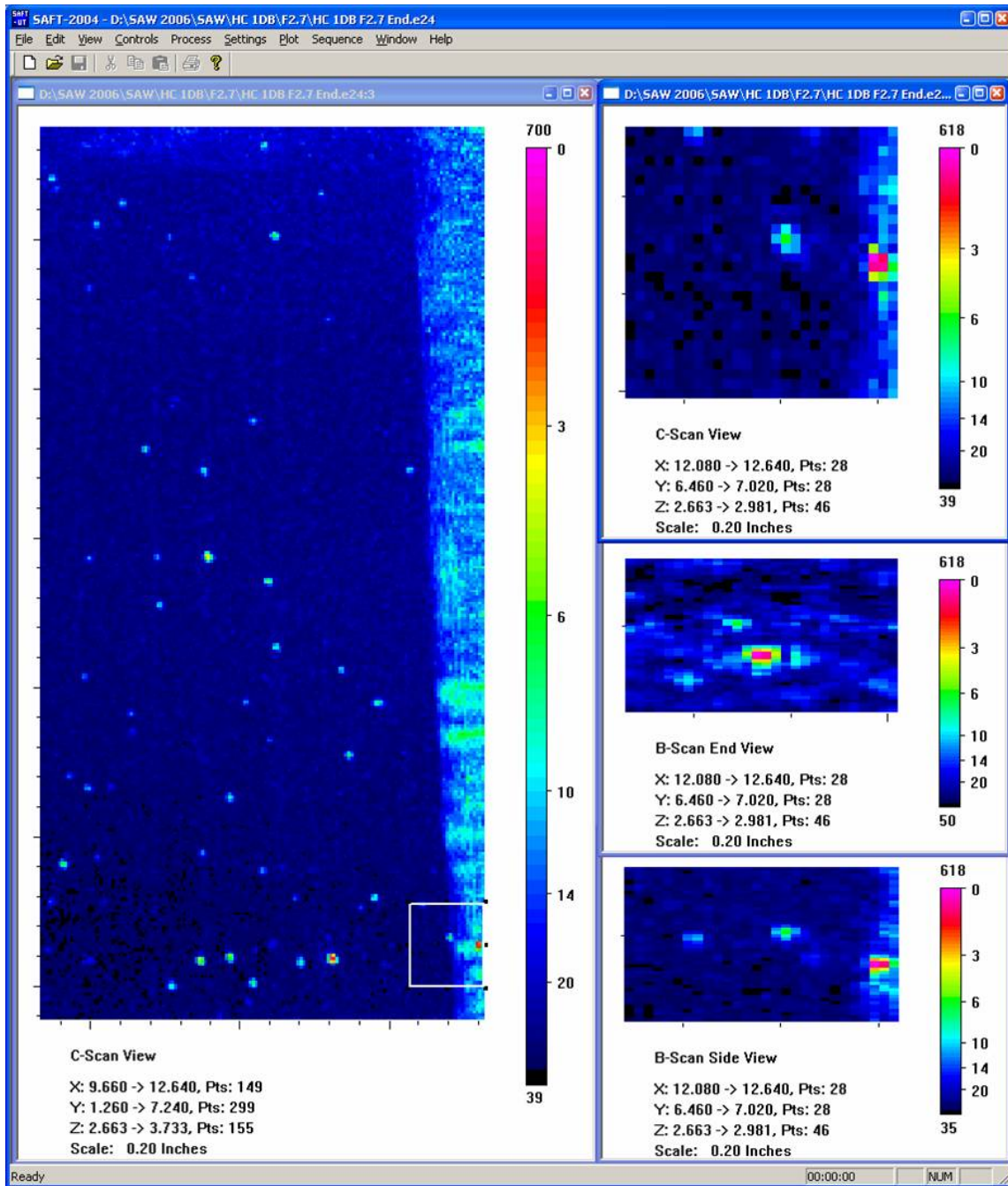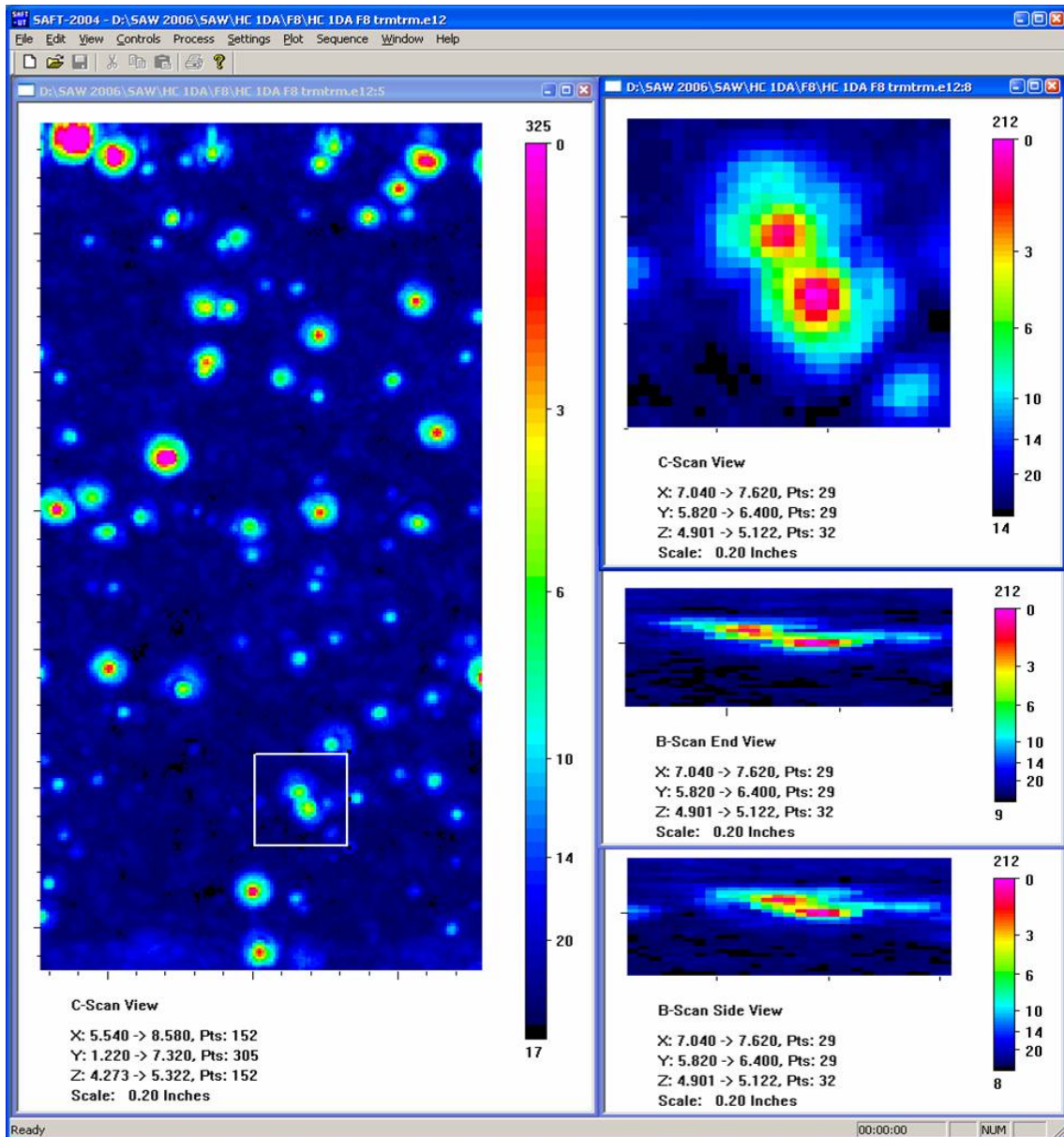
Figure A.9.b F4 Immersion Testing Images of Small Fabrication Flaw: *HC4A*. **This figure shows the same material and flaw(s) as the previous figure but with twice the resolving power. The ultrasonic immersion probe was a 10 MHz F4 and as such has a lateral resolution of 1.2 wavelength or 0.7 mm. Here the flaw is resolved both laterally and in depth with a through-wall size of 2.5 mm.**
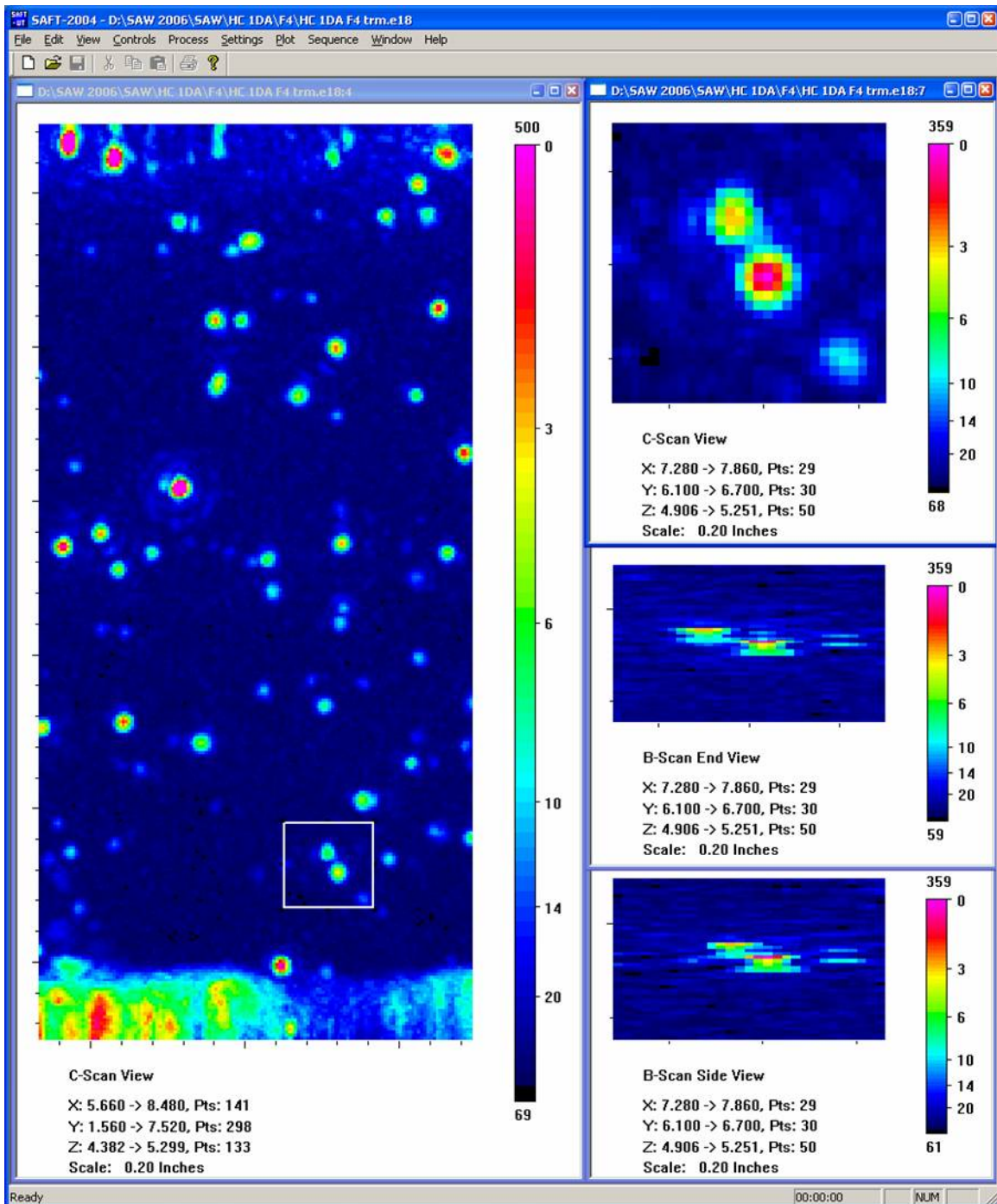
Figure A.9.c F2.7 Immersion Testing Images of Small Fabrication Flaw: *HC4A*. **This figure shows the same material and flaw as the previous figures. Here the flaw is resolved to a through-wall size of 2.0 mm.**

Figure A.10.a 10 MHz F8 Immersion Testing Images of Small Fabrication Flaw: *HC5A*. This figure shows immersion testing data of a 7-mm flaw indication from the weld-normal testing of large weld segments. The flaw indication is identified in the box drawn in the SAFT-UT image on the left in the figure. A close up of the flaw in the C-scan view (top right) shows 2 unresolved flaws.

Figure A.10.b F4 Immersion Testing Images of Small Fabrication Flaw: *HC5A***. This figure shows the same material and flaw(s) as the previous figure but with twice the resolving power. The ultrasonic immersion probe was a 10 MHz F4 and as such has a lateral resolution of 1.2 wavelength or 0.7 mm. Here the two flaws are resolved both laterally and in depth. The through-wall sizes are 2.0 mm and 2.5 mm.**
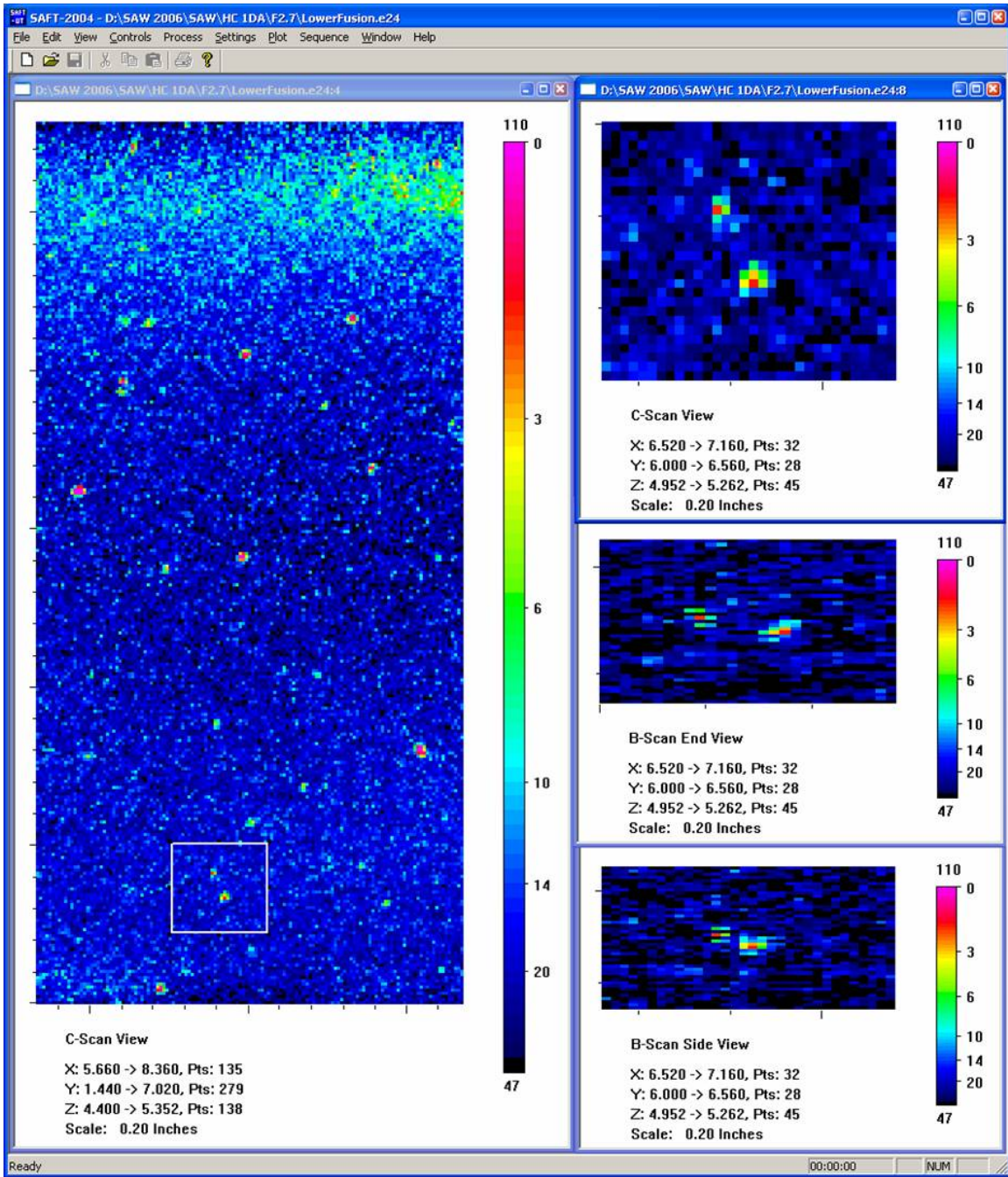
Figure A.10.c F2.7 Immersion Testing Images of Small Fabrication Flaw: *HC5A*. **This figure shows the same material and flaw(s) as the previous figures. Here the two flaws are resolved to through-wall sizes of 1.0 mm and 1.5 mm.**
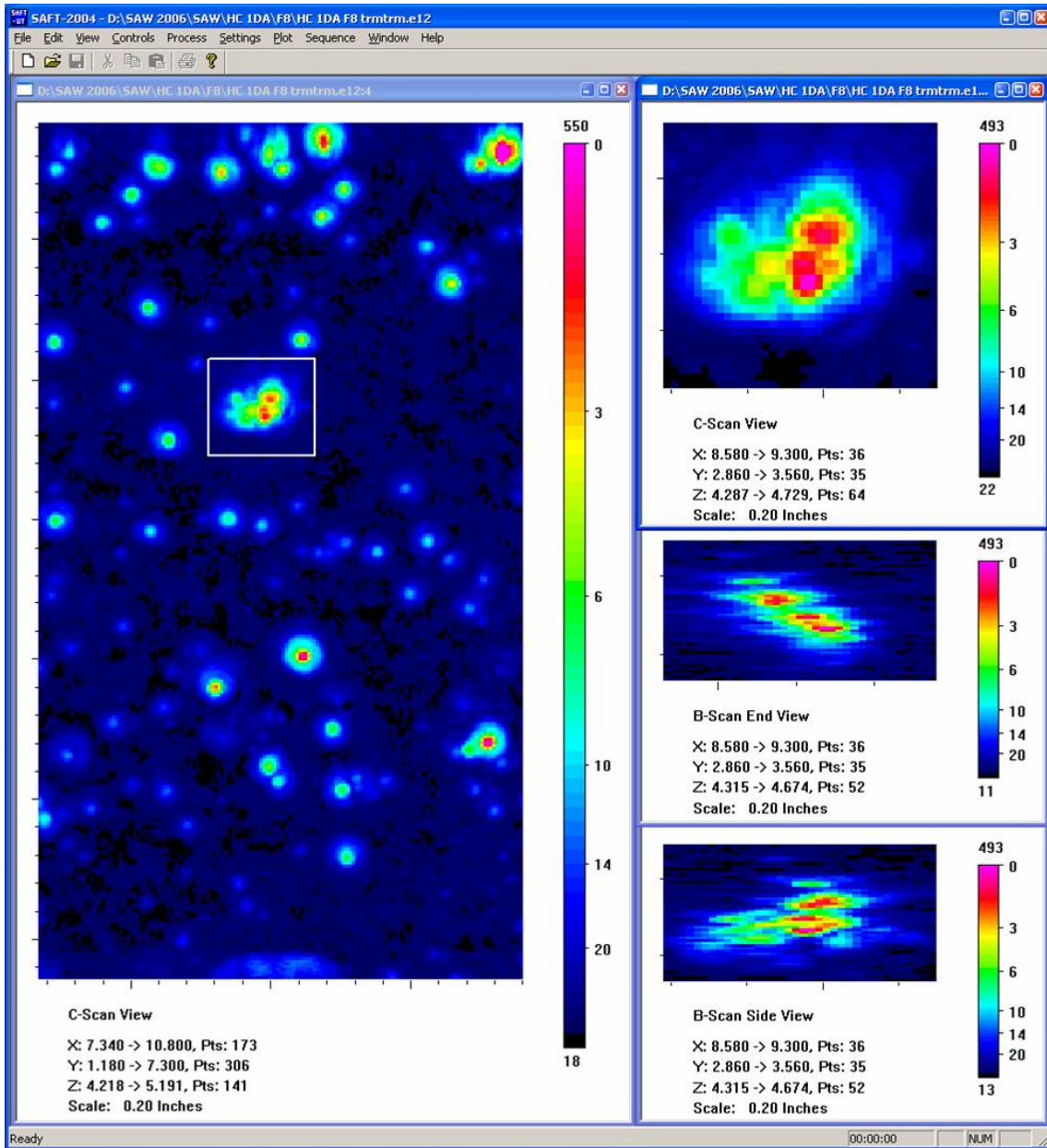
Figure A.11.a 10 MHz F8 Immersion Testing Images of Small Fabrication Flaw: *HC5B*. **This figure shows immersion testing data of a complex flaw indication from the weld-normal testing of large weld segments. The flaw indication is identified in the box drawn in the SAFT-UT image on the left in the figure.**
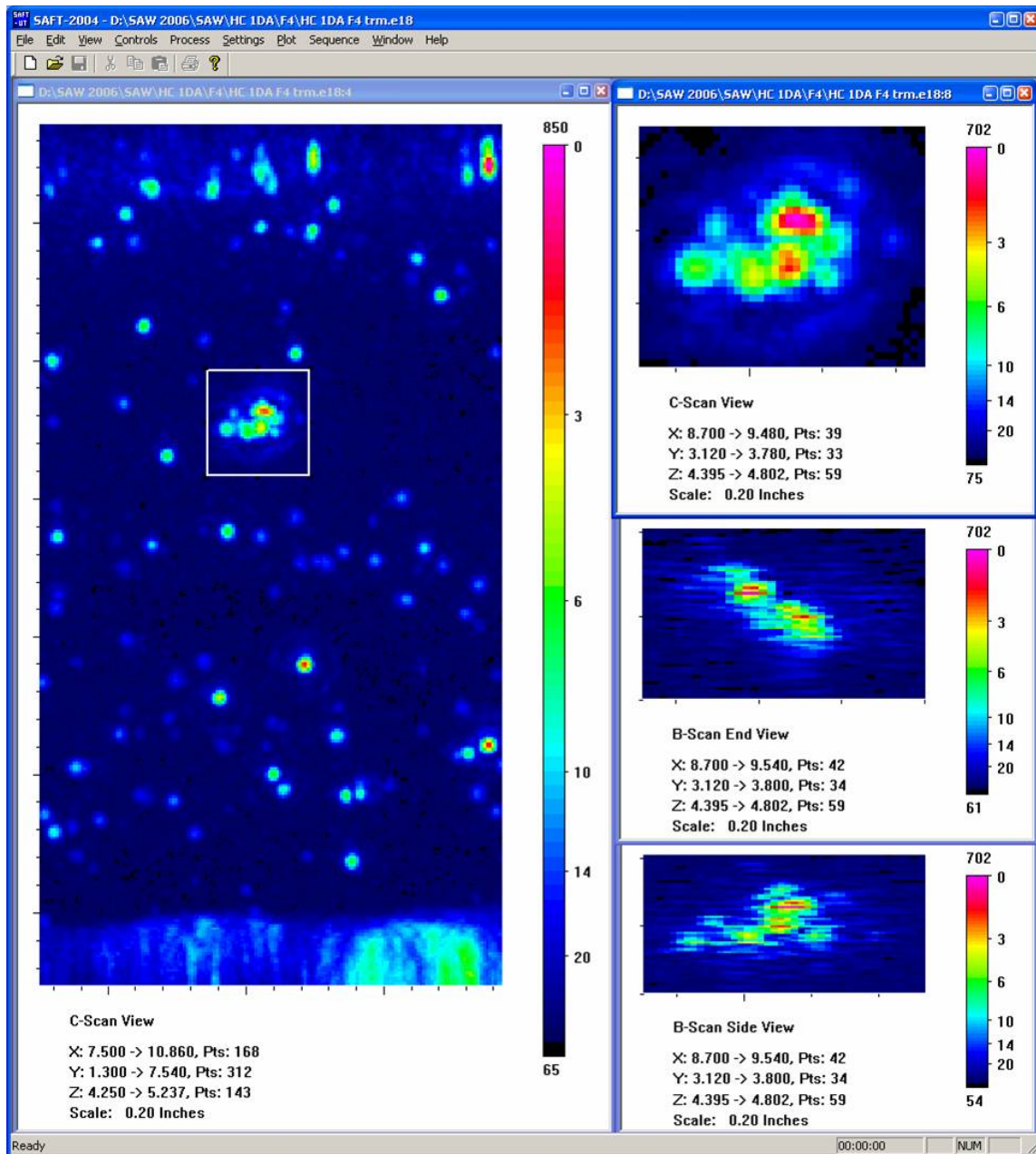
Figure A.11.b F4 Immersion Testing Images of Small Fabrication Flaw: *HC5B*. **This figure shows the same material and complex flaw as the previous figure but with twice the resolving power. The ultrasonic immersion probe was a 10 MHz F4 and as such has a lateral resolution of 1.2 wavelength or 0.7 mm.**
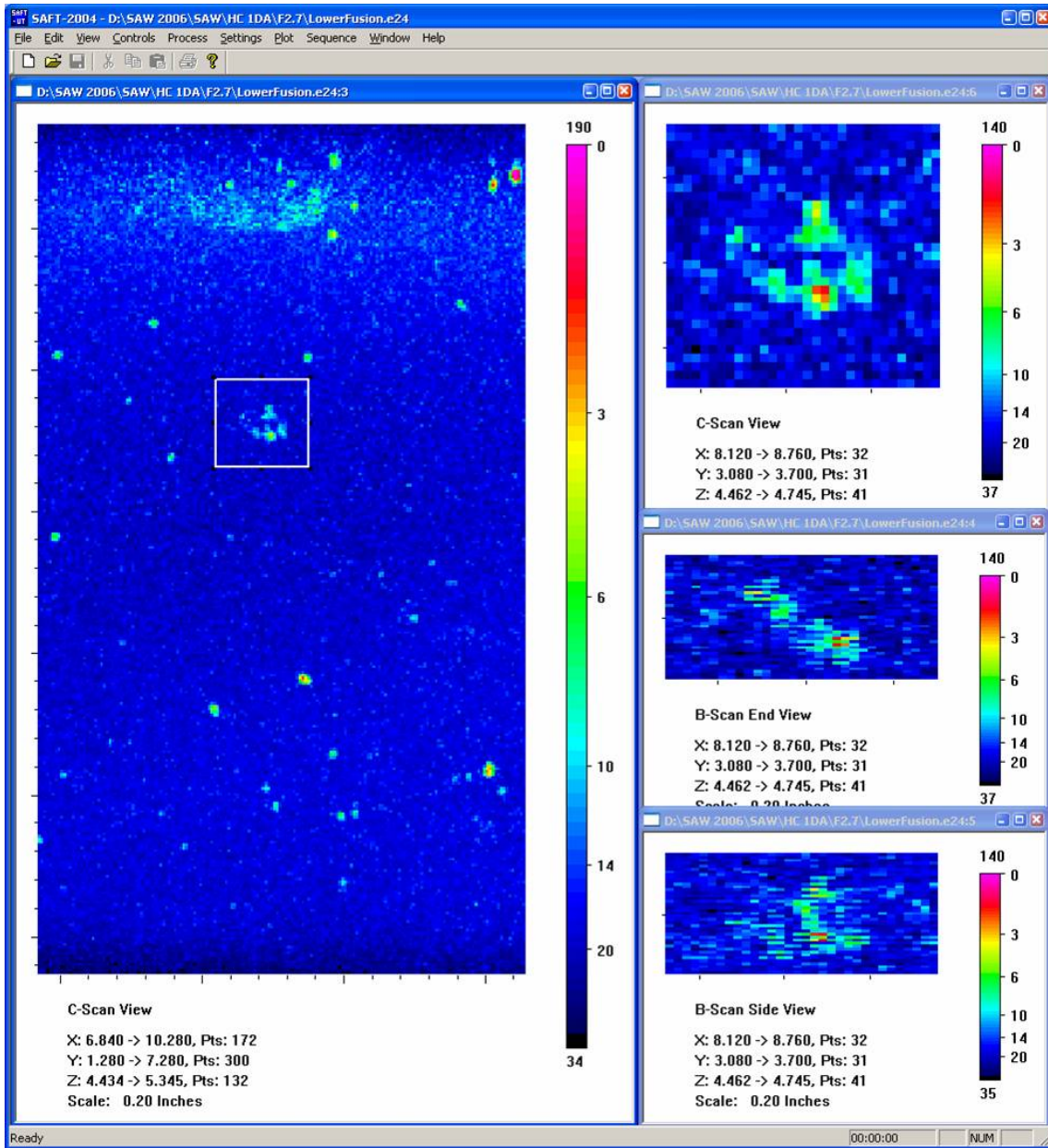
Figure A.11.c F2.7 Immersion Testing Images of Small Fabrication Flaw: *HC5B*. This figure shows the same material and complex flaw as the previous figures. Here the complex flaw is resolved to two flaws with through-wall sizes of 2.5 mm and 2.5 mm.
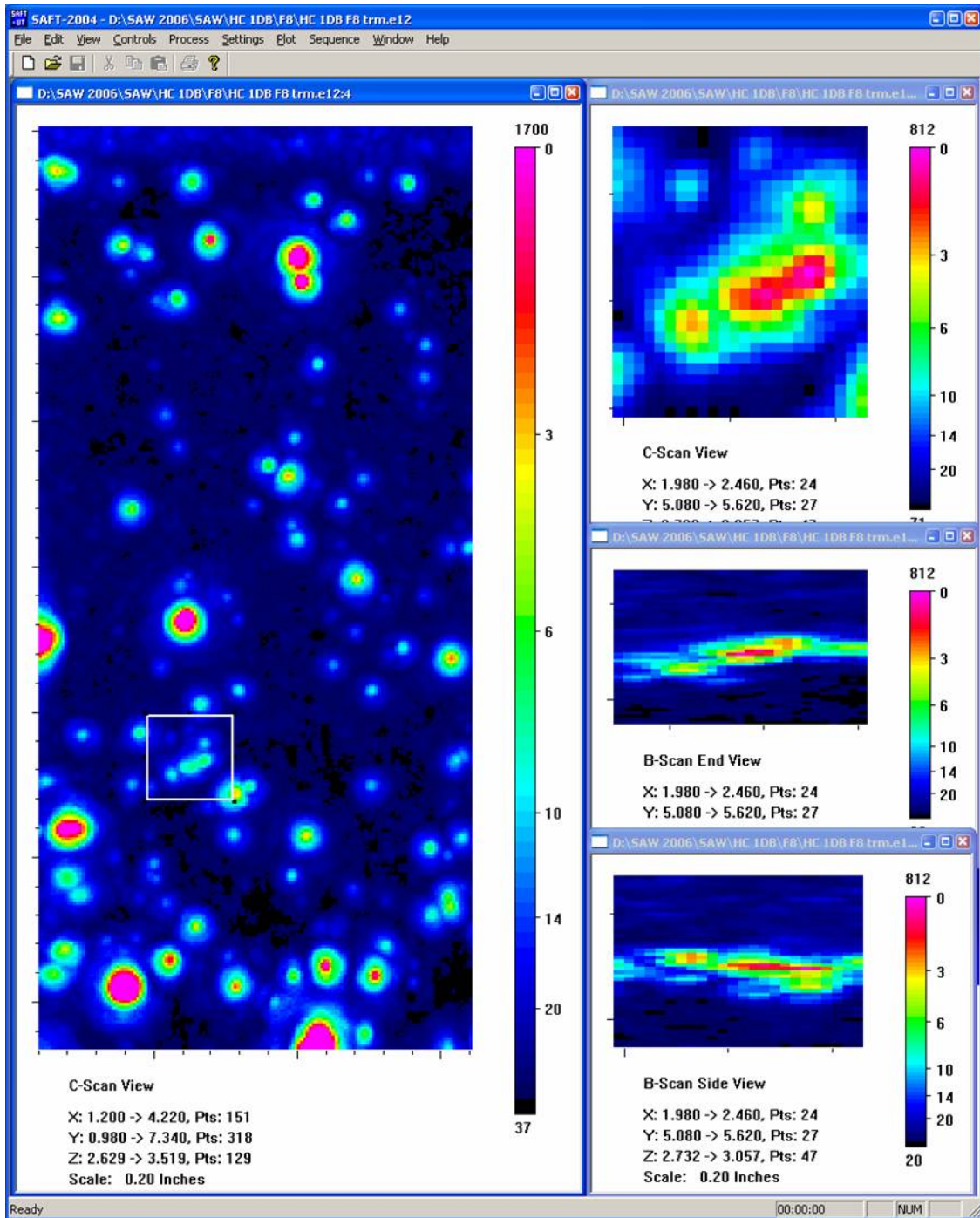
Figure A.12.a 10 MHz F8 Immersion Testing Images of Small Fabrication Flaw: *HC6A*. This figure shows immersion testing data of a 7-mm flaw indication from the weld-normal testing of large weld segments. The flaw indication is identified in the box drawn in the SAFT-UT image on the left in the figure. A close up of the flaw in the C-scan view (top right) shows 4 unresolved flaws.
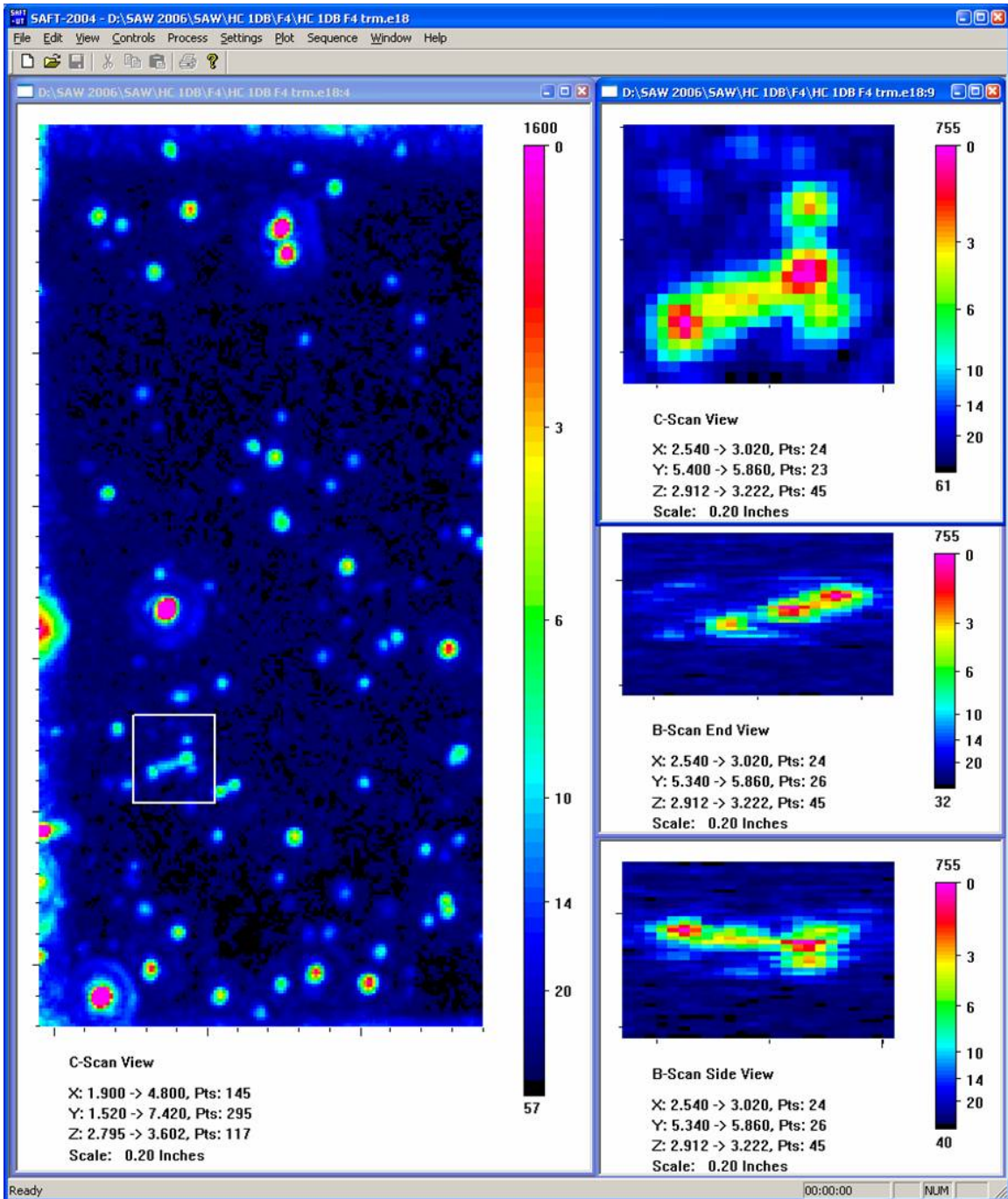
Figure A.12.b F4 Immersion Testing Images of Small Fabrication Flaw: *HC6A*. **This figure shows the same material and flaw(s) as the previous figure but with twice the resolving power. The ultrasonic immersion probe was a 10 MHz F4 and as such has a lateral resolution of 1.2 wavelength or 0.7 mm. Here the four flaws are resolved both laterally and in depth to 2 flaws. The through-wall sizes are 1.5 mm and 4.5 mm.**
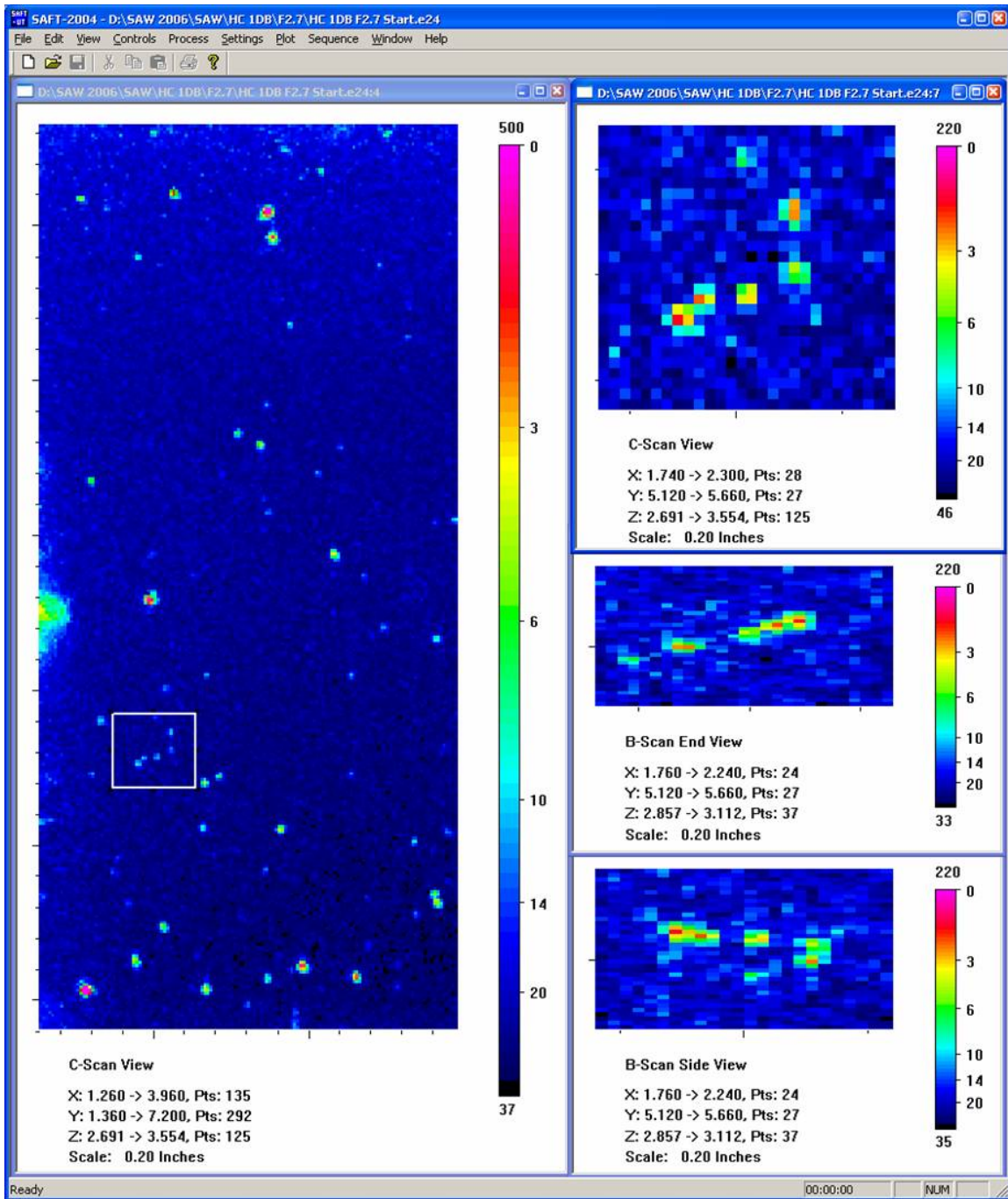
Figure A.12.c F2.7 Immersion Testing Images of Small Fabrication Flaw: *HC6A*. **This figure shows the same material and flaw(s) as the previous figures. Here the four flaws are resolved to through-wall sizes of 1.5 mm, 2.0 mm, 2.0 mm and 1.5 mm.**

Appendix B

Metallography

Appendix B

Metallography

In this appendix, two small flaws imaged in Appendix A with high-resolution ultrasound are confirmed to be small by metallography. Figure B.1 shows a metallograph of flaw RB2A at 10x. Flaw is in the fusion zone of the weld with the base metal. Base metal is on the left in the figure. The heat affected zone of the base metal is 4.0 mm wide as shown. Flaw is inside the weld metal. Figure B.2 is a metallograph of the same flaw at 70x. Flaw measures 0.8 mm vertically in the figure. The vertical axis is the through-wall dimension. The high-resolution ultrasound measured this flaw at 1.5 mm $\pm$ 0.5 mm as shown in Figure A.2.c on page A.6. Figure B.3 is a metallograph of flaw HC5B at 10x. Flaw is in the fusion zone of the weld with the base metal. Base metal is on the left in the figure. The heat affected zone of the base metal is 2.5 mm wide as shown. Flaw cluster is a collection of small isolated flaws. The high-resolution ultrasound shows this flaw cluster in Figure A.11.c on page A.32.
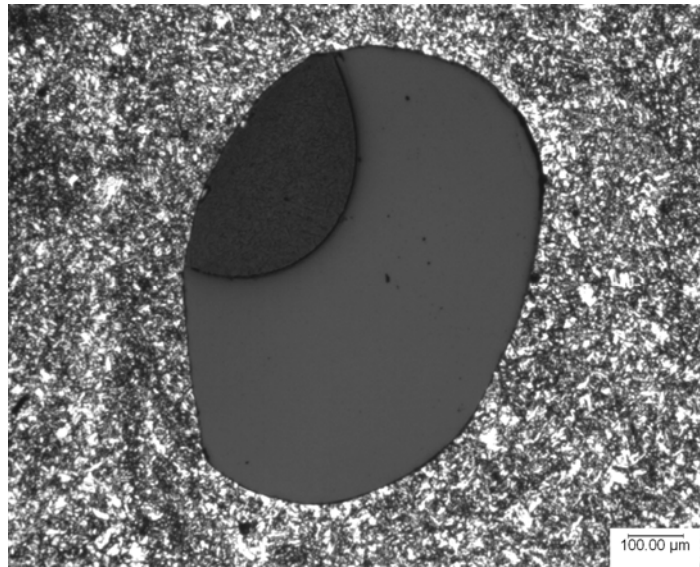

Figure B.1 Metallograph of Flaw RB2A at 10x
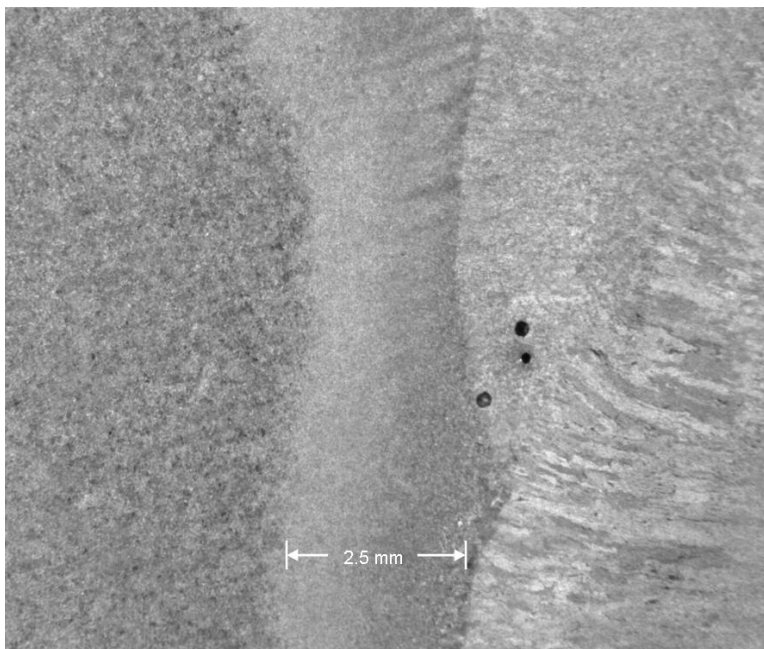
Figure B.2 Metallograph of Flaw RB2A at 70x

Figure B.3 Metallograph of Flaw HC5B at 10x

Distribution

Nuclear Regulatory Commission

TL Chan
NRC/NRR
Mail Stop O-9 H6

RO Hardies
NRC/RES
Mail Stop C5A24M

AL Hull
NRC/RES
Mail Stop C5A24M

MA Mitchell
NRC/NRR
Mail Stop O-9 H6

D Naujock
NRC/NRR
Mail Stop O-9 H6

5   WE Norris
NRC/RES
Mail Stop C5A24M

CA Nove
NRC/NRR
Mail Stop O-9 H6

IG Prokofiev
NRC/RES
Mail Stop C5A24M

TJ Sullivan Jr.
NRC/NRR
Mail Stop O-9 H6

D Terao
NRC/NRO
Mail Stop T-7 F1

RL Tregoning
NRC/RES
Mail Stop C5A24M

MJ Case
NRC/RES
Mail Stop C5A24M

Offsite

J. Lareau
Westinghouse
2000 Day Hill Road
Windsor, CT 06095

WF Miller
118 Hanover Drive
Pottstown, PA 19464

GP Selby
EPRI NDE Center
1300 Harris Blvd.
Charlotte, NC 28262

JC Spanner, Jr.
EPRI NDE Center
1300 Harris Blvd.
Charlotte, NC 28262

50 **Internal Distribution**
Pacific Northwest National Laboratory
P.O. Box 999
Richland, WA 99352

MT Anderson (40)	K5-25
A Ankrum	K6-66
AD Cinson	K5-25
SL Crawford	K5-25
SE Cumblidge	K5-25
AA Diaz	K5-25
SR Doctor	K5-25
M Morra	K5-25
AF Pardini	K5-25
FA Simonen	K5-22
TT Taylor	K5-25
Information Release	PDF